



Current Sheets, Plasmoids and Flux Ropes in the Heliosphere

Part II: Theoretical Aspects

O. Pezzi^{1,2,3} · F. Pecora⁴ · J. le Roux⁵ · N.E. Engelbrecht⁶ · A. Greco⁴ · S. Servidio⁴ · H.V. Malova^{7,8} · O.V. Khabarova^{9,7} · O. Malandraki¹⁰ · R. Bruno¹¹ · W.H. Matthaeus¹² · G. Li⁵ · L.M. Zelenyi⁷ · R.A. Kislov^{9,7} · V.N. Obridko⁹ · V.D. Kuznetsov⁹

Received: 10 October 2020 / Accepted: 15 January 2021
© The Author(s), under exclusive licence to Springer Nature B.V. 2021

Abstract Our understanding of processes occurring in the heliosphere historically began with reduced dimensionality - one-dimensional (1D) and two-dimensional (2D) sketches and models, which aimed to illustrate views on large-scale structures in the solar wind. However, any reduced dimensionality vision of the heliosphere limits the possible interpretations of *in-situ* observations. Accounting for non-planar structures, e.g. current sheets, magnetic islands, flux ropes as well as plasma bubbles, is decisive to shed the light on a variety of phenomena, such as particle acceleration and energy dissipation. In part I of this review, we have described in detail the ubiquitous and multi-scale observations of these magnetic structures in the solar wind and their significance for the acceleration of charged particles. Here, in part II, we elucidate existing theoretical paradigms of the structure of the solar wind and the interplanetary magnetic field, with particular attention to the fine structure and sta-

✉ O. Pezzi
oreste.pezzi@gssi.it

- ¹ Gran Sasso Science Institute (GSSI), Viale F. Crispi 7, 67100 L’Aquila, Italy
- ² Laboratori Nazionali del Gran Sasso (LNGS), INFN, 67100 Assergi, L’Aquila, Italy
- ³ Istituto per la Scienza e Tecnologia dei Plasmi, CNR, Via Amendola 122/D, 70126 Bari, Italy
- ⁴ Dipartimento di Fisica, Università della Calabria, 87036 Rende, CS, Italy
- ⁵ Center for Space Plasma and Aeronomics Research (CSPAR) and Department of Space Science, University of Alabama in Huntsville, Huntsville, AL 35805, USA
- ⁶ Centre for Space Research, North-West University, Potchefstroom, 2522, South Africa
- ⁷ Space Research Institute (IKI) RAS, Moscow, 117997, Russia
- ⁸ Scobeltsyn Nuclear Physics Institute of Lomonosov Moscow State University, Moscow, 119991, Russia
- ⁹ Pushkov Institute of Terrestrial Magnetism, Ionosphere and Radio Wave Propagation of the Russian Academy of Sciences (IZMIRAN), Moscow, 108840, Russia
- ¹⁰ IAASARS, National Observatory of Athens, Penteli, Greece
- ¹¹ Istituto di Astrofisica e Planetologia Spaziali, Istituto Nazionale di Astrofisica (IAPS-INAF), Roma, Italy
- ¹² Department of Physics and Astronomy, University of Delaware, Newark, DE 19716, USA

bility of current sheets. Differences in 2D and 3D views of processes associated with current sheets, magnetic islands and flux ropes are discussed. We finally review the results of numerical simulations and *in-situ* observations, pointing out the complex nature of magnetic reconnection and particle acceleration in a strongly turbulent environment.

Keywords Plasma turbulence · Magnetic reconnection · Particle acceleration · Solar wind

1 Introduction

The heliosphere is a highly structured medium, characterized by the presence of a variety of plasma structures observed over a wide range of scales, from the energy-containing, large scales, to kinetic (Malandraki et al. 2019). As described in Part I of this review, understanding physical processes related to the variety of large-scale plasma structures observed in the solar wind and the magnetosphere implies analyzing their fine structure. The latter, in turn, requires a comprehensive analysis of properties of current sheets (CSs), flux ropes (FRs), and plasmoids. The dipolar nature of the main solar magnetic field and, consequently, of the interplanetary magnetic field (IMF) leads to the formation of the heliospheric current sheet (HCS), which is the largest CS in the heliosphere. Its configuration has historically been modelled as a waved “ballerina skirt” that follows the solar magnetic equator and the Parker IMF spiral shape (Wilcox et al. 1980; Hoeksema et al. 1983). Similarly strong but less long-lived CSs are formed in the solar wind at different helio-latitudes owing to the presence of higher harmonics of the solar magnetic field (see Part I, Sect. 2.1.2). Coronal Mass Ejections (CMEs), often associated with explosive phenomena triggered by magnetic reconnection, as well as their interplanetary counterpart, ICMEs, significantly perturb the heliosphere and its magnetic field, producing shock waves, dubbed interplanetary shocks (ISs) at which strong CSs may occur. ISs can also be produced by long-lived Corotating Interaction Regions (CIRs) or less stable Stream Interaction Regions (SIRs) formed when a fast flow from a coronal hole overtakes the surrounding slow solar wind (Heber et al. 1999). Notably, large-scale structures, such as SIRs, ICMEs and the HCS, coexist with structures of much smaller scales. For example, reconnecting CSs and FRs or plasmoids –whose two-dimensional (2D) counterparts are magnetic islands (MIs)– are often observed not only at the edges but also within complex ICMEs and SIRs/CIRs (see Xu et al. (2011), Khabarova et al. (2016), Khabarova and Zank (2017) and Part I, Sect. 2.1.2). Furthermore, the HCS is often rippled and surrounded by the much wider heliospheric plasma sheet (HPS) in which numerous secondary reconnection regions produce a sea of thin CSs (TCSs), FRs as well as plasma bubbles/blobs/plasmoids (see Adhikari et al. (2019) and Part I, Sect. 2.1). FRs or plasmoids have been also found in the inner heliosphere (Zhao et al. 2020), in the Earth’s magnetosheath at kinetic scales (Yao et al. 2020), and in laboratory plasmas (Gekelman et al. 2019). This ensemble of structures have a significant impact on the topology of the surrounding IMF, which –in turn– regulates the propagation of charged particles of both heliospheric and galactic origin (see Dalla et al. (2013), Battarbee et al. (2017, 2018), Engelbrecht et al. (2019) and Part I, Sect. 3).

Another keystone of *in-situ* measurements regards the pervasive significance of both plasma turbulence and magnetic reconnection in governing small-scale processes that occur in space plasmas (e.g. Matthaeus and Velli (2011), Zank et al. (2014), Matthaeus et al. (2015), Servidio et al. (2015), le Roux et al. (2015)). In Part I, we discussed the fact that magnetic reconnection and turbulence are always linked. An analogous argument holds for

CSs, the occurrence of which always suggests the formation of FRs/plasmoids/magnetic islands and vice versa. The solar wind, which embeds these magnetic and plasma structures, is a strongly turbulent and intermittent medium, characterized by a complex interplay of different phenomena (Servidio et al. 2009; Matthaeus et al. 2015; Bruno and Carbone 2016). The energy of the magnetic field and bulk speed fluctuations injected at large scales is cross-scale transferred towards smaller scales, at which Hall and kinetic effects can be significant (Servidio et al. 2007, 2015). Spectral steepening (Leamon et al. 1998; Alexandrova et al. 2008; Sahraoui et al. 2009) and dispersive wave effects are routinely observed in the solar wind. These latter are compatible with either strongly turbulent fluctuations not described in terms of linear modes (Alexandrova et al. 2008) or kinetic Alfvén waves (KAWs) (Howes et al. 2008a; Sahraoui et al. 2009; Salem et al. 2012) and whistler waves (Beinroth and Neubauer 1981; Gary et al. 2010; Vasko et al. 2020), although whistler modes possess a smaller power content with respect to the KAW branch (Chen et al. 2013).

Signatures of kinetic effects are often found in the particle velocity distribution function (VDFs) that exhibit non-Maxwellian properties, e.g. temperature anisotropy, heat fluxes, beams and rings (Marsch 2006; Maruca et al. 2011; Servidio et al. 2012, 2015; Valentini et al. 2016; Perri et al. 2020). These non-equilibrium features may drive the onset of microinstabilities (Hellinger et al. 2006; Matteini et al. 2013; Bandyopadhyay et al. 2020b), although understanding the significance of linear instabilities within a turbulent environment is still under debate (Qudsi et al. 2020). The dissipation of turbulent energy is thought to locally occur at small scales (Osman et al. 2011, 2012a,b; Matthaeus et al. 2015; Vaivads et al. 2016), thus ultimately heating the plasma. Fine velocity-space structures have also been recently observed in the magnetosheath (Servidio et al. 2017) and obtained in kinetic simulations performed within solar-wind-like conditions (Pezzi et al. 2018; Cerri et al. 2018) by means of the Hermite decomposition of the plasma VDF (Grad 1949; Tatsuno et al. 2009; Schekochihin et al. 2016). This supports the idea that non-equilibrium features in particle VDF readjust in a very complex way, resembling the development of a enstrophy velocity-space turbulent spectrum (Servidio et al. 2017). The presence of fine velocity-space structures may also enhance the dynamical role of inter-particle collisions (Pezzi et al. 2016b; Pezzi 2017; Pezzi et al. 2019b).

Magnetic reconnection, during which a local breaking of the frozen-in law causes a rapid release of magnetic energy in both flow energy and heating, goes hand in hand with plasma turbulence (Lazarian and Vishniac 1999; Kowal et al. 2011; Lazarian et al. 2015). Indeed, CSs that separate vortices and magnetic islands in plasma turbulence often represent reconnection sites (Retinò et al. 2007; Servidio et al. 2009, 2010; Haggerty et al. 2017; Phan et al. 2018). Furthermore, reconnection exhausts and jets generated by magnetic reconnection can be turbulent themselves (Franci et al. 2017; Pucci et al. 2017a, 2018a) and can also host secondary reconnection regions driven by nonlinear waves and/or instabilities (Lapenta et al. 2015, 2018; Wang et al. 2020). Very recent observations conducted at an unprecedented high-resolution by the Magnetospheric Multi-Scale (MMS) mission (Burch et al. 2016a; Fuselier et al. 2016) allowed, for the first time, to investigate the electron-scale magnetic reconnection by explicitly showing the electron diffusion region and by addressing the relevant question about the physical mechanism that breaks the frozen-in law in a collisionless plasma (Burch et al. 2016b; Le Contel et al. 2016; Torbert et al. 2016, 2018; Breuillard et al. 2018; Chasapis et al. 2018a).

Magnetic reconnection is also a decisive phenomenon in astrophysical plasmas owing to its role in particle acceleration (Lyutikov 2003; Uzdensky 2011). In the planetary magnetospheres and the solar wind, signatures of particle acceleration are observed in the particle energy distribution, that often shows non-Maxwellian higher energy tails described in terms

of kappa (Vasyliunas 1968; Sarris et al. 1976; Christon et al. 1989; Collier 1999) or power-law distributions. Although acceleration mechanisms in the solar wind and magnetospheres have common features, they also present distinctive traits due to the different physical conditions. For example, the maximum particle energies that can be obtained in the Earth's magnetosphere do not exceed a few MeV (Zelenyi et al. 2007) since accelerated particles with gyroradii approximately equal to the magnetospheric scales leak out to the solar wind. In smaller-scale magnetospheres, the maximum acceleration energies are much smaller. For example, in Mercury's magnetosphere, due to repeating substorms and magnetotail dipolarization events, particle energies are estimated to be about 100 keV. In the corona and the solar wind, even single mechanisms act on scales many orders larger, and the mechanisms in combination can contribute to the particle energy gain up to GeV. At the same time, one should note that magnetic reconnection, wave propagation and turbulent processes widely present in the solar wind are limited by MeV energies (see Part I, Sect. 3).

Historically, seminal works by Fermi (1949, 1954) proposed two general acceleration mechanisms based either on the stochastic interaction of particles with randomly moving magnetic clouds/inhomogeneities (second-order Fermi acceleration) or on the systematic acceleration of particles in the case of converging magnetic traps (first-order Fermi acceleration). Several acceleration mechanisms in space have been proposed and are found to be in accordance with *in-situ* observations. For example, the large-scale dawn-dusk electric field can accelerate quasi-adiabatic ions during the so-called Speiser acceleration (Speiser 1965; Lyons and Speiser 1982; Cowley and Shull 1983; Ashour-Abdalla et al. 1993; Zelenyi et al. 2007). Plasma particles can also be energized by Alfvén and cyclotron waves in the proximity of the magnetopause (Drake et al. 1994; Johnson and Cheng 2001; Panov et al. 2008) and heated by ultralow frequency (ULF) waves (Glassmeier et al. 2003; Baumjohann et al. 2006). In presence of a shock (e.g. magnetospheric bow shocks or ICME/CIR/SIR – driven interplanetary shocks) (Thampi et al. 2019; Slavin et al. 2008), nonadiabatic heating, diffusive shock acceleration (DSA), shock drift acceleration (SDA) and also stochastic shock drift acceleration (SSDA) (see Katou and Amano (2019) for a review on SDA) can occur. At variance with SDA, both DSA and SSDA assume the presence of fluctuations (e.g. pre-existing turbulence) on which particles diffuse in order to be accelerated. DSA, first introduced to address cosmic-ray acceleration at supernova remnants (Bell 1978a,b; Blandford and Ostriker 1978), has also been invoked to explain acceleration in solar wind (Zank et al. 2000). However, it is not easy to interpret some *in-situ* observations through the original steady-state DSA model (see Malandraki et al. (2019) for a further discussion). At the same time, SDA and SSDA are efficient in the energization of electrons at planetary bow shocks (Leroy and Mangeney 1984; Burgess 1987; Giacalone 1992; Katou and Amano 2019; Amano et al. 2020).

Other mechanisms of acceleration are directly related to magnetic reconnection. Both reconnection events of solar origin (Higginson and Lynch 2018) and local magnetic reconnection (Khabarova et al. 2015, 2016, 2020b; Adhikari et al. 2019; Malandraki et al. 2019) can lead to particle acceleration. Near the current-sheet X-line, the electric field produced by reconnection can accelerate charged particles (Matthaeus and Lamkin 1986; Ambrosiano et al. 1988). Moreover, Hoshino (2005) found that electrons, trapped by the polarization (Hall) electric field produced by reconnection, are efficiently accelerated owing to a surfing acceleration mechanism. Current sheets are often unstable due to tearing instability (Zelenyi et al. 1984; Malara et al. 1992; Malara and Velli 1996; Tenerani et al. 2015a; Primavera et al. 2019). Electric fields induced by (i) the tearing instability, (ii) the CS destruction (Lutsenko et al. 2005), (iii) dipolarization processes in the terrestrial magnetosphere (Zelenyi et al. 1990; Delcourt and Sauvad 1994; Delcourt 2002; Slavin 2004; Delcourt et al. 2005; Apitenkov et al. 2007; Zhou et al. 2010; Ukhorskiy et al. 2017; Parkhomenko et al. 2019), or

(iv) other fluctuations occurring in the turbulent environment with the presence of magnetic reconnection (Malara et al. 2019) are also able to accelerate charged particles. For example, in the magnetosphere, a power-law tailed energy distribution of energetic particles has been obtained by considering the model of the CS with electromagnetic fluctuations excited by electromagnetic wave ensembles. The occurrence of electromagnetic fluctuations close to the reconnecting CSs also allows explaining additional particle acceleration (additional to the acceleration due to the large-scale electrostatic E_y) often observed in velocity distributions at open field lines (Grigorenko et al. 2013). Temperature and density inhomogeneities across the reconnecting CS may also speed up the formation of secondary plasmoids, as has recently been shown using test-particle (Catapano et al. 2015, 2016, 2017) and PIC simulations (Karimabadi et al. 2013; Lu et al. 2019a) as well as spacecraft observations (Lu et al. 2019b).

Furthermore, numerical simulations show that particles can be efficiently energized due to the contraction of magnetic islands (MIs) (Drake et al. 2006a) and their merging (Drake et al. 2013). The combined role of these different mechanisms and their relative importance has been described by Zank et al. (2014) via analytical solutions, finding that MIs contraction and merging are the dominant acceleration mechanisms. Further models discussing the effect of multiple FRs and the combined role of magnetic reconnection-related acceleration mechanisms and DSA have been developed by le Roux et al. (2015) and Zank et al. (2015b), le Roux et al. (2016), respectively. le Roux et al. (2018) self-consistently coupled energetic particles, for which the transport equation is solved, and MHD turbulence that controls the FRs dynamics. The role of small-scale FRs has been recently considered by le Roux et al. (2019), Mingalev et al. (2019). Magnetic reconnection is thus an efficient mechanism able to accelerate particles locally, at least at levels comparable with DSA (Garrel et al. 2018). An analysis of spacecraft observations also supports these findings. Local particle acceleration at the HCS has been reported, e.g., by Zharkova and Khabarova (2012, 2015). Khabarova et al. (2015, 2016, 2020b), Khabarova and Zank (2017), Adhikari et al. (2019), Malandraki et al. (2019) found observational evidence for local particle acceleration associated with the occurrence of reconnecting CSs and MIs. Recurrent (stochastic or turbulent) magnetic reconnection occurring at the HCS, MIs inside the rippled HCS and smaller CSs within the HPS presumably energizes charged particles via the mechanisms proposed by (Zank et al. 2014, 2015a; le Roux et al. 2015, 2016, 2019). Atypical energetic particle events (AEPEs), not easily explained in terms of the DSA mechanism, are instead well described by local particle acceleration in regions filled with small-scale MIs of width $<\sim 0.001$ AU (Khabarova et al. 2016; Khabarova and Zank 2017). Prior findings regarding locally accelerated ions have recently been systematized by Adhikari et al. (2019), Chen et al. (2019a). A local origin of some suprathermal electrons observed in the solar wind, as reflected in the specific features of pitch-angle electron distributions, has also been suggested by Khabarova et al. (2020b). Explosive particle acceleration (Pecora et al. 2018, 2019b) that combines several types of acceleration mechanisms mentioned above can finally take place, e.g. in the solar corona.

It is important to note that different mechanisms can co-act simultaneously in space plasmas. This can be clearly seen in observations (e.g., Khabarova et al. 2016), Adhikari et al. (2019) and Part I, Sect. 3.1, 3.2). However, this effect may considerably complicate the interpretation of the observed picture (Malandraki et al. 2019). Note that, in presence of turbulent fluctuations, stochastic acceleration of charged particles (of both Fermi types) (Milovanov and Zelenyi 2001; Trotta et al. 2020; Sioulas et al. 2020) and, in general, various acceleration mechanisms mentioned above can operate (Artemyev et al. 2009b; Kobak and Ostrowski 2000; Parkhomenko et al. 2019; Ergun et al. 2020b,a). We also remark here

that Milovanov and Zelenyi (2001) generalized second order Fermi acceleration for systems with long-range correlations of spatial turbulence structures (Comisso and Sironi 2018, 2019). This process can be considered as a transport process in the velocity space. In this perspective, the “random movement” term is usually described by the Gaussian variance $\langle V^2(t) \rangle \sim t$ for velocities of scattered particles $V(t)$. Meanwhile, the Gaussian variance in principle ignores long-range dynamical correlations occurring in turbulent self-organized systems. The effect of correlations appears in multi-scale nonrandom acceleration events that do not comply with standard velocity diffusion. A fractional-dynamic approach solves the issue of describing stochastic acceleration in the presence of the long-range correlations (Milovanov and Zelenyi 1994; Metzler and Klafter 2000, 2004; Zimbardo et al. 2017). Fractional generalization of Einstein’s Brownian motion and the subsequent fractional kinetic equations are believed to provide a powerful framework that can be applied to many physical systems (Perri and Zimbardo 2007, 2012; Zimbardo and Perri 2013; Zimbardo et al. 2015; Zimbardo and Perri 2017). The fractional equation allows incorporating spatial and temporal effects of long-range correlations and is capable of describing both particle super-diffusion (i.e., persistent random walks), and sub-diffusion (anti-persistent random walks) (Zimbardo et al. 2006), while the well-known Fermi acceleration dynamics scales as $V(t) \sim t^{1/3}$ in the true random classical case.

These observations ultimately confirm the idea that heliospheric structures, such as CSs, FRs and plasmoids, have a complex topology and, in general, are far from being planar or spherically-symmetric. Due to both non-stationarity and non-uniformity of the solar wind, acceleration processes can take place everywhere where the electric field is present and the scales of magnetic inhomogeneities are of the order of the proton or electron gyroradii. Plasma turbulence complexly links stream propagation, magnetic reconnection and particle energization in a puzzling multi-scale and multi-process scenario. Owing to strong nonlinearities, numerical simulations are important to properly interpret *in-situ* observations.

Obviously, fully three-dimensional (3D) models retain the complete physical picture of the described phenomena. Indeed, small-scale phenomena (e.g., secondary magnetic reconnection, waves/instabilities and ripples of the HCS) are hardly described within a 2D approach. However, 2D or quasi-2D models have been adopted owing to their capability to properly paint the picture of several physical phenomena, at least at a qualitative level. For example, the basic physics of magnetic reconnection is well depicted employing 2D models (Matthaeus and Lamkin 1986; Ambrosiano et al. 1988). On the other hand, Kowal et al. (2011) stressed the importance of considering the fully 3D space and the presence of a guide field. Moreover, Kowal et al. (2012) pointed out that turbulent fluctuations superimposed to the reconnecting CSs can enhance the acceleration rate since magnetic reconnection becomes fast and a thick volume filled with several multiple reconnecting regions is formed, thus leading to a first-order acceleration mechanism. Other advanced studies have been focused on kinetic simulations, in which it is possible to describe the non-ideal mechanism leading to magnetic reconnection. Several studies, often focusing on the relativistic regime, confirmed that the first-order Fermi mechanism related to reconnection can accelerate particles to energies described by a power-law distribution (Guo et al. 2015, 2016b; Li et al. 2019; Xia and Zharkova 2018, 2020). The fully 3D space guarantees the interplay of several wave modes and instabilities, leading to turbulence (Huang et al. 2017; Lapenta et al. 2015, 2018). The contribution of several drifts has also been analyzed by Li et al. (2017), finding that the major energization is due to the particle curvature drift along the induced electric field. The particle energization created by FR merging has recently been investigated by Du et al. (2018).

It is important to emphasize that even while 3D models include distinctive effects not included in 2D, some very important effects occur in both geometries even if details may

differ. For example, multiple secondary island formation occurs even in 2D incompressible MHD (Matthaeus and Lamkin 1986; Wan et al. 2013). Turbulence also elevates reconnection rates in 2D and 2.5D MHD and Hall MHD (Matthaeus and Lamkin 1985, 1986; Smith et al. 2004) as well as in the more realistic 3D geometry as discussed above. While it is almost always preferable to have a 3D picture of natural phenomena, often the 2D models are preferred because they can achieve larger system sizes and higher Reynolds numbers, these also being important and even crucial parameters in describing observations of natural processes.

We finally remark that the description of solar-wind turbulence has faced similar debates about 2D vs 3D models. The strong wavevector anisotropy of MHD turbulence with respect to the guide field (Shebalin et al. 1983), also supported by spacecraft observations revealing the “Maltese Cross” pattern in the two-dimensional correlation function measurements of solar wind fluctuations (Matthaeus et al. 1990), motivated the development of a two-component model, which is composed by fluctuations with wavevector parallel to the ambient magnetic field (slab) and by fluctuations with wavevector quasi-perpendicular to the ambient magnetic field (2D) (Bieber et al. 1996; Ghosh et al. 1998) (see (Oughton et al. 2017; Oughton and Matthaeus 2020) for recent reviews on MHD turbulence in the solar wind). Moreover, numerical simulations performed in the kinetic regime showed that a 2.5D approach describes well solar-wind dynamics in the inertial range and at sub-proton scales (Servidio et al. 2014, 2015; Wan et al. 2015; Li et al. 2016; Franci et al. 2018), although it has been claimed that a fully 3D approach should be retained to properly model nonlinear couplings at large-scale in the incompressible limit (Howes 2015). A contrasting, and even puzzling, result in the realm of kinetic PIC simulations is that averages of the electromagnetic work conditioned on local values of the current density (a rough equivalent of an Ohm’s law) behaves very similarly in 2.5D and in 3D, and, perhaps surprisingly, both behave very much like collisional MHD (Wan et al. 2016).

This part of the review follows Part I (Khabarova et al. 2020a), which, mainly focuses on providing the general information about the objects of this review and observations of non-planar magnetic structures and their association with particle acceleration. The structure of this part of the review is the following. In Sect. 2 we provide details on some models adopted in order to describe the dynamics of CSs and MIs, with particular emphasis on the formation of their fine structure. We also discuss their stability properties and overview theoretical and numerical models aimed at analyzing the impact of CSs, FRs and MIs on the transport of energetic particles, in particular on galactic cosmic rays in the heliosphere (HCS). Then, in Sect. 3 we speculate about the theoretical approaches usually employed to describe particle acceleration within contracting/merging FRs. Section 4 is dedicated to the description of recent advances in numerical studies of the evolution of plasma turbulence and, in particular, the appearance of numerous discontinuities representing potential reconnection and heating sites. The discussion of the results covers both high-resolution fluid (MHD and Hall MHD) and kinetic simulations. Particle acceleration in such complex environments is described in Sect. 5. Finally, we summarize the discussed results and make conclusions about the past and future development of studies of CRs, FRs/plasmoids and MIs in Sect. 6.

2 Current Sheets: Their Fine Structure, Stability and the Ability to Accelerate Particles

As introduced above, FRs, blobs/plasmoids/bubbles, CSs and MIs are ubiquitous features in the dynamics of astrophysical plasmas. In this section, we revisit the basic dynamics of

current sheets by highlighting, in particular, the formation of their fine structure and their stability properties.

One can roughly classify planar and conic current sheets as either “thick” or “thin” structures based on the ratio of their transverse scale to the proton gyroradius. In the thick CSs, electric currents are supported by plasma drift currents in circular magnetic field gradients, repeating the shapes of large-scale structures themselves. For CSs of this type, the presence of a neutral magnetic surface is not necessary and they are quite stable relative to the tearing mode. Meanwhile, crossings of thin CSs (TCSs) are characterized by the occurrence of the neutral line altogether with a strong jump of the magnetic field in their vicinity. These CSs seem to be a reservoir of free energy. Therefore, it is quite possible that these very common structures in space plasmas are responsible for the energy storage and release, magnetic reconnection, plasma acceleration and other important processes in planetary magnetospheres (Retinò et al. 2007; Ergun et al. 2020b), in the solar wind (Zelenyi et al. 2010, 2011, 2019), and the solar corona (Syrovatskii 1971).

As discussed in Part I of this review, current sheets also exhibit a fine structure. They are multi-layered, containing several TCSs embedded into the main CS of much wider thickness (Malova et al. 2017). Cascading or production of similar current sheets around the main one is a well-known process observed over a wide range of scales. In general, a conglomerate of current sheets formed around the mother current sheet and resembling the multi-scaled heliospheric plasma sheet (HPS) (see Part I) is observed. Below we describe the main physical mechanisms responsible for the formation of the fine structure of current sheets. By developing a quasi-adiabatic model, Zelenyi et al. (2004) demonstrated that CSs are multi-scaled and meta-stable structures that can be quite stable for a long time but then can spontaneously be destroyed by tearing instability. TCSs are also sensitive to the impact of a wide spectrum of kink and oblique waves, which leads to their instability in variable conditions. This process is followed by the explosive CS destruction and the release of the energy excess in a form of plasma acceleration and wave activity. Note that excited waves of different types can generally coexist also after the CS destruction. Electromagnetic turbulence can hence develop in the TCS-filled plasmas. As a result, plasma particles can be accelerated by plasma turbulence, and this mechanism is common for the magnetospheric and the solar wind plasmas.

2.1 Quasi-Adiabatic Model of Thin Current Sheets in Space Plasmas

It should be noted that the first analytical and mathematically-simple model of a thin one-dimensional (1D) current sheet was proposed by Harris (1962). In this model, only the tangential component of the magnetic field was taken into account. Further analysis of proton dynamics in the neutral plane with the reversed magnetic field that also considered a finite but small normal magnetic field was done by Speiser (1965), who showed that in such CSs protons are demagnetized near the neutral plane and their quasi-adiabatic integral of transverse (along z coordinate) oscillations

$$I_z = \frac{1}{2\pi} \oint p_z dz \quad (1)$$

is approximately conserved.

A semi-analytical 1D model of the TCS in the collisionless space plasma was proposed by (Zelenyi et al. 2000, 2004) based on the quasi-adiabatic description of ions with the plasma anisotropic pressure tensor and magnetized electrons in the fluid approximation. In

this model, the general self-consistent system of Vlasov-Maxwell equations has the following simple form:

$$\frac{dB_x}{dz} = \frac{4\pi}{c} (j_{i,y}(z) + j_{e,y}(z)) \quad (2)$$

$$j_{i,y} = e \int v_y f_i(z, v) dv \quad (3)$$

being f_i the ion distribution function and $j_{i,y}$ the ion current density in the y -direction. The ion distribution function can be obtained at any location inside the current sheet by mapping the source distribution from the edges of the TCS to the neutral plane using Liouville's theorem; thus it can be re-written as a function of a quasi-adiabatic integral I_z . Electron current density $j_{e,y}$ can be calculated in the guiding center approach. The detailed description of the basic model and its modifications can be found in Zelenyi et al. (2011) and references therein.

Later, numerical models of TCS were adopted to verify the semi-analytical model (Zelenyi et al. 2004). Comparison of model results with experimental observations from the Cluster satellites in the Earth's magnetotail demonstrated a good agreement between them (Artemyev et al. 2009a). The application of the model to the case of the heliospheric current sheet (HCS) and similarly strong current sheets (SCSs) in the solar wind was made by Malova et al. (2017). The general configuration of the model is shown in Fig. 1(a). Particles move from current sheet edges toward the neutral plane. Within the CS plane, particles are demagnetized and move along serpentine-like orbits; afterwards, they go outward and carry the electric current across the current sheet. Since electrons are magnetized, their curvature electric current dominates in the plane of the neutral sheet. As a result, the electron-determined current flows within a thin current sheet is embedded in a thicker current sheet created by protons, as it is shown schematically in Fig. 1(b). This is in good accordance with observations showing that TCSs are located within much thicker Harris-like background current sheets which can be called plasma sheets analogous to the HPS (see Malova et al. (2018) and Fig. 1 of Part I).

Figure 1(c) displays self-consistent solutions for the module of the tangential component of the magnetic field as a function of the z coordinate. Here the parameter n_r is the relative concentration of quasi-adiabatic particles; it varies from 1 to 0. The black curve corresponds to the case when all particles are quasi-adiabatic ($n_r = 1$ or 100%) and the green curve corresponds to the opposite case of a pure Harris-like current sheet with the isotropic pressure distribution ($n_r = 0$ or there is 0% of quasi-adiabatic particles). From panels (b) and (d) of Fig. 1, one can easily figure out that the background current sheet has a very smooth and wide profile. The corresponding green curve has a width of about 10^2 proton gyro-radii, and the ordered thinner proton current peak is manifested in the central part of CS. The electron current is the narrowest, and at some parameters, it is seen in the region of the neutral plane [Fig. 1(b)]. Panel (b) of Fig. 1 also shows that a very narrow $|\mathbf{B}|$ peak of the proton current becomes noticeable for $n_r \geq 0.3$ (see the case with $n_r = 0.3$, shown by the dark blue curve).

One may conclude that in TCSs electrons may carry only a part of the azimuthal electric current due to curvature drifts, whereas the main part of the cross-sheet current is carried by demagnetized quasi-adiabatic protons (Zelenyi et al. 2011; Malova et al. 2017, 2018). As seen from Figs. 1(b–c), the central part of the multi-scale current sheet is a very narrow structure with a thickness of several proton Larmor radii ρ_L , while the wider background part of the SCS with negligible current density has a thickness $L = 100\rho_L$. Therefore Fig. 1(b–c) demonstrate the multiscale character of a thin current configuration embedded in a much

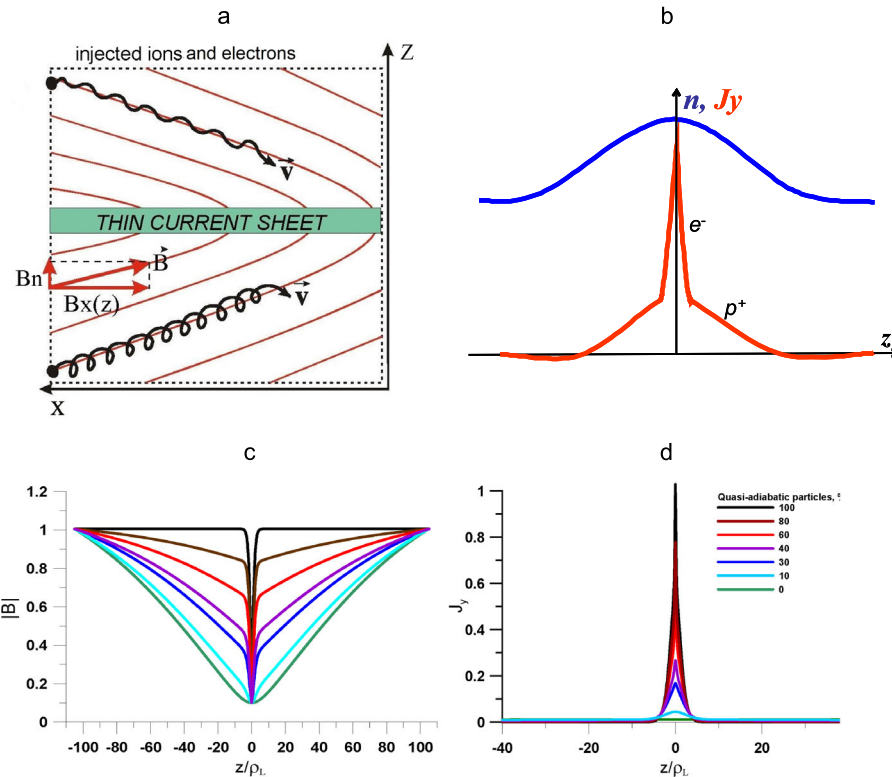


Fig. 1 Multi-scaled structure of SCSs/HCS: (a) General scheme of the model (adapted from Zelenyi et al. (2006)); (b) Schematic view of the embedding of current sheets (adapted from Zelenyi et al. (2006)). Multiscale CSs are embedded in the thicker plasma sheet in which the plasma density tends to constant at the edges, i.e. $n(L) \rightarrow n_0$. Regions of differently-dominated plasma populations can be seen; (c) Self-consistent profiles $|\mathbf{B}(z/\rho_L)|$ (adapted from Malova et al. (2017)); (d) Current density profile $J_y = j_y/enV_{D1}$ within the current sheet (adapted from Malova et al. (2017)). Colored curves correspond to different densities of quasi-adiabatic particles (as a percentage of the total number of particles). Transverse coordinate z showed in the abscissa is normalized to the proton gyroradius ρ_L , $|\mathbf{B}|$ and n are normalized to their values at $100z/\rho_L$

thicker plasma sheet in which the plasma density tends to have an almost uniform distribution, while the current density vanishes in the same region.

2.2 Current Sheet Dynamics and Formation of Multiple Current Sheets in the Solar Wind

The current sheet filamentation *via* tearing instability was proposed as a key factor of sub-storm activity in the Earth's magneto-tail since the early papers (e.g., Coppi et al. (1966)), in which the 1D Harris sheet equilibrium solution has been used for the analysis of current sheets stability. It further was shown that the existence of a finite but small normal component B_z in the current sheet can lead to a strong stabilizing effect due to the electron compressibility (see, e.g. Schindler (1979) and references therein). Many other possible mechanisms of sub-storm triggering were proposed to solve this problem (see details in the review by Zelenyi et al. (2010)). In particular, the stochastic particles motion (Buechner and Zelenyi 1989; Kuznetsova and Zelenyi 1991), pitch angle scattering (Coroniti 1980),

transient electrons (Sitnov et al. 1997, 2002), and current-driven instabilities (Lui 1996, and references therein) were considered and analyzed in detail.

Meanwhile, it was later shown that all these mechanisms cannot destroy the strong stabilization effect of electrons, at least in the Harris-like current-sheet case (Pellat et al. 1991). Over time this paradoxical result had lead to the loss of interest of scientists in the tearing mode as a trigger of substorm onset (Zelenyi et al. 2011). In two decades, experimental observations of the Earth's magnetotail performed during the Cluster mission time made clear that magnetotail TCSs are principally different from well-known Harris-like configurations, therefore some additional factors may control the TCS stability (Runov et al. 2005, 2006; Zelenyi et al. 2003).

These results enabled a solution to the old problem, finally forming the paradigm that associates the substorm activity with the onset of tearing-type instability. The idea that magnetotail current sheets can be unstable only at some narrow regions in the parameter space was for the first time formulated by Galeev and Zelenyi (1976). Further, Zelenyi et al. (2008) investigated this effect in details in the frame of a quasi-adiabatic model of TCS supported by satellite observations. It was concluded that the thinning of the magnetotail current sheet is followed by an increase of the anisotropy in the ion and electron distribution functions. Hence, finally, the magnetotail becomes a new metastable equilibrium with a TCS in the equatorial plane that can spontaneously be destroyed, being accompanied by the processes of fast magnetic reconnection.

Both observational and theoretical studies allow suggesting that tearing instability and magnetic reconnection of thin current sheets can play a substantial role in the formation of a system of multiple current sheets in the solar wind (see, e.g., Wang et al. (1998), Réville et al. (2020) and references therein). More recently, the stability of tearing mode and the onset of fast magnetic reconnection have received a detailed attention (Tenerani et al. 2015a,b; Pucci et al. 2017b, 2018b).

As discussed in Part I, Sect. 2.3.1, crossings of sector boundaries are often associated with prolonged observations of multiple thin current sheets generally following the heliospheric plasma sheet (HPS) shape (see also Liu et al. (2014)). These current sheets with a thickness of several proton gyroradii (Behannon et al. 1981; Khabarova et al. 2015; Xu et al. 2015) are often called strong current sheets (mentioned above in paragraph 2.1) (see Malova et al. (2017)). A possible theoretical interpretation of such events and a typical HPS/HCS crossing observed by a 1 AU spacecraft were discussed by Malova et al. (2018). The corresponding figures are reproduced here as Fig. 2(a) and (b), respectively.

Figure 2(a) shows stable and unstable regions in the parameter space, where b_n is the transverse magnetic component normalized to the total magnetic field at current sheet edges, and ε is the ratio of the thermal velocity to the drift flow plasma velocity. Stability properties of TCSs can be changed during their formation and possible evolution under changing external conditions. An example of this process is shown in Fig. 2(a) with the red arrow that indicates the direction of a possible switch of a TCS from the stable to the unstable state under evolving external conditions, following the decrease in the magnetic transverse component b_n and the relative increase in the plasma flow velocity with respect to the thermal speed (i.e. the decreasing parameter ε , see, e.g., Zelenyi et al. (2009b, 2011)).

Figure 2(b) depicts numerous current sheets observed within the HPS at 1 AU. The beginning of the HPS crossing is characterized by a sharp change in the azimuthal IMF angle direction that was generally stable before. It further becomes very unstable and varies many times for hours along with the corresponding signatures of current sheet crossings in the IMF components and the plasma beta until the IMF direction changes to the opposite. It was acknowledged tens of years ago that studying the nature of multiple SCSs in the solar wind is

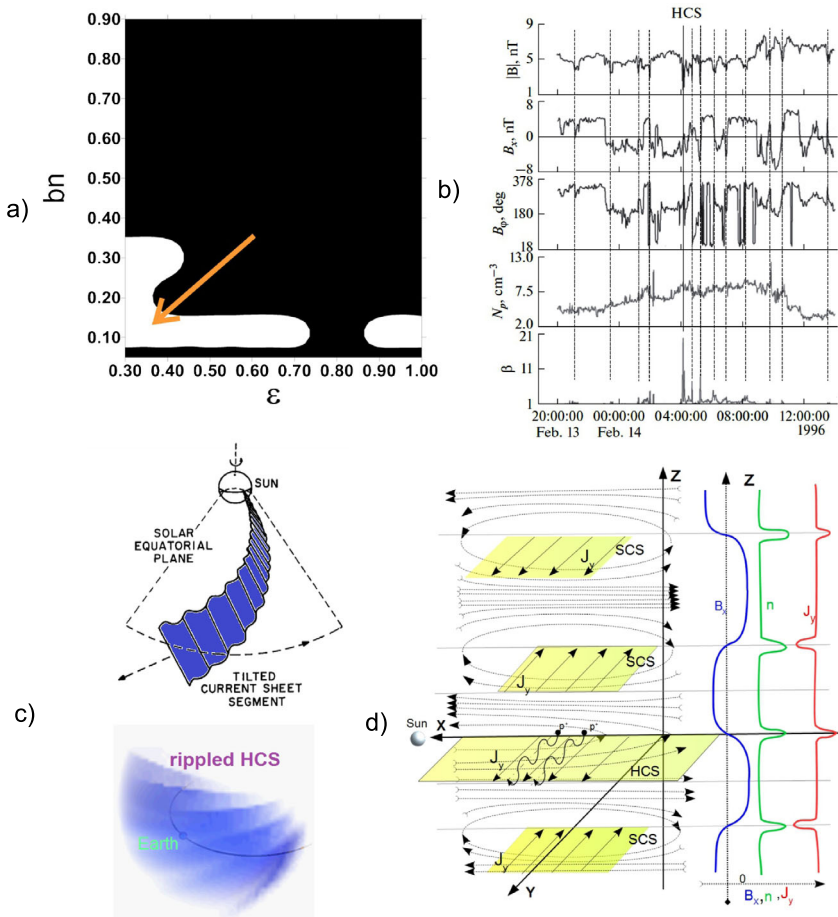


Fig. 2 Current sheet dynamics and multi-sheet current configurations in the solar wind: observations and theoretical interpretations. (a) Stable (black) and unstable (white) regions of a thin current sheet under the tearing mode, according to the model by Zelenyi et al. (2008) (adapted from Zelenyi et al. (2008)). Red arrow indicates a possible direction of the switch of the current sheet state from the stable to unstable. (b) Example of observations of the prolonged HPS/HCS crossing at the Earth's orbit (reproduced from Malova et al. (2018)). From top to bottom: the magnitude of the IMF, the radial component of the IMF in the GSE coordinate system, the azimuthal angle of the IMF, the solar wind density, and the plasma beta. Multiple strong current sheets (indicated by vertical lines) are observed within the HPS. (c) HCS ripples as predicted by Behannon et al. (1981) (upper panel) and observed in the solar wind via interplanetary scintillations (lower panel) (adapted from Khabarova et al. (2015)). (d) Configuration of the magnetic field lines in the vicinity of the HCS (central yellow plane) surrounded by magnetic islands/blobs (left sketch), and corresponding reconstructed profiles of the magnetic field B_x , the electric current j_y and plasma density n

very important for the understanding of current sheet dynamics in the heliosphere. Crooker et al. (1993, 2004) proposed a mechanism of the formation of multiple current sheets due to the large-scale radial folding/bending of the HCS and magnetic tubes with a subsequent formation of giant loops, which, however, was not confirmed. Modern views on this point suggest that both the loops and HCS folding/rippling exist but at far smaller scales, produced by local dynamical processes (see Part I, Sect. 2.3.1).

Generally, two main hypotheses on the formation of a set of multiple current sheets in the solar wind near the HCS have been developed:

- exogenous: the solar corona is the source of current sheets in the solar wind.
- endogenous: wave and reconnection processes locally trigger multiple CSs in the HCS/HPS vicinity.

Note that, the exogenous factor may lead, e.g., to the distortion and the consequent destruction of neutral surfaces originated from the top of coronal streamers (see, e.g., Sanchez-Diaz et al. (2019), and references therein). On the other hand, the two following mechanisms can be attributed to the endogenous factors:

1. The development of wave processes as a result of the impact of non-stationary flowsstreams, owing to which the HCS can possess a folded or highly rippled form with ripples crossed for tens of minutes at 1 AU (Behannon et al. 1981; Khabarova et al. 2015). The rippled HCS is shown in Fig. 2(c). The upper panel is adapted from Behannon et al. (1981). They gave a correct explanation of the fine structure of the HCS/HPS, suggesting the existence of the plissé-like shape of the HCS, crossing of which may be reflected in observations of numerous current sheets. The direction of ripples was suggested to be perpendicular to the radial (sunward) direction, which indeed can be the case either at far heliocentric distances where the Parker spiral twist angle is near 90° or in front of/behind fast streams pushing the HCS (see Fig. 22 and Fig. 30 in Part I of the review). The lower panel in Fig. 2(c) shows observational evidence for the formation of HCS ripples. It is easy to see that the crossing of a ripple can be interpreted as an intersection of pairs of current sheets with the opposite direction of the flowing electric current (Mingalev et al. 2019).
2. The development of current sheet-associated instabilities (mainly, tearing instability) in the solar wind, accompanied by magnetic reconnection and the formation of plasmoids/magnetic islands (see Gosling (2007), Ruffenach et al. (2012), Khabarova et al. (2015), Tenerani et al. (2015a,b), Pucci et al. (2017b), Khabarova and Zank (2017), Adhikari et al. (2019) and Sect. 2.1.4. of Part I). The electric currents can flow at both internal and external surfaces of such closed structures.

It is important to note that the origin of magnetic islands and plasmoids, as well as blobs and bubbles surrounding the HCS, may be of the combined exogenous-endogenous origin (see Part I and Janvier et al. (2014)). The largest of these magnetic structures can be formed due to the splitting of streamer current sheets and subsequent magnetic reconnection during the extension and evolution of streamers in the solar wind (Somov 2013). It is shown that multi-sheet magneto-plasma configurations are unstable in principle (Dahlburg and Karpen 1995), i.e. magnetic fields tend to reconnect, which leads to the formation of magnetic islands contributing to changes of the magnetic surface topology and stratification of the current system within the HCS (Zelenyi and Milovanov 2004; Sanchez-Diaz et al. 2019). An idea about magnetic reconnection of coronal streamers above loops appeared in 1990th (see McComas et al. (1991), Antiochos and DeVore (1999), Wang et al. (2000), Somov (2013)). Later, it was suggested that coronal streamers can eject a series of sequentially arranged magnetic blobs adjacent with magnetic flux ropes into the solar wind. In the plane perpendicular to the neutral surface at the cusp of a streamer, these structures represent a chain of blobs or 2D magnetic islands that can be observed not only in-situ but also in white light (e.g., Wang et al. (2000), Song et al. (2009), Wang and Hess (2018)). This process has been modelled as well (e.g., Higginson and Lynch (2018)). Owing to the impact of the dynamical processes occurring in the surrounding plasma and the development of tearing and

other instabilities, magnetic bubbles/blobs originated from the corona can be distorted, split or merged. As a result, all those structures create an HCS turbulent/intermittent environment consisting of multiple current sheets occurring within the system of numerous magnetic islands. In this perspective, it is clear that a fully 3D approach is quite important in order to properly understand the dynamics of these structures.

Figure 2(d) schematically shows a possible configuration of the HCS surrounded by several magnetic islands. On the right of the sketch, the corresponding profiles of the magnetic field, the plasma and electric current density are shown as a function of the transversal z -coordinate. Such current structures are relatively thin and can be comparable by width with the proton gyroradii. In such current configurations, electrons can be magnetized while protons move along quasi-adiabatic (serpentine-like) orbits (Zelenyi et al. 2004, 2011; Malova et al. 2017). Two protons on quasi-adiabatic trajectories are shown in Fig. 2(d) in the HCS plane.

Therefore, multiple current sheets embedded in the HPS are self-consistent structures with characteristic peaks of the plasma density, the plasma beta and the alternating direction of the electric current in the adjacent current sheets. Owing to their small thicknesses and large spatial scales, such magnetic configurations can be described in the frame of an almost one-dimensional quasi adiabatic model (see (Zelenyi et al. 2004)) in which spatial characteristics in the direction transverse to the current sheet midplane are most important.

2.3 Oblique Low-Frequency Electromagnetic Modes and TCS Stability

As described above, TCSs can become unstable when they are influenced by the electromagnetic modes propagating along the magnetic field. Meanwhile, modes with the wave vector $\mathbf{k} = k\mathbf{e}_x$ in the GSM system of coordinates represents a limiting case of a more general situation when modes propagate in the arbitrary direction with respect to the magnetic field (e.g., for $\mathbf{k} = k\mathbf{e}_y$, these are well-known kink and sausage modes (Lapenta and Brackbill 1997; Daughton 1999; Büchner and Kuska 1999)). These fluctuations could be either symmetric or asymmetric with respect to $z = 0$ plane. A lot of research were devoted to the analysis of all possible instabilities both analytical (Lapenta and Brackbill 1997; Daughton 1999; Yoon and Lui 2001) and numerical (Pritchett et al. 1996; Zhu and Winglee 1996; Büchner and Kuska 1999; Karimabadi et al. 2003).

All these studies were limited to the case of 1D Harris equilibrium with $B_z \neq 0$. Meanwhile, it is known that real TCSs cannot be described by this model (see above). Some alternative approaches were suggested by Sitnov et al. (2004), who studied lower-hybrid drift perturbation in the y -direction, although considering electrons as a cold neutralizing background. Silin et al. (2002) studied electromagnetic perturbations in current sheets, in the limit of an infinitely thin 1D current sheet (so-called Syrovatsky's sheet). Moreover, Zelenyi et al. (2009a) showed that different values of the growth rate are possible in TCSs as a function of angle θ with respect to the direction of magnetic field lines. This implies that different types of wave modes can exist at the neutral plane of the magnetotail simultaneously to form a complex turbulent structure (Milovanov et al. 2001).

Zelenyi et al. (1998) suggested analyzing the problem from another perspective. In particular, they studied the state of the magnetotail after that all linear CS modes grew up and nonlinearly interacted with each other (see Zelenyi et al. (1998) for details about such interaction). It is important to point out that the resulting CS state keeps an intrinsic variability, i.e. modes may grow and decay, but on average, the system remains steady. Such a system is, hence, in the so-called non-Equilibrium Steady State (NESS). In the NESS state, particles (e.g., ions as suggested in Zelenyi et al. (1998)) supporting the cross-tail current in

the current sheet drift through current sheet-associated magnetic turbulence and are scattered by magnetic fluctuations. The fluctuating part of the electric current is determined by this scattering and controls the parameters of magnetic fluctuations via Maxwell equations. Magnetic fluctuations, in turn, govern peculiarities of ion scattering. Therefore, the fluctuating part of the electric current and magnetic fluctuations are coupled self consistently, while the average current should have an exact value supporting the current sheet magnetic field reversal considered as a boundary condition.

Technically, methods of fractal geometry appear to be very effective to describe particle scattering in the ensemble of multi-scale magnetic fluctuations with certain fractal properties. This analysis uniquely defines the fractal measures of turbulence necessary for the self-consistency of a system. The final task is to convert these measures to the observable standard characteristics of turbulence, such as Fourier spectra. Zelenyi et al. (1998) adopted a simple assumption, namely, the Taylor hypothesis that magnetic structures are frozen into the bulk of moving plasma and their characteristics are determined by the Doppler effect in the frame of an observer/spacecraft. Bringing all these considerations together, Zelenyi et al. (1998) obtained the so-called universal shape of the spectra of magnetic fluctuations: $\delta B/B \sim k^{-7/3}$, where k is the wavenumber. Certainly, such spectral indexes are expected to exist as “universal” only within the frequency (wavelength) domain in which the Taylor hypothesis operates. A theoretical analysis predicted that there should be well-defined spectral breaks at large- and small k boundaries of the universal interval. An analysis of numerous satellite observations brought together by Zelenyi et al. (1998) confirmed that the spectral index of 7/3 is indeed quite common for magnetospheric processes in numerous cases.

2.4 Effects of the Occurrence of Current Sheets, Flux Ropes and Magnetic Islands for the Transport of Energetic Particles in the Heliosphere

Beyond the importance to accelerate particles, that will be the content of next section, drift along HCS as well as drift due to gradients in and the curvature of the heliospheric magnetic field (HMF) play an integral role in the modulation of galactic cosmic rays, as evinced by more than half a century of neutron monitor (e.g. Caballero-Lopez et al. 2019, and references therein) and spacecraft observations (e.g. Gieseler et al. 2017), of cosmic-ray intensities. The characteristic 22-year cycle of alternating peaks and plateaux corresponding respectively to negative and positive heliospheric magnetic field polarities seen from neutron monitor observations can in principle be explained by invoking the drift patterns of charged particles in the heliosphere, where, in the former case positively charged cosmic rays drift Earthwards along with the heliospheric current sheet, and in the latter from the polar regions (see, e.g., Jokipii et al. 1977; Jokipii and Thomas 1981; Burger et al. 1985; Potgieter 2013). This has led to implementing these effects, especially CSs drift, in cosmic ray transport codes since earlier works by Jokipii and Kopriva (1979) and Kota and Jokipii (1983) as well as in subsequent studies. Implementing drift effects due to the HCS in such a code is, however, not a straightforward endeavour, and several approaches to this problem have been implemented in the past. For example, the approach of Kota and Jokipii (1983) numerically calculated the required drift velocities, while studies like those of Strauss et al. (2012) and Pei et al. (2012) numerically calculate perpendicular particle distances from a modelled HCS, using this distance as an input for an approximate expression for the current sheet drift speed which is calculated assuming a locally flat sheet (see also Burger et al. (1985)). The approach of Burger (2012) calculates drift velocities directly by assuming a transition function over the HCS and has also been successfully implemented in CR modulation studies (e.g. Engelbrecht and Burger 2015). All of these approaches, however, treat

the HCS as a differentially thin surface, doubtlessly motivated by the fact that high energy galactic cosmic rays have large Larmor radii, this being the characteristic length scale associated with drift processes in a scatter-free environment Forman et al. (1974), which are assumed to be much greater than the thickness of the current sheet. This quantity is observed to be approximately 10^4 km at 1 au, and to increase with heliocentric radial distance (see, e.g., Smith et al. 2001). Turbulence in the HMF does, however, act so as to reduce the drift scale, and hence drift effects, as has been shown theoretically (e.g. Bieber and Matthaeus 1997), from numerical CR modulation studies (e.g. Ferreira et al. 2003; Burger et al. 2008) and from numerical test-particle simulations of diffusion and drift coefficients (e.g. Minnie et al. 2007; Tautz and Shalchi 2012). Various approaches have been taken to model this effect (for a review, see Burger and Visser 2010), which imply that the assumption that drift processes would be unaffected by physical processes taking place within the finite thickness of the HCS may not always be correct. To investigate this, the turbulence-reduced drift length scale proposed by Engelbrecht et al. (2017) is used in what is to follow, as it yields results for the turbulence-reduced drift coefficient in reasonable agreement with numerical simulations of that quantity in various turbulence scenarios, and has been used successfully in *ab initio* CR modulation studies (e.g. Moloto et al. 2018). This length scale is given by

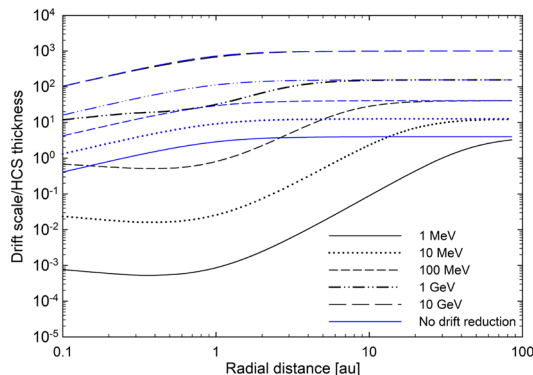
$$\lambda_A = R_L \left[1 + \frac{\lambda_\perp^2}{R_L^2} \frac{\delta B_T^2}{B_0^2} \right]^{-1}, \quad (4)$$

where R_L denotes the maximal Larmor radius to which this drift scale reduces to for low levels of turbulence, δB_T^2 the total transverse magnetic variance, B_0 the HMF magnitude, and λ_\perp the perpendicular mean free path. The inherent three-dimensionality of heliospheric magnetic turbulence has long been taken into account in the various scattering theories used to describe the diffusion of charged particles. An example of this is the study of Bieber et al. (1994), who invoke the observed composite slab/2D nature of turbulence at Earth (see, e.g., Matthaeus et al. 1990; Bieber et al. 1996) to resolve the then long-standing issue of parallel mean free paths derived from the quasilinear theory of Jokipii (1966) for magnetostatic turbulence being considerably smaller than expected from simulations (Palmer 1982). Since then, more advanced theories of particle scattering take this geometry into account, and require also as key inputs information as to the behaviour of turbulence power spectra (see, e.g., Matthaeus et al. 2003; Shalchi 2009; Ruffolo et al. 2012), being sensitive in particular to the behaviour of the 2D turbulence spectrum at low wavenumbers (Shalchi et al. 2010; Engelbrecht and Burger 2015) (see Dundovic et al. (2020) for a recent review of theoretical models and test-particle simulations). For demonstration, as input for Eq. (4) an expression of the perpendicular mean free path derived by Engelbrecht and Burger (2015) from a scattering theory proposed by Shalchi (2010) will be employed, given by

$$\lambda_\perp \approx a^2 C_{-1} \lambda_\parallel \frac{\delta B_{2D}^2}{B_0^2} \log \left[\frac{3\lambda_{out} + 2\sqrt{\lambda_\parallel \lambda_\perp}}{3\lambda_{2D} + 2\sqrt{\lambda_\parallel \lambda_\perp}} \right], \quad (5)$$

with C_{-1} a normalisation constant for the 2D turbulence power spectrum employed in that study, $a^2 = 1/3$ a constant chosen based on the results of numerical test particle simulations of the perpendicular diffusion coefficient by Matthaeus et al. (2003), while the parallel mean free path λ_\parallel is modelled using the quasilinear theory result employed by Burger et al. (2008). The quantity λ_{2D} denotes the length scale at which the break between the energy-containing and inertial ranges occurs on the 2D turbulence power spectrum, and λ_{out} the length scale at which the energy range begins. The spectrum employed by Engelbrecht and Burger (2015)

Fig. 3 Ratio of proton turbulence-reduced drift scale (black lines) and Larmor radius (blue lines) at various energies to the HCS thickness, as a function of heliocentric radial distance in the solar ecliptic plane



to derive Eq. (5) is assumed to decrease with decreasing wavenumber at scales larger than λ_{out} , following physical considerations as discussed by Matthaeus et al. (2007). Observationally, it is unclear how to model this latter quantity, given uncertainties as to observations of turbulence quantities (see, e.g., Goldstein and Roberts 1999), and various estimates for this quantity, which can have a considerable effect on perpendicular mean free paths, have been proposed. Adhikari et al. (2017) argue that the largest turbulent injection scale should correspond with the solar rotation rate, while Engelbrecht and Burger (2013) found that scaling of this quantity being proportional to the 2D correlation scale, as modelled using the Oughton et al. (2011) turbulence transport model, would lead to the differential galactic CR proton intensities computed with their ab initio modulation code to be in reasonable agreement with observations. The quantity λ_{out} can, however, be indirectly calculated if it is assumed that magnetic island sizes can give one a measure of the 2D ultrascale Matthaeus et al. (2007). Engelbrecht (2019b) does this by making use of observed magnetic island sizes reported by Khabarova et al. (2015) and calculating corresponding values for λ_{out} from an expression for the 2D ultrascale derived from an observationally-motivated form for the 2D turbulence power spectrum (the same as that used to derive Eq. (5)). The results are quite close to the scaling used by Engelbrecht and Burger (2013) for this quantity, and are used as inputs for Equations (5) and (4).

To roughly ascertain the validity of the assumption of a negligibly thin HCS, the ratio of the proton drift scale to the HCS thickness is plotted in Fig. 3 as a function of heliocentric radial distance, for the purposes of simplicity in the solar ecliptic plane, and assuming a Parker HMF. For the purposes of comparison, the current sheet thickness is assumed to scale as $\sim r$, with a value of 10^4 km at Earth (Smith et al. 2001). Turbulence quantities are modelled using the simple power-law scalings employed by Engelbrecht (2019a) (based on the turbulence transport model results of Chhiber et al. (2019)). The ratios are also only evaluated to 85 au, as these assumptions are no longer valid in the heliosheath. Figure 3 shows ratios of the drift scale to HCS thickness for both the weak scattering (blue lines) and turbulence-reduced (black lines) cases at various energies. A ratio considerably larger than one would imply that physical processes occurring within the current sheet could safely be neglected when the transport of particles is modelled. For the weak-scattering drift length scale, this ratio is greater than unity for all proton energies considered, barring for a small distance in the very inner heliosphere at 1 MeV. When the effects of turbulence on the drift scale are taken into account, the picture changes considerably. At the highest energies, corresponding to galactic CR protons above 100 MeV, and beyond $\sim 1 - 10$ au, the ratio is very large. Below this energy, and in the very inner heliosphere, it quickly drops below unity,

and considerably so at the lowest energies shown. The implication is that the finite thickness of the current sheet, as well as the detailed physics thereof, need to be taken into account when the transport of such particles is being studied. This is especially relevant given the recent interest in the effects of drift on solar energetic particles (see, e.g., Dalla et al. 2013; Marsh et al. 2013), and has to some degree been taken into account (e.g. Battarbee et al. 2018; Engelbrecht et al. 2019). It is nevertheless also surprising that relatively low-energy (≤ 100 MeV) galactic protons may also be influenced by these effects, and that the detailed physics of the HCS might also need to be incorporated in CR transport models.

3 Kinetic Transport Theory of Energetic Particle Acceleration by Small-Scale Flux Ropes

Irrespective of whether small-scale magnetic flux ropes (SMFRs) originate in a turbulent plasma through magnetic reconnection at large-scale (primary) current sheets or because of the presence of a significant guide/background magnetic field in the turbulent plasma, they form a dynamic turbulence component that generates electric fields through processes like contraction and merging (reconnection) of neighbouring SMFRs that can accelerate particles. Evidence from simulations suggest an efficient acceleration of charged particles traversing regions filled with dynamic SMFRs that can result in power-law spectra for energetic particles as first pointed out by Matthaeus et al. (1984) and Ambrosiano et al. (1988) and confirmed later by many others such as Gray and Matthaeus (1992), Dmitruk et al. (2004), Drake et al. (2006a, 2010, 2013), Li et al. (2015, 2017, 2018).

Theoretical explanation of the main SMFR acceleration mechanisms in the simulations often rely on kinetic transport theories constructed based on the first and second adiabatic invariants combined with magnetic flux conservation (e.g., Drake et al. (2006a, 2013), Zank et al. (2014)), guiding center kinetic transport theory (e.g., Dahlin et al. (2016, 2017)), and the closely related focused transport theory (le Roux et al. 2015, 2018; Li et al. 2018). These theoretical approaches, besides providing familiar non-resonant acceleration concepts for SMFRs, also show promise in reproducing simulation results of acceleration on macro scales (scales larger than the magnetic island size) where the limitation of nearly gyrotropic particle phase angle distributions inherent in these approaches is less problematic (e.g., Li et al. (2018)). This opened up the possibility that such kinetic transport theories can be used to model particle acceleration by SMFRs on large scales in the solar wind, which is computationally beyond the capability of full kinetic particle simulations of acceleration especially.

This promise prompted Zank et al. (2014) and le Roux et al. (2015, 2018) to develop kinetic focused transport theories that unify the main non-resonant SMFR acceleration mechanisms identified in simulations. Expressed in terms of guiding center kinetic theory, the main acceleration mechanisms are: (i) parallel guiding center motion acceleration by the parallel reconnection electric field generated when neighboring SMFRs form secondary (small-scale) reconnecting current sheets between them to merge (e.g., Oka et al. (2010)), (ii) curvature drift acceleration by the motional electric field generated when SMFRs contract or merge (e.g., Drake et al. (2006a, 2013), Li et al. (2017, 2018)), (iii) Lagrangian betatron acceleration which involves magnetic moment conservation when the magnetic field strength in the plasma drift flow frame slowly varies in time and space. This mechanism includes grad-B drift acceleration by the motional electric field generated in contracting and merging SMFRs (e.g., Dahlin et al. (2016, 2017)). In focused transport theory the same acceleration mechanisms manifest in terms of non-uniform plasma flow effects in SMFRs. In this

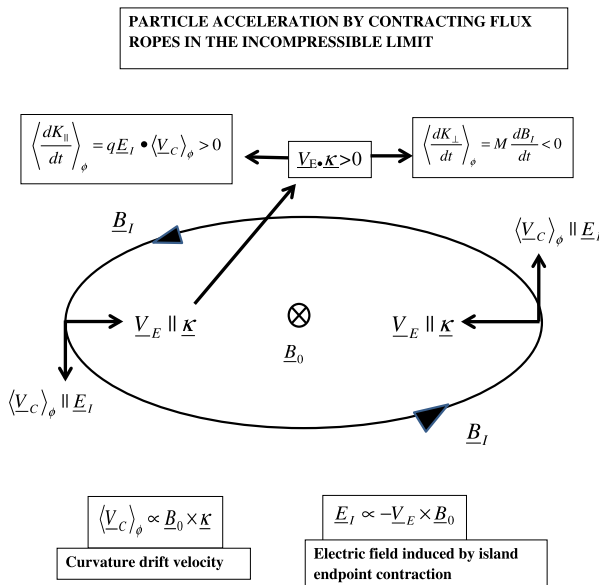


Fig. 4 A schematic diagram of energetic ion acceleration by a contracting quasi-2D SMFR in the incompressible limit (reproduced from le Roux et al. (2018)). Shown is the island (twist) magnetic field component \mathbf{B}_I of the SMFR structure in the 2D plane perpendicular to the locally uniform guide field (axial) component \mathbf{B}_0 of the SMFR pointing into the page. \mathbf{V}_E is the contraction velocity (plasma drift velocity) at the endpoints of the island, and $\kappa = (\mathbf{b} \cdot \nabla) \mathbf{b}$ is the magnetic curvature vector which points in the same direction as the contraction velocity. Thus, for a contracting island $\mathbf{V}_E \cdot \kappa > 0$. This ensures parallel kinetic energy gain from curvature drift acceleration by the in-plane electric field $\mathbf{E}_I \approx -\mathbf{V}_E \times \mathbf{B}_0$ induced by contraction because $q\mathbf{E}_I \cdot \langle \mathbf{V}_C \rangle_{\phi} \propto \mathbf{V}_E \cdot \kappa > 0$, where $\langle \mathbf{V}_C \rangle_{\phi}$ is the curvature drift velocity, but perpendicular kinetic energy loss from Lagrangian betatron acceleration (combination of betatron and grad-B drift acceleration) because $MdB/dt \propto -\mathbf{V}_E \cdot \kappa < 0$, where M is the magnetic moment (see Eq. (6) and its discussion)

context the main SMFR acceleration mechanisms identified in kinetic particle simulations are SMFR compression acceleration, SMFR incompressible parallel shear flow acceleration referring to the SMFR shear flow tensor in the limit of a SMFR flow with a zero divergence, while acceleration by the parallel reconnection electric field is the same as in guiding center kinetic theory (Zank et al. 2014; le Roux et al. 2015, 2018). Having studied how the SMFR acceleration mechanisms in focused transport theory and guiding center kinetic transport theory are connected, le Roux et al. (2018) concluded that: (i) SMFR compression acceleration can be viewed as combining curvature drift momentum gain from the motional electric field induced by magnetic island compression with Lagrangian betatron momentum gain (momentum gain from unified betatron and grad-B drift acceleration) due to the increasing magnetic field strength resulting from magnetic island compression (magnetic-island-containing area shrinks as a result). (ii) SMFR incompressible parallel shear flow acceleration can be interpreted as combining curvature drift momentum gain in the motional electric field generated by magnetic island contraction or merging with competing Lagrangian betatron momentum loss from the decreasing magnetic field strength resulting from magnetic island contraction or merging (magnetic-island-containing area is conserved). For illustration of shear-flow acceleration in contracting magnetic islands, see Fig. 4, in merging magnetic islands, see Fig. 5, and in contracting SMFRs, see Fig. 6. Figure 5 also illustrates parallel guiding center motion acceleration by the parallel reconnection electric field gen-

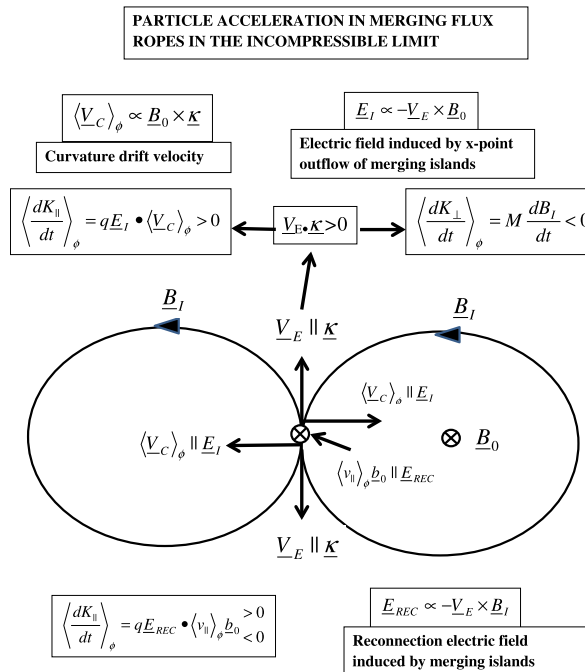


Fig. 5 A schematic diagram of ion acceleration by two merging (reconnecting), quasi-2D flux ropes in the incompressible limit (reproduced from le Roux et al. (2018)). Shown is the island magnetic field \mathbf{B}_I in the 2D plane perpendicular to a uniform guide field component \mathbf{B}_0 pointing into the page. \mathbf{V}_E is the x-point plasma outflow drift velocity in the merging area at the center of the merging magnetic islands pointing in the same direction as the magnetic curvature vector $\kappa = (\mathbf{b} \cdot \nabla) \mathbf{b}$. Thus, in the merging region (reconnecting area) $\mathbf{V}_E \cdot \kappa > 0$, resulting in parallel kinetic energy gain from curvature drift acceleration and perpendicular kinetic energy loss from Lagrangian betatron acceleration (see Eq. (6) and the caption of Fig. 4). In the center of the merging area, the reconnection electric field $\mathbf{E}_{REC} = -\mathbf{V}_E \times \mathbf{B}_I$ points into the page. Energetic particle guiding center motion along/against \mathbf{B}_0 results in parallel kinetic energy gain/loss from the reconnection electric field

erated in the merging process. (iii) Focused transport theory also includes an acceleration mechanism connected to parallel guiding center motion momentum gain or loss from the non-inertial force associated with the parallel component of the acceleration of the plasma flow in SMFRs (le Roux et al. 2018). This mechanism can be traced back as being part of the term in guiding center kinetic theory describing the effect of the electric field on drift inertia that also is the source of the curvature drift acceleration mechanism. From the SMFR focused transport equations, diffusive Parker type transport equations were derived assuming that on large spatial scales in the solar wind pitch-angle scattering will inevitably result in near-isotropic accelerated energetic particle distributions (the diffusive approximation). Accordingly, the distributions were expanded out to the second anisotropic moment in pitch-angle space using Legendre polynomials (Zank et al. 2014; le Roux et al. 2015). By inspecting the SMFR focused transport equation it is clear that SMFR compression acceleration, first advocated by Zank et al. (2014) and later also by le Roux et al. (2015, 2018), Li et al. (2018), Du et al. (2018), can be considered as the only true 1st order Fermi SMFR acceleration mechanism because it involves energy gain without competing energy losses. In the Parker transport equation limit, however, SMFR compression acceleration appears

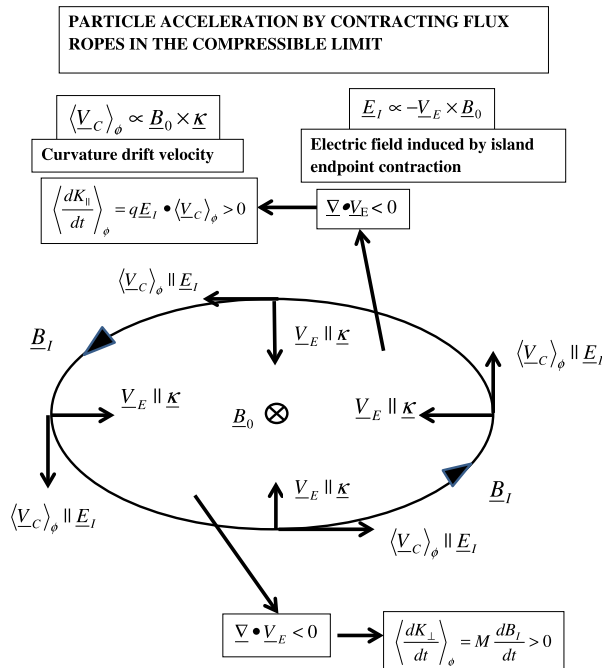


Fig. 6 A schematic diagram of ion acceleration in a compressible contracting quasi-2D SMFR (reproduced from le Roux et al. (2018)). Shown is the island magnetic field (twist component) B_I in the 2D plane perpendicular to a uniform guide field component B_0 pointing into the page. In the compressible limit the divergence of the contraction velocity $\nabla \cdot V_E < 0$ results in perpendicularly kinetic energy gain of energetic particles from the Lagrangian betron acceleration term $M dB_I/dt \propto -\nabla \cdot V_E > 0$ (see Eq. (6) and its discussion) because the island magnetic field strength increases with time (Eq. (6)). Since $\nabla E \cdot \kappa > 0$ for compressible contraction, there is also parallel kinetic energy gain from curvature drift acceleration, but because $|\nabla \cdot V_E| \gg V_E \cdot \kappa > 0$ in the compressible limit, perpendicularly kinetic energy gain from Lagrangian betatron acceleration is expected to be dominant

to be a 1st order Fermi acceleration only in terms of the dominating isotropic part of the distribution function because SMFR compression acceleration also contributes to 2nd order Fermi acceleration through second anisotropic moment of the particle distribution (le Roux et al. 2018). Because the second moment of the distribution function is small compared to the dominating isotropic part of the distribution function, the net compression acceleration for the total distribution function still yields 1st Fermi acceleration mechanism consistent with the focused transport equation. In contrast, SMFR incompressible parallel shear flow acceleration in the Parker transport equation is intrinsically a second order Fermi acceleration mechanism during significant pitch-angle scattering with net acceleration originating from the second anisotropic moment in the particle distribution expansion. In the focused transport equation this mechanism acts like a 1st order Fermi acceleration mechanism when pitch angle scattering is weak because shear-flow acceleration tends to beam particles along the magnetic field so that energy losses become negligible. This is consistent with discussions by Drake et al. (2010) of incompressible magnetic island contraction leading to 1st order Fermi acceleration because the betatron energy losses are negligible compared to curvature drift acceleration when pitch-angle scattering is weak. SMFR parallel guiding center motion acceleration by both the parallel reconnection electric field force and by the parallel

component of the non-inertial force associated with the acceleration of the plasma flow also yield 2nd order Fermi acceleration in the Parker transport equation limit of focused transport theory, but with the difference that net acceleration comes from the 1st anisotropic moment of the particle distribution function expansion. Thus, for a purely isotropic particle distribution only first Fermi SMFR acceleration will be operative (see also, Drake et al. (2010)), while the other mechanisms need a distribution with a pitch-angle anisotropy to yield a net acceleration effect.

3.1 The Small-Scale Flux Rope Acceleration Mechanisms

3.1.1 A Guiding Center Kinetic Theory Perspective

SMFRs detected near Earth have cross sections of $L_I \sim 0.01 - 0.001 \text{ AU}$ (Cartwright and Moldwin 2010; Khabarova et al. 2015) where energetic protons, e.g., have gyro-radii $r_g \ll L_I$ for a wide range of energies that easily includes energies in the MeV range. Thus, standard guiding center kinetic theory, which is restricted to gyro-radii much less than scale of the electromagnetic field in the plasma, is well suited for modeling energetic particle acceleration in SMFR regions up to several MeV as observed (e.g., Khabarova and Zank (2017)). In guiding center kinetic theory, the gyro-phase-averaged rate of change in kinetic energy for energetic charged particles interacting with dynamic SMFRs can be expressed in different ways:

$$\begin{aligned}
 \left\langle \frac{dK}{dt} \right\rangle_{\phi} &\approx \left[q \mathbf{E} \cdot \left(v_{\parallel} \mathbf{B} + m v_{\parallel} \mathbf{b} \times \frac{d\mathbf{b}}{dt} + \frac{mv_{\parallel}^2}{qB} \mathbf{b} \times \boldsymbol{\kappa} \right) \right]_{\parallel} \\
 &+ \left[M \frac{\partial B}{\partial t} + q \mathbf{E} \cdot \left(\frac{M}{q} \frac{\mathbf{B} \times \nabla \mathbf{B}}{B^2} + \frac{M}{q} (\nabla \times \mathbf{b})_{\parallel} \mathbf{b} \right) \right]_{\perp} \approx \\
 &\left[q E_{\parallel} v \mu + m v \mu \left(\mathbf{V}_E \cdot \frac{d\mathbf{b}}{dt} \right) + m v^2 \mu^2 (\mathbf{V}_E \cdot \boldsymbol{\kappa}) \right]_{\parallel} \\
 &+ \left[(1 - \mu^2) M' \left(\frac{\partial B}{\partial t} + (\mathbf{V}_E \cdot \nabla) B \right) + (1 - \mu^2) B \frac{dM'}{dt} \right]_{\perp} \approx \\
 &\left[q E_{\parallel} v \mu - m v \mu \left(\frac{d\mathbf{V}_E}{dt} \cdot \mathbf{b} \right) + m v^2 \mu^2 (\mathbf{V}_E \cdot \boldsymbol{\kappa}) \right]_{\parallel} \\
 &+ \left[-m v^2 \frac{1}{2} (1 - \mu^2) [(\mathbf{V}_E \cdot \boldsymbol{\kappa}) + (\nabla \cdot \mathbf{V}_E)] \right]_{\perp}
 \end{aligned} \tag{6}$$

where q is the net particle charge, v_{\parallel} is the parallel guiding velocity component, \mathbf{b} is the unit vector along the SMFR magnetic field, $\boldsymbol{\kappa} = (\mathbf{b} \cdot \nabla) \mathbf{b}$ is its magnetic curvature, M is the magnetic moment of a gyrating particle, $\mathbf{E} \cdot \mathbf{b} = E_{\parallel}$ is the parallel reconnection electric field component associated with merging SMFR pairs, μ is the cosine of the particle pitch angle, \mathbf{V}_E is the electric field drift (plasma drift) velocity (velocity at which the SMFR magnetic field is contracting or merging), and M' is the maximum magnetic moment (magnetic moment when $\mu = 0$).

In Eq. (6), first and second line, the basic SMFR acceleration mechanisms are grouped in terms of parallel kinetic energy changes (terms in first square bracket) and perpendicular kinetic energy changes (terms in second square bracket). The mechanisms are: (1) Parallel

guiding center motion acceleration by the parallel reconnection electric field component E_{\parallel} generated in reconnection regions between merging neighbouring SMFRs (first term in first square bracket), (2) the effect of the electric field force on the drift inertia term minus curvature drift acceleration (second term in first square bracket in which $d/dt = \partial/\partial t + (\mathbf{V}_E \cdot \nabla)$), (3) curvature drift acceleration by the motional electric field induced by contracting or merging SMFRs (third term in the first square bracket), (4) betatron acceleration due to time variations in the SMFR magnetic field strength (first term in the second square bracket), (5) grad-B drift acceleration by the motional electric field induced by contraction and merging of SMFRs (second term in the second square bracket) and, (6) parallel drift acceleration by $E_{REC\parallel}$ (the last term in second square bracket). Direct comparison of the terms in the first two lines of Eq. (6) with the corresponding terms in the third and fourth lines reveals that one can express the curvature drift acceleration term in terms of $\mathbf{V}_E \cdot \boldsymbol{\kappa}$ (advection of curved SMFR magnetic field at plasma drift velocity), and the grad-B drift acceleration term in terms of $(\mathbf{V}_E \cdot \nabla)B$ (advection of the perpendicular gradient in SMFR magnetic field strength at the plasma drift velocity). This version of the grad-B drift acceleration term can be combined with the betatron acceleration term into a Lagrangian betatron acceleration expression $M'dB/dt = M'(\partial B/\partial t + (\mathbf{V}_E \cdot \nabla)B)$ that tracks the time and spatial variations in the SFMR magnetic field strength B following the SMFR flow due to contraction or merging processes (first two terms in second square bracket, in line three of Eq. (6)) (e.g., Dahlin et al. (2016, 2017)). Comparison of the last terms in line two and line four indicates that approximate conservation of the magnetic moment M requires a small E_{\parallel} value. Furthermore, comparing the terms in the fourth line with those in the sixth line of Eq. (6) reveals that the Lagrangian betatron acceleration expression can be related to a combination of the $\mathbf{V}_E \cdot \boldsymbol{\kappa}$ and the $\nabla \cdot \mathbf{V}_E$ terms, assuming approximate magnetic moment conservation (i.e. a small E_{\parallel} -value). Thus, Lagrangian betatron acceleration is a competition between incompressible SMFR contraction or merging ($\mathbf{V}_E \cdot \boldsymbol{\kappa} > 0$) resulting in energy loss because $dB/dt < 0$ and compressible contraction or merging ($\nabla \cdot \mathbf{V}_E < 0$) resulting in energy gain because $dB/dt > 0$. Inspection of the middle term in the first square bracket and the corresponding middle terms in lines 3 and 5 of Eq. (6) reveals how the drift inertia term in line one was converted into a term modelling parallel guiding center motion acceleration by the parallel component of the non-inertial force associated with the acceleration of the plasma drift velocity $d\mathbf{V}_E/dt$.

Combining the first two terms of the fifth line and separately the last term in the fifth line with the first term in the sixth line of Eq. (6), results in the expression

$$\left\langle \frac{dK}{dt} \right\rangle_{\phi} \approx v\mu \left(q\mathbf{E}_{REC} - m\frac{d\mathbf{V}_E}{dt} \right) \cdot \mathbf{b} + mv^2 \frac{1}{2} (3\mu^2 - 1) (\mathbf{V}_E \cdot \boldsymbol{\kappa}) - mv^2 \frac{1}{2} (1 - \mu^2) (\nabla \cdot \mathbf{V}_E) \quad (7)$$

The combined term containing $\mathbf{V}_E \cdot \boldsymbol{\kappa}$ in Eq. (7) unifies curvature drift acceleration with Lagrangian betatron and parallel drift acceleration, but it seems that the last term associated with $\nabla \cdot \mathbf{V}_E$ combines Lagrangian betatron acceleration with parallel drift acceleration only without a contribution from curvature drift acceleration. The latter raises a question because this contradicts the standard Parker cosmic-ray transport equation in which the $\nabla \cdot \mathbf{V}_E$ -term has been shown to combine curvature drift acceleration with Lagrangian betatron and parallel drift acceleration (Kota 1977; Webb et al. 1981). By introducing the shear flow

tensor into the bottom line of equation Eq. (6) using the relationship

$$\mathbf{V}_E \cdot \boldsymbol{\kappa} = -\mathbf{b} \cdot (\mathbf{b} \cdot \nabla) \mathbf{V}_E = -\left[b_i b_j \sigma_{ij} + \frac{1}{3} (\nabla \cdot \mathbf{V}_E) \delta_{ij} \right] \quad (8)$$

where we relate the magnetic curvature advection term, $\mathbf{V}_E \cdot \boldsymbol{\kappa}$, to the parallel shear-flow term, $\mathbf{b} \cdot (\mathbf{b} \cdot \nabla) \mathbf{V}_E$, which in turn is expressed in terms of the shear-flow tensor σ_{ij}

$$\sigma_{ij} = \frac{1}{2} \left[\frac{\partial V_{Ei}}{\partial x_j} + \frac{\partial V_{Ej}}{\partial x_i} - \frac{2}{3} (\nabla \cdot \mathbf{V}_E) \delta_{ij} \right] \quad (9)$$

one finds that

$$\begin{aligned} \left\langle \frac{dK}{dt} \right\rangle_{\phi} &\approx v\mu \left(q\mathbf{E}_{REC} - m \frac{d\mathbf{V}_E}{dt} \right) \cdot \mathbf{b} - mv^2 (3\mu^2 - 1) \mathbf{b} \cdot (\mathbf{b} \cdot \nabla) \mathbf{V}_E \\ &\quad - \frac{1}{3} mv^2 (\nabla \cdot \mathbf{V}_E) + \frac{1}{3} mv^2 \frac{1}{2} (3\mu^2 - 1) (\nabla \cdot \mathbf{V}_E) \end{aligned} \quad (10)$$

In Eq. (10) the $\mathbf{b} \cdot (\mathbf{b} \cdot \nabla) \mathbf{V}_E$ -term can be viewed as a combination of curvature drift acceleration with Lagrangian betatron and parallel drift acceleration acting collectively as plasma drift parallel shear flow acceleration in SMFRs. The first $\nabla \cdot \mathbf{V}_E$ -term in Eq. (9) is exactly the $\nabla \cdot \mathbf{V}_E$ -term appearing in the standard Parker cosmic-ray transport equation that has been shown before to combine curvature drift acceleration with Lagrangian betatron and parallel drift acceleration. The last $\nabla \cdot \mathbf{V}_E$ -term in Eq. (10) depends on the factor $(3\mu^2 - 1)$ just like the $\mathbf{b} \cdot (\mathbf{b} \cdot \nabla) \mathbf{V}_E$ -term, providing evidence that it too unifies curvature drift acceleration with Lagrangian betatron and parallel drift acceleration. The difference between the two $\nabla \cdot \mathbf{V}_E$ -terms is that the first term accelerates the isotropic part of the distribution function while the second term affects the energy of particles belonging to the anisotropic part of the particle distribution as discussed above (for more details, see le Roux et al. (2018)).

3.1.2 The Connection Between Guiding Center Kinetic and Focused Transport Theory

By doing the substitution $\mathbf{V}_E = \mathbf{U}_{\perp}$ (which follows from specifying the macroscale electric field in contracting and merging SMFRs as the induced motional electric field $\mathbf{E} = -\mathbf{U} \times \mathbf{B}$ where \mathbf{U} is the plasma flow velocity in SMFRs) in Eq. (10), we get the expression

$$\begin{aligned} \left\langle \frac{dK}{dt} \right\rangle_{\phi} &= v\mu \left(q\mathbf{E} - m \frac{d\mathbf{U}_{\perp}}{dt} \right) \cdot \mathbf{b} - \frac{1}{2} (1 - \mu^2) (\nabla \cdot \mathbf{U}_{\perp}) \\ &\quad - \frac{1}{2} (3\mu^2 - 1) \mathbf{b} \cdot (\mathbf{b} \cdot \nabla) \mathbf{U}_{\perp} \end{aligned} \quad (11)$$

This expression reveals the close connection between standard guiding-center kinetic theory and focused transport kinetic theory that we use to model particle acceleration by dynamic small-scale flux ropes because, according to focused transport theory, the relative momentum rate of change is given by

$$\begin{aligned} \frac{1}{p} \left\langle \frac{dp}{dt} \right\rangle_{\phi} &= \mu \left(\frac{q\mathbf{E}}{p} - \frac{1}{v} \frac{d\mathbf{U}}{dt} \right) \cdot \mathbf{b} - \frac{1}{2} (1 - \mu^2) (\nabla \cdot \mathbf{U}) \\ &\quad - \frac{1}{2} (3\mu^2 - 1) \mathbf{b} \cdot (\mathbf{b} \cdot \nabla) \mathbf{U} \end{aligned} \quad (12)$$

The main difference is that guiding-center kinetic theory describes particle acceleration in terms of the non-uniform plasma drift velocity $\mathbf{V}_E = \mathbf{U}_\perp$, whereas focused transport theory does it in terms of the total non-uniform plasma flow velocity in SMFRs. Thus, from the perspective of focused transport theory, we have four SFMR acceleration mechanisms. From left to right in Eq. (12) they are acceleration by the parallel reconnection electric field force, the parallel non-inertial force due to the acceleration of the SMFR flow, compression of the SMFR flow, and parallel SMFR shear flow. These mechanisms form the basis of our focused and Parker transport theories for energetic particle acceleration by and propagation through a field of dynamic SMFRs.

3.2 Focused and Parker Transport Equations for Particle Acceleration by SMFRs

By applying standard perturbation analysis to the focused transport equation containing Eq. (12) we derived a modified focused transport equation that models how energetic particles respond in a statistical average sense on large spatial scales to both the non-uniform solar wind flow and interplanetary magnetic field, and to a collection of dynamic SMFRs advected with the solar wind flow (le Roux et al. 2015, 2018). The derivation was done assuming that SMFR dynamics occur mainly in a 2D plane perpendicular to the guide field (axial) component B_0 of the SMFR assuming a strong guide field (Birn et al. 1989; Dmitruk et al. 2004). The 2D plane contains the magnetic island (twist) component B_I of the SMFR and the SMFR flow U_I determining contraction or merging of the magnetic island. In the inner heliosphere, it appears that assuming a strong guide field so that $B_I/B_0 \ll 1$ is reasonable (Smith et al. 2006). For simplicity, no distinction is made in the derivation between the guide field and the background magnetic field. This approach has some support from observational evidence that the SMFR guide field is aligned with the solar wind spiral magnetic field (Zheng and Hu 2018). The modified focused transport equation is presented compactly as

$$\begin{aligned} \left(\frac{df}{dt} \right)_{sw} = & -\nabla \cdot \left[\left\langle \frac{d\mathbf{x}}{dt} \right\rangle^I (\varepsilon_I) f \right] - \frac{1}{p^2} \frac{\partial}{\partial p} \left[p^2 \left\langle \frac{dp}{dt} \right\rangle^I (\varepsilon_I) f \right] \\ & - \frac{\partial}{\partial \mu} \left[\left\langle \frac{d\mu}{dt} \right\rangle^I (\varepsilon_I) f \right] \\ & + \frac{\partial}{\partial \mu} \left[D_{\mu\mu}^I (\varepsilon_I) \frac{\partial f}{\partial \mu} + D_{\mu p}^I (\varepsilon_I) \frac{\partial f}{\partial p} \right] \\ & + \frac{1}{p^2} \frac{\partial}{\partial p} \left[p^2 \left(D_{p\mu}^I (\varepsilon_I) \frac{\partial f}{\partial \mu} + D_{pp}^I (\varepsilon_I) \frac{\partial f}{\partial p} \right) \right] \end{aligned} \quad (13)$$

where $f(x, p, \mu, t)$ is the energetic charged particle distribution. On the left-hand side of this equation, $(df/dt)_{sw}$ represents the standard focused transport equation for energetic particle transport in the non-uniform solar wind flow and interplanetary magnetic field (e.g., Isenberg (1997)). On the right-hand side, there are additional terms to model the interaction of energetic particles with dynamic SMFRs. In the top line $\langle dp/dt \rangle^I$ models the average energetic particle momentum rate of change in response to average SMFR quantities (the average SMFR compression, parallel shear flow, parallel reconnection electric field due to SMFR merging, and the parallel acceleration of the SMFR flow). In the absence of pitch-angle scattering, the acceleration is coherent but can become stochastic if particles undergo

significant pitch-angle scattering. In the bottom line, D_{pp}^I signifies the variance in the energetic particle rate of momentum change due statistical fluctuations in the SMFR quantities expressed in terms of the variance in the SMFR compression, parallel shear flow, parallel reconnection electric field, and the parallel acceleration of the SMFR flow (for more details, see le Roux et al. (2015, 2018)). Recently, a simplified telegrapher type Parker transport equation was derived from the modified focused transport equation by assuming that on large spatial scales the energetic particle distribution will inevitably become nearly isotropic due to significant levels of pitch-angle scattering (le Roux et al. 2019). This was accomplished by expanding the energetic particle distribution function $f(x, p, \mu, t)$ out to the second moment with respect to μ with aid of Legendre polynomials and deriving the zeroth, first and second moments of the modified focused transport equation (see also Zank et al. (2014), le Roux et al. (2015, 2018)). The first and second moment equations were simplified to enable a closed evolution equation for the isotropic part of the distribution function $f_0(x, p, t)$ in the form of a telegrapher type Parker transport equation. Discussion of the simplifications can be found in le Roux et al. (2019). The telegrapher type Parker transport equation we derived is given by

$$\begin{aligned}
 & \frac{3\kappa_{\parallel}^I}{v^2} \frac{\partial}{\partial t} \left[\frac{\partial f_0}{\partial t} + (\mathbf{U}^{coh} \cdot \nabla) f_0 - (\nabla \cdot \mathbf{U}^{coh}) \frac{p}{3} \frac{\partial f_0}{\partial p} \right. \\
 & \left. - \frac{1}{p^2} \frac{\partial}{\partial p} \left(p^2 D_{pp}^{Istoch} \frac{\partial f_0}{\partial p} \right) \right] \\
 & + \frac{\partial f_0}{\partial t} + \left[\mathbf{U}^{coh} - \frac{1}{3p^2} \frac{\partial}{\partial p} (p^3 (U_{EA}^{coh} - U^{Istoch}) \mathbf{b}) \right] \cdot \nabla f_0 \\
 & - [(\nabla \cdot \mathbf{U}^{coh}) + (\nabla \cdot (U_{EA}^{coh} + U^{Istoch}) \mathbf{b})] \frac{p}{3} \frac{\partial f_0}{\partial p} \\
 & = \nabla \cdot (\kappa_{\parallel}^I \mathbf{b} \mathbf{b} \cdot \nabla f_0) + \frac{1}{p^2} \frac{\partial}{\partial p} \left[p^2 (D_{pp}^{coh} + D_{pp}^{Istoch}) \frac{\partial f_0}{\partial p} \right] \\
 & + \frac{2}{3} p U_{EA}^{coh} (\mathbf{b} \cdot \nabla) \frac{\partial f_0}{\partial p}
 \end{aligned} \tag{14}$$

In Eq. (14) the superscript ‘coh’ refers to a combination of background solar wind and average SMFR quantities, whereas the superscript ‘Istoch’ indicates the variance of fluctuating SMFR quantities only. Accordingly, U^{coh} models the net advection effect on energetic particles stemming from the combination of the solar wind velocity with the mean plasma flow velocity in dynamic SMFRs, $U_{EA}^{coh} \mathbf{b}$ represents the net parallel advection effect on energetic particles from the average parallel component of the electric field and of the acceleration of the plasma flow in the background solar wind and in SMFRs, and $U^{Istoch} \mathbf{b}$ refers to the average, field-aligned advection effect produced by the variance of statistical fluctuations in SMFR fields. κ_{\parallel}^I denotes the parallel diffusion coefficient as a consequence of particle pitch-angle scattering by random magnetic mirroring forces in SMFRs (for more information, see le Roux et al. (2015, 2016, 2018)). Furthermore, there are two categories of second-order Fermi acceleration in Eq. (14). D_{pp}^{coh} models second-order Fermi acceleration when particles undergoing pitch-angle scattering on macro scales respond to the average parallel electric field and acceleration of the plasma flow, the parallel shear flow tensor, and the flow compression for both the background solar wind and SMFRs, whereas D_{pp}^{Istoch} describes second-order Fermi acceleration when particles experience the variance effects from fluctuations in the same SMFR quantities. The more familiar diffusive Parker trans-

port equation can be recovered by neglecting the additional transport terms in the top line of Eq. (14). Besides the well-known telegrapher term (first term in line one of Eq. (14) containing the second-order time derivative, there are also less familiar additional telegrapher terms involving second and third-order partial derivatives (rest of terms in line one and two of Eq. (14)). The telegrapher Parker transport equation addresses a deficiency in the diffusive Parker transport equation where some particles propagate to larger distances than physically possible by restoring causality. However, the causality in particle transport is only restored for leading edge particle pulses that are nearly isotropic, that is, for particles that experience significant pitch-angle scattering. This kind of telegrapher equation is less accurate when it comes to model unscattered particle escape from the acceleration site during early times, resulting in a cutoff in the particle distribution spatially that is too abrupt so that the maximum distance particles reach as a function of time is underestimated (e.g., Effenberger and Litvinenko (2014), Malkov and Sagdeev (2015)). Since we model energetic particle acceleration inside the SMFR acceleration region on macro scales, where particles are expected to be scattered by low-frequency wave turbulence and by fluctuating magnetic mirroring forces inside these structures to maintain near-isotropic distributions, the telegrapher Parker equation should be applicable.

3.3 Solutions of the Diffusive Parker Transport Equation for Acceleration by SMFRs

Various analytical steady-state solutions for spatial transport in planar geometry, but also some in spherical geometry, were found for simplified versions of the diffusive Parker transport equation, that is, Eq. (14) neglecting telegrapher terms in the top line (e.g., Zank et al. (2014, 2015a), le Roux et al. (2015, 2016), Zhao et al. (2018), le Roux et al. (2019)). The solutions either emphasized first-order Fermi due to the average SMFR compression and/or acceleration by the mean parallel reconnection electric field in the mixed-derivative transport term (see last term in Eq. (14)) generated during SMFR merging (Zank et al. 2014, 2015a; Zhao et al. 2018), or second-order Fermi acceleration involving the variance in the SMFR compression/parallel shear flow and/or 1st order Fermi acceleration (le Roux et al. 2015, 2016, 2019). Irrespective of whether first-order or second-order Fermi SMFR acceleration in the solutions was emphasized, two key predictions were made that was verified by spacecraft data analysis: (1) the accelerated particle flux form spatial peaks in the SMFR acceleration region so that the flux amplification factor downstream of the particle injection point increases with particle energy, and (2) the accelerated particle spectra evolve through the SMFR region by becoming harder downstream of the injection location (Zank et al. 2015a; le Roux et al. 2016; Zhao et al. 2018; Adhikari et al. 2019; le Roux et al. 2019; Khabarova et al. 2016). In the new work le Roux et al. (2019) present both time-dependent and steady-state analytical solutions of Eq. (14) in planar geometry in which all the basic SMFR acceleration mechanisms present in the underlying focused transport theory (see Eq. (12)) are unified. The solutions are based on solving a simplified version of the telegrapher Parker transport equation Eq. (14) in which the solar wind flow velocity is defined in the x-direction as $\mathbf{U}_0 = U_0 \mathbf{e}_x$ and the background magnetic field is specified in the x-z-plane according to the expression $\mathbf{B}_0 = B_0 (\cos(\psi) \mathbf{e}_x + \sin(\psi) \mathbf{e}_z)$ where ψ is the spiral magnetic field angle (the angle between \mathbf{B}_0 and \mathbf{U}_0). The transport equation is

$$\begin{aligned} \tau_{SC}^I \frac{\partial^2 f_0}{\partial t^2} + \frac{\partial f_0}{\partial t} + U_0^I \frac{\partial f_0}{\partial x} + \langle v_{COM}^I \rangle \frac{p}{3} \frac{\partial f_0}{\partial p} = \\ = \kappa_{xx}^I \frac{\partial^2 f_0}{\partial x^2} + \frac{1}{p^2} \frac{\partial}{\partial p} \left(p^2 D_{pp}^I \frac{\partial f_0}{\partial p} \right) + \frac{2}{3} U_E^I \frac{\partial}{\partial x} \left(p \frac{\partial f_0}{\partial p} \right) - \frac{f_0}{\tau_{esc}} + \end{aligned} \quad (15)$$

$$+ \frac{dN/dt}{4\pi p_0^2} \delta(x - x_0) \delta(p - p_0)$$

where in the first term, the telegrapher term, τ_{SC} , is the time scale for particle pitch-angle scattering by random magnetic mirroring forces in SMFRs. For simplicity, the other telegrapher terms in the top line of Eq. (14) were neglected. In the third term in Eq. (15), the advection term, the effective advection velocity in the x-direction $U_0^I = U_0 - U_E^I$, where U_0 is the background solar wind velocity, and $U_E^I = (3\kappa_{\parallel}^I/v) \langle v_{REC}^I \rangle \cos(\psi)$ is an advective velocity along the background magnetic field \mathbf{B}_0 projected in the x-direction using the factor $\cos(\psi)$. The U_E^I advection effect is associated with particle interaction with the mean parallel reconnection electric field in numerous merging SMFRs generating an average relative momentum rate of change $\langle v_{REC}^I \rangle$. The fourth term in Eq. (15) contains the mean SMFR compression rate $\langle v_{COM}^I \rangle$ to model first-order Fermi SMFR acceleration, while the first term on the right hand side of Eq. (15) includes the diffusion coefficient in the x-direction κ_{xx}^I , which is related to the parallel diffusion coefficient κ_{\parallel}^I according to the expression $\kappa_{xx}^I = \kappa_{\parallel}^I \cos^2(\psi)$. In the second term on the right of Eq. (15) we find the total momentum diffusion coefficient for second-order Fermi acceleration by SMFRs $D_{pp}^I = p^2 D_0^I = D_{pp}^{Icoh} + D_{pp}^{Istoch}$ where D_{pp}^{Icoh} refers to second-order Fermi acceleration when particles undergo pitch-angle scattering on macro scales in response to the average parallel electric field and acceleration of the plasma flow, the parallel shear flow tensor, and the flow compression in SMFRs, whereas D_{pp}^{Istoch} describes second-order Fermi acceleration when particles experience the variance effects from fluctuations in the same four SMFR quantities. This is followed by the third mixed derivative transport term which determines particle acceleration by the mean parallel reconnection electric field in numerous merging SMFRs. The second last term determines the rate of particle escape from the SMFR region which depends on the escape time scale τ_{esc} (see also, Zhao et al. (2018)) whereas the last term represents a particle source in which particles in a thin spherical momentum shell with radius p_0 are continuously injected at a rate dN/dt in the SMFR region at location $x = x_0$. As an example, we present the steady-state solution of Eq. (15) which is

$$f_0(x, p) = \frac{1}{2\pi} \left(\frac{dN/dt}{4\pi p_0^3} \right) \sqrt{\frac{1}{\bar{D}_0^I \kappa_0^I}} e^{\frac{1}{2} \frac{U_0^I + q U_E^I / 3}{\kappa_0^I} (x - x_0)} \left(\frac{p}{p_0} \right)^{-\frac{q}{2}} K_0(2\sqrt{\alpha\beta}) \quad (16)$$

where K_0 is the modified Bessel function of the first kind and

$$\begin{aligned} \bar{D}_0^I &= D_0^I \left[1 - \frac{1}{9} \frac{(U_E^I)^2}{\kappa_0^I D_0^I} \right] \\ q &= 3 \left[1 - \frac{1}{9} \frac{\langle v_{COM}^I \rangle - U_0^I U_E^I / \kappa_0^I}{D_0^I} \right] / \left[1 - \frac{1}{9} \frac{(U_E^I)^2}{\kappa_0^I D_0^I} \right] \\ \alpha &= \frac{1}{4\kappa_0^I} \left[(x - x_0)^2 + \frac{\kappa_0^I}{D_0^I} \left[\ln \left(\frac{p}{p_0} \right) - \frac{1}{3} \left(\frac{U_E^I}{\kappa_0^I} \right) (x - x_0) \right]^2 \right] \\ \beta &= \left(\frac{1}{2} \frac{U_0^I}{\kappa_0^I} \right)^2 \kappa_0^I + \left(\frac{q}{2} \right)^2 \bar{D}_0^I + \frac{1}{\tau_{esc}} \end{aligned} \quad (17)$$

The solution includes all four SMFR acceleration mechanisms listed in the underlying focused transport equation (see Eq. (12)) that appears in the Parker transport equation as first-

order Fermi acceleration, second-order Fermi acceleration, and acceleration by the mixed-derivative transport term. By taking limits of the solution, the basic characteristics of observations of energetic particle acceleration and transport through a dynamic SMFR region in the solar wind, namely, energetic particle distribution spatial peak formation and spectral hardening as discussed above. If $\ln^2(p/p_0) \gg (x - x_0)^2$ in the parameter α in $K_0(2\sqrt{\alpha\beta})$, one finds that

$$f_0(x, p) \propto e^{-\frac{U_0}{2\kappa_0^I}(x-x_0)} \left(\frac{p}{p_0}\right)^{-\frac{1}{2}\left[q+|q|\sqrt{1+(2/q)^2\tau_{D_0^I}\left[\frac{1}{\kappa_0^I}+1/\tau_{esc}\right]}\right]} \quad (18)$$

In the opposite limit $\ln^2(p/p_0) \ll (x - x_0)^2$

$$f_0(x, p) \propto e^{-\frac{1}{2}\left[\left|\frac{U_0}{\kappa_0^I}(x-x_0)\right|\sqrt{1+4\tau_{D_0^I}\left[\frac{(q/2)^2}{\tau_{D_0^I}}+1/\tau_{esc}\right]}-\frac{U_0}{\kappa_0^I}(x-x_0)\right]/\kappa_0^I} \left(\frac{p}{p_0}\right)^{-\frac{q}{2}} \quad (19)$$

where $\tau_{\kappa_0^I} = \kappa_0^I/U_0^2$ is the diffusion time scale and $\tau_{D_0^I} = 1/D_0^I$ is the time scale for second-order Fermi acceleration. In Eq. (18) and Eq. (19) we let $U_E^I = 0$, thus removing the effects of average parallel reconnection electric field in the mixed-derivative transport term and in spatial advection ($U_0^I = U_0$) in Eq. (15), but not in second-order Fermi acceleration. The mixed-derivative transport term was found to counteract spatial peak formation by forming a plateau in the accelerated particle distribution contrary to observations (Zank et al. 2014). Both solution limits Eq. (18) and Eq. (19) indicate that, because energetic particle diffusive transport occurs against the solar wind flow upstream of the particle injection point at $x = x_0$ ($x < x_0$), the particle distribution decays exponentially with increasing upstream distance from the injection point (thus no spatial peak in the particle distribution). Since diffusive transport unfolds in the direction of the solar wind flow downstream of the injection point ($x > x_0$) during acceleration, the particle distribution increases exponentially with increasing distance downstream when sufficiently close to the injection point because then limit Eq. (18) applies. However, sufficiently far downstream of the injection point, the particle distribution at lower energies decays first with increasing distance because then limit Eq. (19) is applicable. The decay at higher energies occurs progressively further downstream of the particle source when Eq. (19) becomes applicable at those distances. Thus, peaks form in the accelerated downstream distribution that shifts increasingly to larger distances downstream with increasing particle energy. Consider the accelerated particle spectra. Close to the injection point the particle spectra form power laws steeper than $f_0(p) \propto (p/p_0)^{-q/2}$ at most energies above the injection energy ($p > p_0$) because Eq. (18) is valid. With increasing distance from the injection point expression in Eq. (18) holds progressively at increasingly high particle energies only while at lower energies (Eq. (19)) applies where the spectrum approaches the harder power law $f_0(p) \propto (p/p_0)^{-q/2}$ for a growing energy interval. Thus, with increasing distance downstream of the injection point the accelerated particle spectrum becomes increasingly hard on average while assuming a more exponential character as it bends over more strongly at lower energies. Inspection of Eq. (18) also reveals that more efficient particle escape results in a steeper spectrum (Zhao et al. 2018) and a larger spatial diffusion coefficient produces a harder spectrum as particles sample more SMFRs in a given time interval.

3.3.1 Second Order Fermi SMFR Acceleration

Zhao et al. (2018) and Adhikari et al. (2019) had great success in reproducing the observed features of accelerated ions in SMFR regions at 1 AU and 5 AU in the equatorial plane

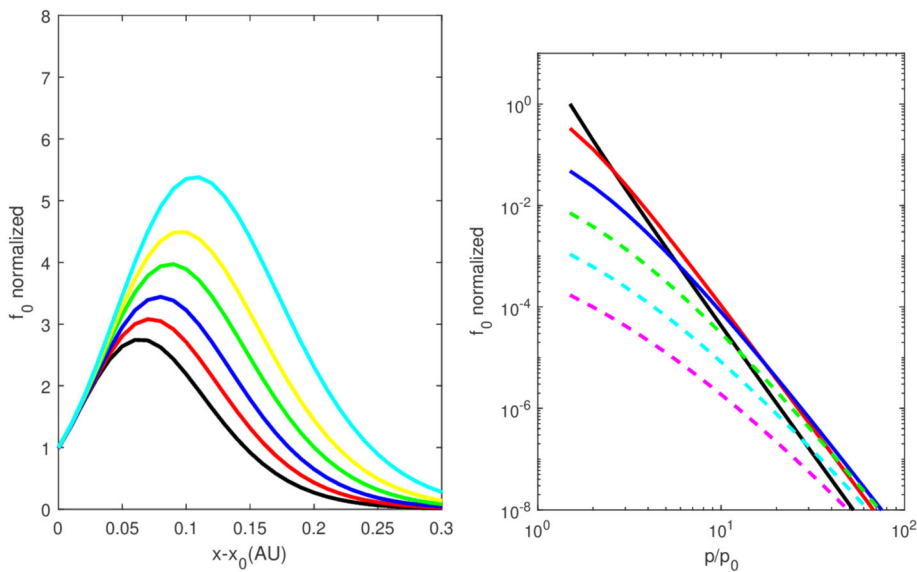


Fig. 7 The 1D steady-state analytical solution (Eq. (16)) for energetic proton 2nd order Fermi acceleration by SMFRs in a uniform SMFR region in the vicinity of 1 AU (reproduced from le Roux et al. (2019)). The solution combines second order Fermi acceleration due the variance in the SMFR compression rate and in the SMFR incompressible parallel shear flow. Left panel: The direction-averaged proton distribution function $f_0(x, p)$ as a function of distance in AU relative to the particle injection position x_0 ranging from $x - x_0 = 0 - 0.3$ AU in the downstream direction (in the direction of the solar wind flow) for the particle energies 144 keV (black), 256 keV (red), 0.44 MeV (blue), 0.81 MeV (green), 1.44 MeV (yellow), and 3.31 MeV (cyan). The energy intervals were chosen to fall inside the energy intervals in the observed energetic flux enhancements at 1 AU in Fig. 10 of Khabarova and Zank (2017). The different curves for $f_0(x)$ were normalized to a value of 1 at $x - x_0 = 0$ AU to reveal the amplification factor of f_0 from the particle injection location to the peak in $f_0(x)$ further downstream for each particle energy. Since the differential intensity as a function of kinetic energy T is $j_T(T) = p^2 f_0(p)$, the amplification factor for f_0 also serves as the amplification factor for j_T . Right panel: Normalized $f_0(x, p)$ as a function particle momentum p in the solar wind frame normalized to p_0 (the injection momentum). The spectra are displayed for the following values of $x - x_0$: 0 AU (solid black), 0.05 AU (solid red), 0.1 AU (solid blue), 0.15 AU (dashed green), 0.2 AU (dashed cyan), and 0.25 AU (dashed magenta). The curves were multiplied with the same factor so that the black curve has a value of one at the minimum momentum $p/p_0 = 1.5$. At $p/p_0 = 1$ the proton kinetic energy $T \approx 1$ keV while at the maximum momentum $p/p_0 = 100$, $T \approx 10$ MeV

using an analytical steady-state solution of their Parker transport equation in which 1st order Fermi SMFR compression acceleration appears to be the dominant acceleration mechanism, but without considering second-order Fermi SMFR acceleration or connecting the acceleration and transport time scales to SMFR properties. In Fig. 7 we illustrate steady-state solution (Eq. (16)) in the limit where second-order Fermi SMFR acceleration due to the variance in the SMFR compression and parallel shear flow is the dominant acceleration mechanism. The left panel in Fig. 7 shows the spatial variation in the accelerated proton distribution function amplification factor for different particle energies downstream of the injection point at $x - x_0 > 0$ by choosing an amplification factor of one for all energies at the injection location. The theoretical maximum amplification factor varies between $\sim 2.8 - 5.4$ for proton energies in the range $0.144 - 3.31$ MeV, thus increasing with energy. Figure 10 of Khabarova and Zank (2017), based on a superposed epoch analysis of energetic ion flux enhancements in the vicinity of 126 thin primary reconnecting current sheet events at 1 AU,

suggests that the average intensity maximum amplification factor of energetic ion flux varies between $\sim 4.5 - 7.5$ in the energy range $0.112 - 4.75$ MeV (LEMS30 detector of EPAM instrument on the ACE spacecraft), and between $\sim 3.5 - 5.5$ in the energy range $0.066 - 4.75$ MeV (LEMS120 detector of EPAM) with the largest amplification factor occurring at the highest energies. The latter range of maximum amplification factors agrees best with the analytical results. The analytical solution also predicts a systematic shift in the position of the maximum amplification factor. It varies from $\sim 0.05 - 0.1$ AU from low to high particle energies downstream of the injection point that does not appear to be present in the observations averaged over many events in Fig. 10 of Khabarova and Zank (2017). Although such a shift does not appear to be present in Fig. 10 of Khabarova and Zank (2017), it is present in energetic ion observations of SMFR acceleration behind an interplanetary shock from the Ulysses spacecraft at ~ 5 AU reported by Zhao et al. (2018), and in anomalous cosmic ray observations from the Voyager 2 spacecraft behind the solar wind termination shock (Zank et al. 2015a).

In Fig. 7, right panel, we present the corresponding accelerated energetic proton spectra from our analytical solution for second-order Fermi acceleration at the particle injection point (solid black curve), and at increasing distances further downstream of the injection location: 0.05 AU (solid red curve), 0.1 AU (solid blue curve), 0.15 AU (dashed green curve), 0.2 AU (dashed cyan curve), and 0.25 AU (dashed magenta curve). The spectra are normalized so that the distribution function at the injection point has a value of one at the lowest momentum shown which is $p/p_0 = 1.5$, where p_0 is the injection momentum specified to be at a suprathermal proton kinetic energy of $T \approx 1$ keV. At the particle injection location the accelerated spectrum is close to a power law, being slightly softer than $f_0(p) \propto p^{-5}$ (in terms of differential intensity it is somewhat harder than $j_T(T) \propto T^{-1.5}$) except at the lowest momenta where the spectrum steepens somewhat. Inspection of the spectral evolution with increasing distance downstream of the injection point reveals that the spectra become progressively harder and more exponential so that spectra at low energies are considerably harder compared to high energies. If one would fit a power law to the exponential spectrum at 0.2 AU downstream of the injection location (dashed cyan curve), the spectrum would be approximately a $f_0(p) \propto p^{-4}$ ($j_T(T) \propto T^{-1}$) above ~ 100 keV ($p/p_0 > 10$). This basic trend of spectral hardening and increasing exponential nature of accelerated proton spectra produced by SMFRs with increasing distance inside the SMFR region is consistent with SMFR acceleration events at 1 AU reported by Adhikari et al. (2019). The variation in the power-law index through the SMFR region from ~ -1.5 to ~ -1 for particle energies ~ 100 keV $< T < 1$ MeV in the second event discussed by Adhikari et al. (2019) is close to the result reported here. A similar hardening trend in the energetic particle spectra through an SMFR at ~ 5 AU was detected in Ulysses data as reported by Zhao et al. (2018).

We conclude that one can potentially reproduce the observed flux amplification of energetic ions as a function of particle energy and the evolution of the accelerated spectra through SMFR regions at 1 AU by focusing solely on second-order Fermi SMFR acceleration of energetic ions in response to statistical fluctuations (variance) in the compression and the parallel shear flow in SMFRs, and we found that this can be accomplished with reasonable SMFR parameters (for more detail, see le Roux et al. (2019)). Based on the SMFR parameters that we used we found that stochastic acceleration by the variance in the parallel reconnection electric field is the dominant second-order Fermi acceleration mechanism. Unfortunately, we were unable to model particle acceleration for this mechanism using the solution of Eq. (16) because this analytical solution only holds for $D_0^I = D_{pp}^I/p^2$ being a constant while for this mechanism D_0^I depends on particle speed. Second-order Fermi acceleration involving the variance in the SMFR parallel shear flow was the second most efficient,

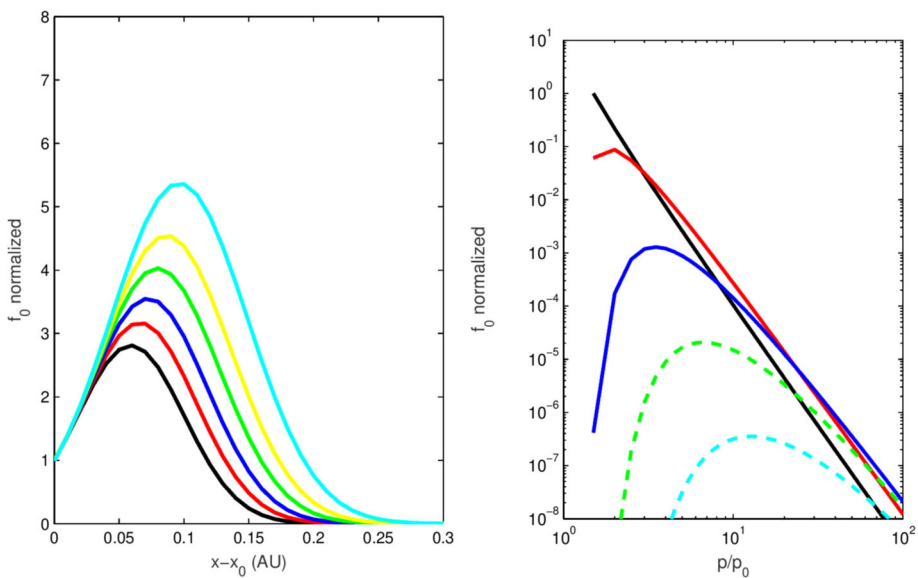


Fig. 8 The 1D steady-state solution for energetic proton first order Fermi acceleration or mean SMFR compression acceleration in a uniform SMFR region in the vicinity of 1 AU (Eq. (16)) (reproduced from le Roux et al. (2019)). Left panel: The same format as Fig. 7, left panel. Right panel: Same format as Fig. 7, right panel

while second-order Fermi acceleration due to the variance in SMFR compression was the least efficient. However, due to our limited knowledge of the SMFR parameters that enter into the acceleration expressions, and because of limitations of the analytical solutions, it is difficult to draw definitive conclusions about the ranking of the different second-order Fermi acceleration mechanisms associated with the variance in SMFR fields. Further progress requires intensifying data analysis of SMFR acceleration events, while at the same time increasing the sophistication of the solutions.

3.3.2 First Order SMFR Fermi Acceleration

Consider Fig. 8 where we show an analytical solution of Eq. (16) in the limit where first-order Fermi acceleration of energetic ions in response to the mean compression rate of SMFRs in an SMFR region at 1 AU is the dominant acceleration mechanism. Inspection of the results in the left panel for the spatial variation in the amplification factor in the accelerated particle distribution downstream of the particle injection point shows that they are remarkably similar to the results in Fig. 7 for second-order Fermi acceleration. In other words, with both first and second-order second Fermi SMFR acceleration the observed enhanced energetic ion flux in SMFR regions at 1 AU in Fig. 10 of Khabarova and Zank (2017) were reproduced reasonably well. The SMFR parameters specified in the first-order Fermi solution closely follow those used in the second-order Fermi solution, except for the characteristic cross-section of SMFRs that was reduced by a factor of four. However, the reduced value falls within the range of possibility given the little that we know of the statistics of SMFR parameters in SMFR acceleration regions in the solar wind, thus accentuating the need for more detailed analysis of SMFR properties in SMFR acceleration regions. As can be seen in Fig. 8, right panel, similar to the results for second-order Fermi acceleration, the modelled

accelerated spectra for first-order Fermi acceleration are power laws at the particle injection point, exhibiting the same rollover trend qualitatively at lower particle energies downstream of the injection point (see also Zhao et al. (2018), Adhikari et al. (2019)). Quantitatively, however, the spectral rollover trend at lower particle energies and overall increasing spectral hardening downstream of the injection location is notably stronger in the case of first-order Fermi acceleration due to the cutoff in the downstream spectrum at the injection momentum. This illuminates a key difference between the first Fermi acceleration solution, where all the particles that arrive downstream of the injection point have been accelerated systematically to momenta larger than the injection momentum to form the low-energy cutoff at the injection momentum, and the second-order Fermi solution where particles arriving downstream experienced stochastic acceleration which lowers the probability for a low-energy cutoff at the injection momentum. This predicted difference in the spectral evolution for the two acceleration mechanisms downstream of the injection point might potentially help identify the dominant operating SMFR acceleration mechanism in observations. Based on the evolution of the spectral power-law index through the SMFR region in SMFR acceleration event two of Adhikari et al. (2019), the event with spectral power-law indices closest to our results, the less strong spectral hardening in the second-order Fermi acceleration case is closer to the observed hardening trend. More SMFR acceleration events need to be studied before conclusions can be drawn with confidence. The success of our SMFR acceleration results for both first-order Fermi acceleration (see also Zhao et al. (2018), Adhikari et al. (2019)) and second-order Fermi acceleration is partially due to the term for particle escape from the SMFR region which ensured steepened accelerated particle spectra with more realistic slopes. The particle escape term reflects the need for more sophisticated solutions that specify finite boundaries for the SMFR acceleration region and allow for multi-dimensional transport. It must be pointed out that the need for steeper accelerated spectra in the solution can partly be the result of modelling particle acceleration in the test particle limit. The considerable pressure in the accelerated test particle spectra indicates that the energy exchange between the particles and SMFRs should be modelled self-consistently, thus contributing also to steeper accelerated particle spectra (le Roux et al. 2016, 2018).

4 Numerical Modeling of Magnetic Reconnection, Formation of Coherent Structures, Their Dynamics and Corresponding Properties of Turbulence

Magnetic reconnection is a fundamental process that occurs ubiquitously in both space and laboratory plasmas. This process consists of an intense magnetic energy release that heats and accelerates particles (Drake et al. 2006a; Hesse et al. 2016). One way in which reconnection may be triggered is via the tearing instability of thin current sheets. In a recent work (Pucci et al. 2018b), it has been discussed the critical aspect ratios for the fastest tearing mode growth times, required to reach values comparable to ideal time-scales for current sheet equilibria that are different from the Harris current sheet.

It is now widely accepted that magnetic reconnection takes place in turbulent environments, where an energy cascade, from large to smaller spatial scales, is present (Matthaeus et al. 2015; Bruno and Carbone 2016). The interplay of magnetic reconnection and plasma turbulence is hence decisive for assessing the role of this process in natural systems and can include the effects of turbulence on magnetic reconnection and, vice-versa, the influence of reconnection on turbulence (Matthaeus and Velli 2011; Karimabadi et al. 2013). For example, it has been observed that turbulence can increase the reconnection rate

(Matthaeus and Lamkin 1986; Smith et al. 2004; Lapenta 2008; Loureiro et al. 2009; Lazarrian and Vishniac 1999; Kowal et al. 2011, 2012; Lazarrian et al. 2015). Analogously, plasma jets generated by reconnection can also supply energy for sustaining the turbulent cascade (Lapenta 2008; Pucci et al. 2017a, 2018a; Cerri et al. 2017). All the above, recent studies suggest that the intense current sheets naturally produced by turbulence, and that represent the boundaries of magnetic islands, might be the preferred sites of magnetic reconnection. For this reason, reconnection is a crucial ingredient of turbulence itself (Matthaeus and Lamkin 1986; Servidio et al. 2010). These small-scale coherent structures are also thought to be the sites of inhomogeneous dissipation, where kinetic effects and plasma heating are concentrated (Servidio et al. 2011a, 2012, 2015; Osman et al. 2011, 2012b; Greco et al. 2012; Wu et al. 2013; Wan et al. 2015), together with local accelerations of energetic particles (Comisso and Sironi 2018, 2019; Pecora et al. 2018).

Due to the strong nonlinearity of complex, multi-scale plasmas, the adoption of high-resolution numerical simulations is mandatory. Therefore, for practical reasons, considerable progress in the area of reconnection and turbulence has been made in the context of reduced dimensionality models that have an ignorable coordinate, or a weak dependency along the magnetic field as in the case of Reduced MHD (Rappazzo et al. 2017) (see Oughton et al. (2017) for a recent review). Much of the progress in 3D turbulent reconnection has been either experimental (Brown et al. 2006) or in a 3D numerical setup that is in effect nearly-2D (Kowal et al. 2009; Daughton et al. 2011). It is obvious that the full 3D case is substantially more complex and much less understood, both theoretically (Schindler et al. 1988; Priest and Pontin 2009) and from the point of view of simulations (Dmitruk and Matthaeus 2006; Borgogno et al. 2005; Lapenta et al. 2015, 2016).

Weakly 3D cases, often studied in Reduced MHD, have interesting properties (Oughton et al. 2017). For weakly 3D setups, it has been confirmed that some 2D-like effects persist (Rappazzo et al. 2007; Daughton et al. 2011). There are however some fundamentally 3D effects that occur even in Reduced MHD. An example is in the study of the geometry of current sheets and the trajectories of field lines that pass through them (Zhdankin et al. 2013; Wan et al. 2014; Rappazzo et al. 2017). In 2D rectilinear geometry the presence of a current sheet in one plane guarantees that a similar current sheet will be present at all other planes at different distances along the ignorable coordinate. Furthermore the central field line, the X-line, pass through each of these identical current sheet. This is in essence a trivial restatement of two-dimensionality. However in the weakly 3D Reduced MHD case (Wan et al. 2014) the behavior of field lines passing through current sheets do not have this property. Instead, a field line passing through an X-point central to a current sheet on one plane, will likely depart nearby current sheets on nearby planes. Consequently X-points are usually found at varying distances relative to what had been their coincident current sheet. But of course reconnection in MHD only occurs when the X-point is co-located with a strong current, so this meandering has a leading order effect on where reconnection occurs and how strong it will be (Wan et al. 2014). This inherently 3D effect is further complicated by the fact that current sheets in reduced MHD have a finite extent along the guide field (Zhdankin et al. 2013). Further study also showed (Rappazzo et al. 2017) that reduced MHD current sheets tend to wander in the transverse directions *diffusively*, while field lines also wander randomly, but somewhat independently of the current sheets. This is clearly a much more complex scenario than the 2D case, even though Reduced MHD is only weakly 3D. This complexity will however have potentially major impact on physical phenomena such as nanoflares (Rappazzo et al. 2007; Gomez et al. 2000).

In general, it is well established that turbulence plays an essential role in accelerating the reconnection process both in 2D (Matthaeus and Lamkin 1986) and in 3D

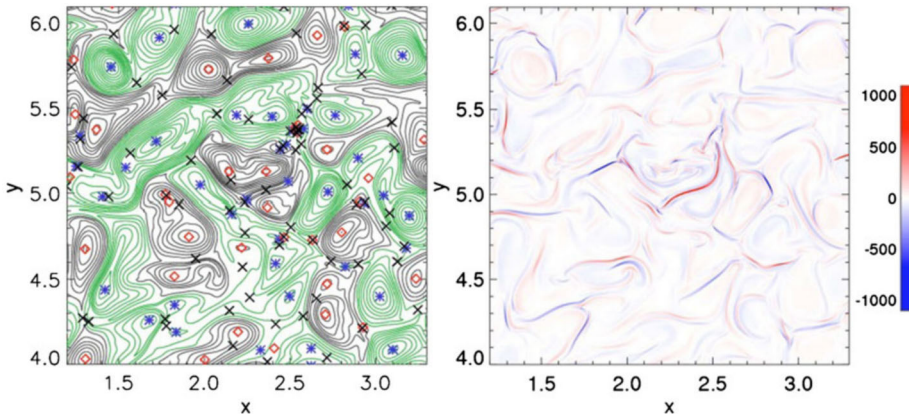


Fig. 9 2D MHD simulation result, showing the concurrency of current sheets and magnetic reconnection sites. Left: Contour plot of the magnetic potential a with the position of all the critical points: O-points (blue stars for the maxima and red open diamonds for the minima) and X-points (black), from a small section of a high-resolution 2D MHD simulation. Right: Shaded contour plot of the current density j in the same region. In between magnetic islands, intense current density peaks are present. Several reconnection sites are observed associated with current sheets (reproduced from Servidio et al. (2010))

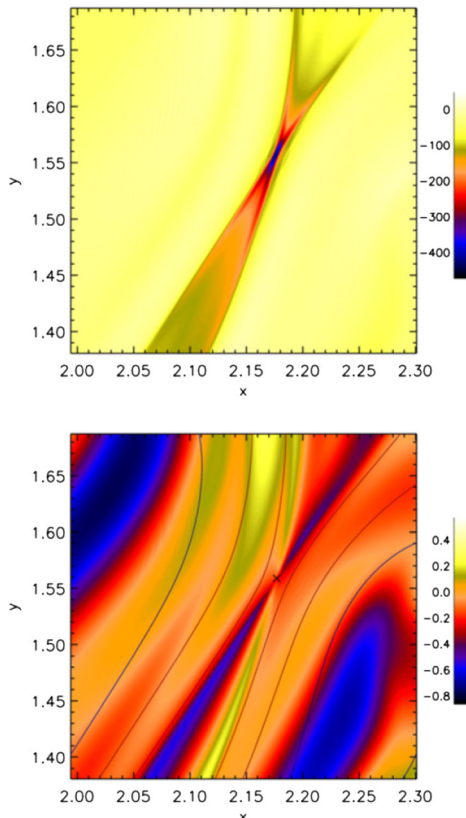
(Lazarian and Vishniac 1999). While the physics of reconnection revealed in the 2D can be applied in some circumstances to 3D, it is likely also that there are essential physical effects that occur in reconnection only in a strongly 3D systems, not the least of which is the very nature of reconnection itself in a full 3D representations (see, e.g., Priest and Pontin (2009)). These challenging problems have not been included in any complete way in the present review, where we concentrated, instead, on the progress in understanding reconnection in a turbulent environment which is very well magnetized and anisotropic.

First numerical attempts to model magnetic reconnection were based on an MHD approach, where the plasma is treated as a collisional magneto-fluid. Turbulence tends to dynamically generate relaxed regions –where non-linearities are depleted– separated by sheets of strong gradients (i.e. current) (Matthaeus et al. 2015), where magnetic reconnection can occur (Matthaeus and Montgomery 1980; Carbone and Veltri 1990; Retinò et al. 2007; Servidio et al. 2009, 2010, 2011b; Rappazzo et al. 2010). Figure 9 shows the in-plane magnetic field lines with X-points and O-points identified (left), and the associated current sheets (right), for a 2D magnetohydrodynamics (MHD) simulation (Servidio et al. 2010). A sea of interacting magnetic island, with boundaries characterized by intense current sheets, is found. Current sheets are often co-located with reconnection sites.

The *in-situ* observations conducted with the Cluster mission have revealed that physical ingredients beyond the pure MHD description –namely the Hall and the kinetic terms– can have a significant role in characterizing the magnetic reconnection process (Øieroset et al. 2001; Vaivads et al. 2004; Retinò et al. 2007; Sundkvist et al. 2007). Indeed, their effects become important when characteristic dynamical scales are comparable with the ion skin depth $d_i = c/\omega_{pi}$ (ω_{pi} being the ion plasma frequency). This motivated huge numerical efforts to include these ingredients and a variety of numerical simulations, ranging from Hall-MHD to Vlasov-Maxwell, have been performed.

The Hall term, which brings the dynamics of whistler waves and dispersive effects into the system, increases the reconnection rate (Ma and Bhattacharjee 2001; Birn et al. 2001; Smith et al. 2004; Lu et al. 2010; Papini et al. 2019), while the distribution of reconnec-

Fig. 10 2D Hall-MHD simulation result, indicating the typical quadrupolar structure of the reconnection site due to the Hall term. Top: Contour plot of the out-of-plane component of the current j_z in a sub-region of the simulation box. The bifurcation of the sheet and the typical structure of a reconnection region are clearly visible. Bottom: A contour plot of the out-of-plane component of the magnetic field b_z , in the same sub-region. The magnetic flux α is also represented as a line contour. A quadrupole in the magnetic field can be identified, revealing the presence of Hall activity (reproduced from Donato et al. (2012))



tion rates become broader than the MHD case (Donato et al. 2012). At variance with the pure MHD case, the magnetic energy is more frequently released through explosive, catastrophic events, that lead to fast magnetic reconnection onset (Cassak et al. 2005, 2007). The topology of the current sheets also changes and a quadrupolar structure of the out-of-plane magnetic field is observed (Fig. 10), as expected from theory (Sonnerup 1979).

Several efforts have been performed to understand at which extent MHD and Hall-MHD models, based on a collisional closure, properly describe turbulence in almost collisionless systems where the collisional closure may not be valid (e.g., Pezzi et al. (2017b), Perrone et al. (2018), González et al. (2019), Papini et al. (2019)). In general, Hall MHD simulations retain turbulence properties (spectral features, intermittency, reconnection...) up to the sub-proton range of wavenumbers. However, together with the presence of the Hall physics, genuinely kinetic effects are also significant at scales $l \sim d_i$ (Valentini et al. 2008, 2011a,b; Howes et al. 2008b; Parashar et al. 2009, 2018; Schekochihin et al. 2009; TenBarge et al. 2013; TenBarge and Howes 2013; Matteini et al. 2013; Franci et al. 2015, 2018, 2020; Vásconez et al. 2015; Valentini et al. 2016; Parashar and Matthaeus 2016; Pucci et al. 2016; Cerri et al. 2017; Cerri and Califano 2017; Pezzi et al. 2017a,b,c; Grošelj et al. 2017; Hellinger et al. 2019; Califano et al. 2020). Indeed, since magnetic reconnection onsets in a weakly-collisional plasma, the plasma is free to explore the full phase-space and can exhibit non-equilibrium features, such as temperature anisotropy, rings, beams of accelerated particles along or across the local magnetic field (Osman et al. 2011, 2012b; Servidio et al. 2015). Both hybrid, where electrons are assumed to be fluid while protons are kinetic, and

fully-kinetic models have been employed to gain insights on the magnetic reconnection onset at kinetic scales (Birn et al. 2001; Mangeney et al. 2002; Zeiler et al. 2002; Pritchett 2008; Scudder and Daughton 2008; Lu et al. 2010; Zenitani et al. 2011; Greco et al. 2012; Aunai et al. 2013; Wu et al. 2013; Karimabadi et al. 2013; Leonardis et al. 2013; Valentini et al. 2014; Wan et al. 2015; Lapenta et al. 2015, 2016, 2020; Shay et al. 2018). Kinetic simulations are usually employed within two different numerical approaches: Particle-In-Cell (PIC) and Eulerian Vlasov codes. Since the computational cost of PIC algorithms is in general smaller with respect to low-noise Eulerian codes, PIC codes are able to capture the full plasma dynamics (including electron scales, although with unrealistic electron to ion mass ratio). However, at variance with noise-free Eulerian algorithms, PIC codes are affected by statistical noise and may fail in providing a clean description of small-scale fluctuations and particle distribution functions in phase space. Very recently, first Eulerian fully-kinetic codes have been implemented to describe plasma dynamics at electron scales without noise (Schmitz and Grauer 2006; Umeda et al. 2009, 2010; Tronci and Camporeale 2015; Delzanno 2015; Umeda and Wada 2016, 2017; Ghizzo et al. 2017; Juno et al. 2018; Roytershteyn et al. 2019; Skoutnev et al. 2019; Pezzi et al. 2019a).

The introduction of the kinetic physics leads to several novelties regarding magnetic reconnection (Burch et al. 2016b; Torbert et al. 2018; Shuster et al. 2019; Chen et al. 2019c; Jiang et al. 2019). In the diffusion region, collisionless and collisional plasma processes affect the change of magnetic field topology. Within a general fluid framework, non-ideal mechanisms are modelled through a resistive term, which can take into account both electron-ion collisions as well as the presence of an anomalous resistivity produced by wave-particle interactions and/or turbulence. Owing to poor collisionality, non-ideal effects are induced by collisionless processes, such as electron pressure tensor gradients and electron inertia effects. It is thus decisive to describe the system through kinetic model to evaluate the role of these terms in shaping magnetic reconnection.

Within the hybrid framework, it has been reported that kinetic effects are concentrated close to intense current sheets (Valentini et al. 2007, 2014, 2016, 2017; Servidio et al. 2012, 2015; Greco et al. 2012). The role of alpha particles in characterizing kinetic scales turbulence has been analyzed in the detail showing that both protons and alpha particles are not in thermal equilibrium and manifest a preferentially perpendicular heating (Gary et al. 2003; Hellinger et al. 2005; Ofman and Viñas 2007; Ofman et al. 2011; Perrone et al. 2011, 2013, 2014a,b; Maneva et al. 2013, 2014, 2015; Maneva and Poedts 2018; Valentini et al. 2016). Figure 11 displays four indicators of non-Maxwellian features in the proton distribution function in the proximity of a current sheet, identified through the Partial Variance of Increments (PVI) method (Greco et al. 2009). Recently a similar proxy of non-Maxwellianities based on the entropy density has been adopted by Liang et al. (2019, 2020), Pezzi et al. (2020). The ϵ parameter (panel (a)), which locally quantifies deviations of the proton VDF with respect to the associated Maxwellian distribution clearly shows a broad region of significant non-Maxwellianity surrounding the X-point. Out-of-equilibrium features emerge as temperature anisotropy (b) as well as higher VDF moments such as heat fluxes (c) and kurtosis (d). Note also that the heat flux is peaked in the exhaust region, this resembling the presence of outflows.

As suggested above, velocity-space is complexly structured in view of wave-particle interactions and turbulent cascade. Recently the Hermite decomposition of the proton distribution function has been adopted to highlight this complexity (Grad 1949; Tatsuno et al. 2009; Pezzi et al. 2016a; Schekochihin et al. 2016; Servidio et al. 2017). Indeed, the distribution function is decomposed in velocity-space by adopting a 3D Hermite transform,

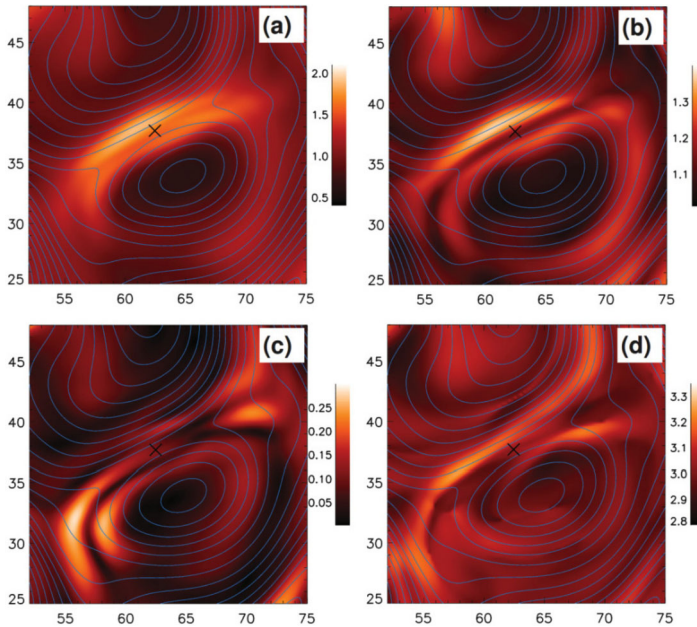


Fig. 11 Hybrid Eulerian Vlasov simulation results, indicating the concentration of kinetic effects close to current sheets. Contour plots of several indicators of non-Maxwellian features in the proton velocity distribution function, in the vicinity of an intense current sheet, identified through the PVI method (black cross in all panels): (a) ϵ parameter, that evaluates the local deviation of the distribution function from the associated Maxwellian (in per cent); (b) Proton temperature anisotropy $T_{\perp}/T_{||}$, being the parallel direction evaluated with respect to the local magnetic field; (c) heat flux, evaluated as the third-order moment of the proton distribution function; and (d) kurtosis (fourth-order moment) of the proton distribution function. (reproduced from Greco et al. (2012))

whose one-dimensional basis is:

$$\psi_m(v) = \frac{H_m\left(\frac{v-u}{v_{th}}\right)}{\sqrt{2^m m! \sqrt{\pi} v_{th}}} e^{-\frac{(v-u)^2}{2v_{th}^2}}, \quad (20)$$

where u and v_{th} are now the local proton bulk and thermal speed, respectively, and $m \geq 0$ is an integer (we simplified the notation suppressing the spatial dependence). The above projection quantifies high-order corrections to the particle velocity DF. A highly distorted DF produces plasma enstrophy (Knorr 1977), defined as

$$\Omega(\mathbf{x}, t) \equiv \int_{-\infty}^{\infty} \delta f^2(\mathbf{x}, \mathbf{v}, t) d^3 v = \sum_{\mathbf{m} > 0} [f_{\mathbf{m}}(\mathbf{x}, t)]^2, \quad (21)$$

where δf indicates the difference from the ambient Maxwellian and $f_{\mathbf{m}} \equiv f_{\mathbf{m}}(m_x, m_y, m_z)$ is the Hermite coefficient, from which the enstrophy spectrum $P(\mathbf{m}) = \langle f_{\mathbf{m}}(\mathbf{x}, t)^2 \rangle$ is defined. From this last quantity, reduced spectra (e.g. along perpendicular and/or parallel direction, as well as omnidirectional) can be evaluated. By taking advantage of highly accurate measurements from the Magnetospheric MultiScale mission (MMS), an enstrophy velocity-space cascade, revealed by evaluating the Hermite spectrum of the ion distribution function, has

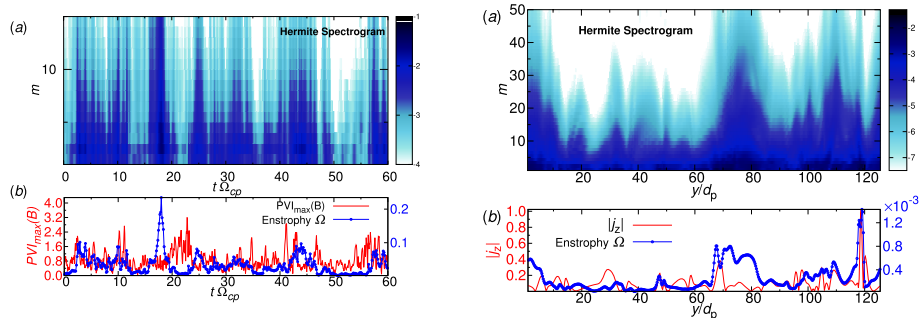


Fig. 12 Magnetospheric Multi-Scale (MMS) in-situ observations (left columns) and Eulerian Hybrid Vlasov-Maxwell simulation (right columns) results, showing that the Hermite velocity-space cascade is intermittent and it is more developed close to intense current sheets. Left: Hermite spectrogram (top) and profile of the maximum PVI index for the magnetic field (i.e. magnetic field gradient, current density) bottom) as a function of time, from the MMS observations. Right: Hermite spectrogram (top) and profile of the current density j_z , together with the plasma enstrophy Ω (bottom), as a function of the spatial position in an one dimensional cut of the simulation (adapted from Pezzi et al. (2018)). The Hermite spectrogram displays the evolution of the Hermite spectrum as a function of time and/or space

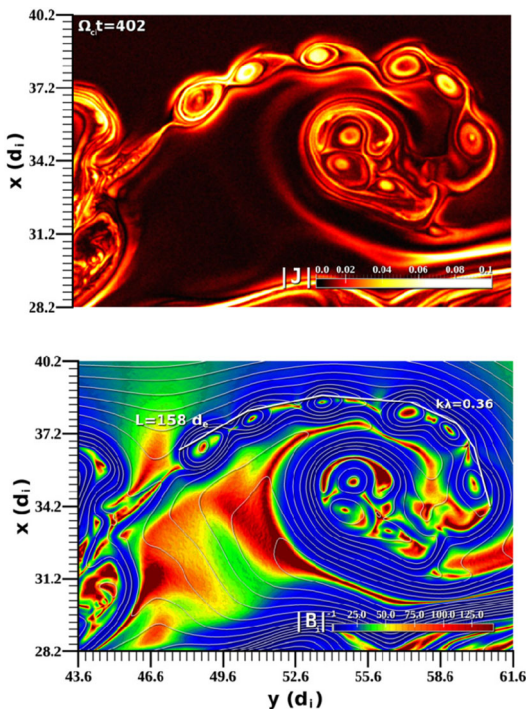
been observed in the Earth's magnetosheath (Servidio et al. 2017) and also in hybrid Vlasov-Maxwell simulations (Pezzi et al. 2018; Cerri et al. 2018). A Kolmogorov-like phenomenology has been also proposed to interpret the observed slopes of the Hermite spectrum. Here we want to further stress that the presence of this phase-space cascade is spatially intermittent and it is more developed close to current sheets (Fig. 12). This indicates that magnetic reconnection triggers non-thermal features in the distribution of particles, as also pointed out from *in-situ* observations and PIC simulations (Drake et al. 2006b, 2014; Shay et al. 2007, 2014, 2016; Hesse et al. 1999, 2017; Pritchett 2013, 2016; Lapenta et al. 2017).

Thanks to the unprecedented-resolution observations MMS (Burch et al. 2016a; Fuselier et al. 2016; Torbert et al. 2016, 2018), electron scale reconnection has become finally accessible and have shown a complex picture where a nested set of diffusion regions, whose size range from ion to electron scales (Hesse et al. 2016). Fully-kinetic models need to be adopted to characterize the process at such small scales. Figure 13 show the occurrence of several secondary islands, which are unstable for tearing instability. The size of these reconnection sites is comparable with electron scales.

At small scales, the dissipation of turbulent energy is thought to occur. Although it is well accepted that turbulence efficiently transfers energy from large to smaller scales (Verma et al. 1995; Vasquez et al. 2007; Sorriso-Valvo et al. 2007; Marino et al. 2008; Hadid et al. 2018; Andrés et al. 2019), it is not clear which physical mechanisms –among a variety of proposed ones– are controlling the dissipation process (Vaivads et al. 2016; Matthaeus et al. 2020). Actually, several different definitions of the *word* dissipation have been recently proposed. One approach analyzes the dissipation associated with a peculiar phenomenon, either a kind of fluctuations (e.g. KAW and whistler) (Chandran et al. 2010; Salem et al. 2012; Gary et al. 2016; Vech et al. 2017; Sorriso-Valvo et al. 2018, 2019) or magnetic reconnection (Drake et al. 2010; Servidio et al. 2011a; Osman et al. 2011, 2012a,b; Wu et al. 2013; Shay et al. 2018).

Within the reconnection community, there has been a particular emphasis on examining the electromagnetic work on particles, i.e. $j \cdot E$ (j the electric current density, E the electric field) as a dissipation proxy (Sundkvist et al. 2007; Zenitani et al. 2011; Wan et al. 2015). This has been instrumental in identifying a large number of active reconnection sites

Fig. 13 2D fully-kinetic PIC simulation results ($m_i/m_e = 100$), showing the generation of secondary tearing islands at electron scales in a small sub-portion of the simulation box. Top: Contour plot of J showing the formation of chains of tearing islands. Bottom: Contour plot of the in-plane magnetic field B , highlighting the fact that tearing modes are formed in regions where the in-plane magnetic field is weak. Contours of vector potential a are also displayed. (reproduced from Karimabadi et al. (2013))



in MMS data (Burch and Phan 2016; Fuselier et al. 2017; Wilder et al. 2018). However it has also been demonstrated in MMS analysis (Chasapis et al. 2018b) that some current sheets that are found to be reconnecting, with measures such as $j \cdot E$ indicating conversion of magnetic energy into particle energy, are actually *cooling* locally. This is not a paradox, since fundamental Vlasov-Maxwell theory shows that electromagnetic work exchanges energy with microscopic *flows*, while the actual conversion into internal energy of each species α is accomplished by $\Pi_{ij}^\alpha \nabla_i u_j^\alpha$ the contraction of the pressure tensor with fluid velocity gradients of each species Yang et al. (2017a,b). Further decomposed into a compressive part (pressure-dilatation) and an incompressive part (pressure-strain, or “Pi-D”) these quantities have recently been studied as direct channels of dissipation into heat (Yang et al. 2017a,b; Chasapis et al. 2018b; Pezzi et al. 2019c; Matthaeus et al. 2020). It is important to note that within a collisional closure the pressure strain interaction is approximated by a viscosity (Braginskii 1965) and becomes irreversible; however in the Vlasov-Maxwell case, lacking collisions, these terms are sign-indefinite, just as are the electromagnetic work and the turbulence scale-to-scale transfer (Matthaeus et al. 2020). Recently the statistical distribution of the Pi-D interaction has been examined in MMS data (Bandyopadhyay et al. 2020a), and found to be consistent, in detail, with statistics from kinetic plasma simulation. It is encouraging that these highly fluctuating quantities in turbulent plasma give rise to statistical distributions that have reproducible properties.

The *field-particle correlator* has been furthermore proposed to point out features of particular phenomena associated with dissipation, e.g. Landau damping (Klein and Howes 2016; Chen et al. 2019b; Klein et al. 2020). Although in general their role is thought of being weak (Speiser 1965; Kasper et al. 2008; Maruca et al. 2011; Chhiber et al. 2016), collisional effects have been very recently also adopted to describe the ultimate dissipation,

that produces an irreversible entropy growth (TenBarge et al. 2013; Pezzi et al. 2015, 2016b; Pezzi 2017; Pezzi et al. 2019b; Navarro et al. 2016; Vafin et al. 2019).

We conclude this section by highlighting that the support that numerical simulations can provide for interpreting and understanding *in-situ* observations is far from being exhausted. Indeed, magnetic reconnection is a multiscale phenomenon which goes “hand-in-hand” with turbulence evolution (Matthaeus and Velli 2011). Several issues need to be additionally addressed to clarify this puzzling picture. As introduced above, several simulations are performed in a reduced two-dimensional geometry, while the full three-dimensional case is much more complex and needs to be understood in detail. Another caveat concerns the unrealistic ion-to-electron mass ratio and the reduced box-size, that respectively affect the separation of different dynamical scales (i.e. the possibility to couple large and small scales) and the feasibility to achieve realistic Reynolds number. In this perspective, very recently, it has been proposed to couple different models, such as kinetic and global MHD (Daldorff et al. 2014; Drake et al. 2019). Finally, based on the MHD treatment, magnetic reconnection is associated with the introduction of irreversibility in the system. However, in a weakly-collisional plasma, the transition to an irreversible dynamics is a long-standing challenge (Navarro et al. 2016; Pezzi et al. 2016b, 2019b). For a discussion of the relationship between collisional and collisionless cases, see (Matthaeus et al. 2020).

5 Theory of Particle Acceleration in Dynamical Flux Ropes/Magnetic Islands

Charged particle dynamics depends on the stochastic motion of magnetic field lines, whose random displacement affects the diffusion of particles both across and along the mean magnetic field (Jokipii and Parker 1969). In fact, particles gyrate along the magnetic field but, if the field is turbulent, they spread in the perpendicular direction, “jumping” from one field line to another (Jokipii 1966; Chandran et al. 2010; Ruffolo et al. 2012). The turbulent nature of the fields that scatter particles, makes the analytical treatment rather difficult. Because of this, we still lack an exact and universal theory to describe diffusion (Bieber and Matthaeus 1997; Hussein and Shalchi 2016; Dundovic et al. 2020).

Currently, among all diffusion theories, the nonlinear guiding centre (NLGC) (Matthaeus et al. 2003) and its variations Ruffolo et al. (2012), Shalchi (2009) give a rather accurate prediction of the diffusion coefficient for systems with a three-dimensional (3D) geometry. However, a fully 3D numerical description of plasma turbulence requires huge computational efforts that can be streamlined by reducing the dimensionality of the problem. If a strong guiding magnetic field is present, turbulence becomes anisotropic and both 2D and 2.5D models become good approximations (Dobrowolny et al. 1980a,b; Shebalin et al. 1983; Matthaeus and Lamkin 1986; Oughton et al. 1994; Dmitruk et al. 2004). Due to this anisotropy, structures and phenomena related to turbulence, such as current sheets and reconnecting magnetic islands (Matthaeus and Lamkin 1986; Greco et al. 2009; Servidio et al. 2011a), magnetic field topology changes and energy conversion (Parker 1957; Matthaeus et al. 1984; Ambrosiano et al. 1988; Servidio et al. 2009, 2015), mainly occur due to dynamics in the plane perpendicular to the main field (Bruno and Carbone 2016). In Pecora et al. (2018), a 2D version of 3D NLGC has been developed and tested with the 2.5D hybrid-PIC (Particle In Cell with kinetic ions and fluid electrons) simulation campaign described in (Servidio et al. 2016). As turbulence develops, large-scale structures interact and smaller vortices and sharp current sheets appear, as shown in Fig. 9. In particular, these magnetic structures represent magnetic islands (sections of three-dimensional flux tubes), and intense

current sheets are associated to regions of strong magnetic gradients, in between reconnecting magnetic islands (Matthaeus and Montgomery 1980; Servidio et al. 2015). Particles' trajectories show that they can be either trapped in magnetic vortices (Ambrosiano et al. 1988; Ruffolo et al. 2003; Dmitruk et al. 2004; Tooprakai et al. 2007, 2016; Seripienlert et al. 2010), or scattered by magnetic discontinuities such as current sheets (Rappazzo et al. 2017).

While at short times particles can be trapped in topological structures, typically a stochastic transport regime is achieved after rather long time intervals and can be statistically described within the theory of diffusion, based for example, on the relation

$$\langle \Delta s^2 \rangle = 2D\tau$$

where $\Delta s = \mathbf{x}(t_0 + \tau) - \mathbf{x}(t_0)$ is the displacement of a particle, with \mathbf{x} being its position vector, D the diffusion coefficient, and the average operation $\langle \dots \rangle$ is taken over all the particles (Chandrasekhar 1943; Batchelor 1976; Wang et al. 2012). The diffusive description can be applied after initial transients, the simplest of which is referred to as the ballistic regime (Servidio et al. 2016). When applicable, particles must also escape from topological trapping in small flux tubes Tooprakai et al. (2007) prior to achieving diffusive transport. Generally speaking, transient regimes will last until particles sample uncorrelated correlated magnetic fields. As long as particles motion is followed for times shorter than the particle Lagrangian magnetic field correlation time, their motion cannot be found to be stochastic. This correlation time can be thought as the time one particle needs to move from one large scale magnetic vortex (island) to another. Low energy particles have longer correlation times as they cannot easily escape from vortices. Generally, the shape of trajectories suggests whether a particle has experienced trapping or scattering events, or both. Indeed, some particles have closed orbits that are a manifestation of trapping phenomena, while others show sharp turnovers that suddenly bend their trajectory when they experience strong local discontinuities (Drake et al. 2010; Haynes et al. 2014).

When charged particles move in a turbulent plasma, local properties and modifications in the topology, such as island contractions and magnetic reconnection, are possible acceleration mechanisms as discussed in previous sections. Among these, one that can lead straight to particle acceleration is the electric field parallel to the local magnetic field (Sturrock 1966; le Roux et al. 2001; Comisso and Sironi 2018). Particles with acceleration values that exceed the variance of the distribution are found to be non-uniformly distributed in space. These particles tend to cluster where the parallel electric field is more intense, mostly on the flanks of magnetic islands. This supports the idea that accelerating particles are located close to regions where dynamical activity is occurring, notably along boundaries of interacting flux tubes, and near the associated current sheets, suggesting an association with magnetic reconnection. An example of this acceleration mechanism taking place is shown in Fig. 14.

Particles can also be accelerated by perpendicular electric fields including betatron and curvature drift mechanisms that were discussed at some length in Sect. 3. It should be noted that much of the elegant formal theory presented in those preceding sections was based on conservation of adiabatic invariants and correspondingly, on guiding center drift theory Rossi and Olbert (1970). While applicable in many situations, the basis of this set of approximations is not always defensible; in particular adiabatic conservation laws such as conservation of magnetic moment are very sensitive to the presence of resonant power in the spectrum (Dalena et al. 2012). In this regard a test particle study in a hierarchical reduced MHD model Dalena et al. (2014) found that in early stages of acceleration, parallel electric field is most important, but later, the most energetic particles are found in a so-called

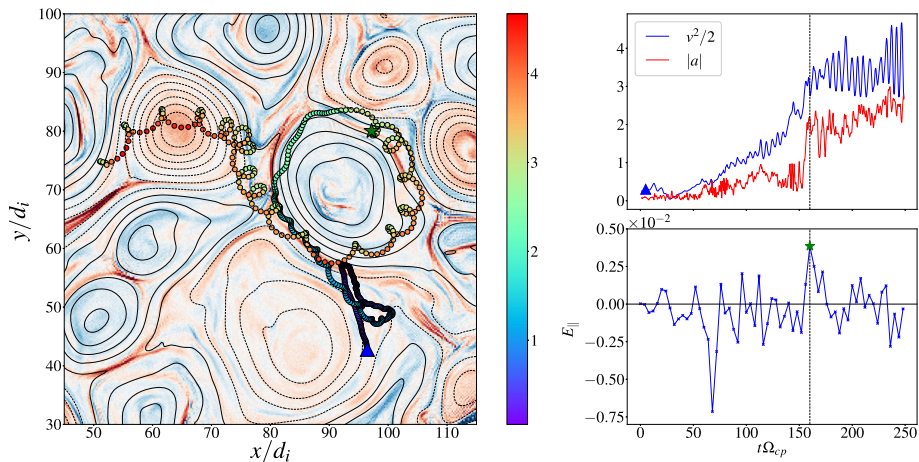


Fig. 14 Snapshot of turbulence simulation when one particle is subject to a peak of the parallel electric field, located at the flank of the magnetic island in which it is trapped (adapted from Pecora et al. (2018)). At the same time, the particle experiences an increase in acceleration and kinetic energy and is able to escape from the island (the trajectory starts at the blue triangle and the colour code represents particle's kinetic energy)

betatron distribution, with parallel streaming relatively suppressed. The affected particles are typically trapped for extended periods of time in the acceleration region. The interaction with the electric field is found to be in the perpendicular direction and resonant in the time domain as seen by the accelerated particles. The locus of this acceleration is near magnetic boundaries of flux tubes as they are compressed due to interaction with neighboring flux tubes. There is a suggestion that the mechanism is limited by eventual pitch angle isotropization. As far as we are aware a transport theory describing this mechanism has not yet been developed.

Coherent structures, such as current sheets, contribute to non-Gaussian statistics and therefore to intermittency which is a fundamental property of turbulence and can be associated with kinetic effects such as particle acceleration (Marsch and Tu 1997; Sorriso-Valvo et al. 1999; Osman et al. 2012b; Greco et al. 2012; Servidio et al. 2015; Wan et al. 2015). A well-established proxy to locate regions in which such structures appear is the Partial Variance of Increments (PVI) technique (Greco et al. 2009). In turbulence simulations, it has been found that the regions of large parallel electric field occur in correspondence of magnetic discontinuities rather than in smooth regions, at the boundaries of the magnetic islands as previously shown in Fig. 15 of Greco et al. (2009).

Along with the parallel electric field, another feature has emerged to be extremely relevant in the process of acceleration and energization of particles. For energization to be effective, there must be a sort of spatial resonance between particle and diffusive characteristic scales. In particular, the gyroradius has to be comparable with Taylor dissipation length, $\lambda_T = \sqrt{\langle \delta b_\perp^2 \rangle / \langle j_z^2 \rangle}$, (qualitatively, the in-plane length of the largest current sheet). In Pecora et al. (2019b) this resonance is achieved in low- β simulations and particles are more effectively energized with respect to those in large- β plasmas. Indeed, changing plasma β does not change turbulence scales such as correlation and Taylor lengths, but it modifies plasma's thermal energy and hence particles' gyroradii. These local spatial resonances, at low β , make the magnetic moment no longer a constant of the motion, leading to acceler-

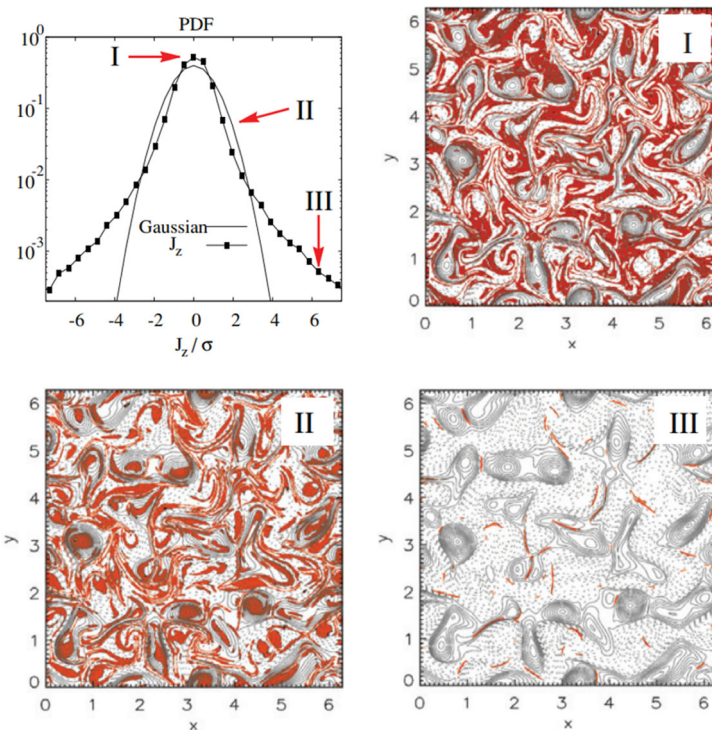


Fig. 15 PDF of the out-of-plane electric current density J_z from a 2D simulation, compared to a reference Gaussian (reproduced from Greco et al. (2009)). For each region I, II, and III, magnetic field lines (contours of constant magnetic potential $A_z > 0$ solid, $A_z < 0$ dashed) are displayed; the coloured (red) regions are places where the selected band (I, II, or III) contributes

ation and eventually to energization, reminiscent of the nonadiabatic betatron mechanism described above (Dalena et al. 2014).

On the other hand, in larger- β plasma simulations, a consistent percentage of particles have a Larmor radius that is larger than the Taylor length, meaning that particles barely notice the current sheets during their gyrating motion and no resonance is possible, resulting in lower to none energization features.

Energization processes are ubiquitous in the whole universe and are not confined within the heliospheric description. High-energy particles, cosmic rays, black holes jets, all require a slightly different description that takes into account relativistic effects and strongly magnetized environments. As for non-relativistic plasmas, observations are tightly related to numerical simulations, especially when dealing with far unfathomable places. Magnetically dominated regions are a source of strong reconnection events and simulations show that acceleration of particles takes place as a two-stage process. First, the electric field acts as a primary source of acceleration in what can be considered an injection phase. Subsequently, many different processes, such as stochastic interaction with turbulent fluctuations, curvature drift and magnetic islands contraction, can take place and result in a Fermi-like acceleration (Guo et al. 2015, 2016a,b; Huang et al. 2017; Ball et al. 2018; Comisso and Sironi 2019; Trotta et al. 2020).

There is a lot of observational evidence about the structured texture, previously depicted with simulations, of space plasmas at different spatial scales (Schatten 1971;

Bruno et al. 2001; Borovsky 2008; Khabarova and Zank 2017; Malandraki et al. 2019; Verscharen et al. 2019). As discussed also in Part I of this review, cross-sections of 3D structures such as elongated plasmoids, flux ropes and blobs of different origins, are 2D magnetic islands. The presence of these structures, on-average aligned with the Parker spiral, was suggested by (Borovsky 2008), following the spaghetti solar wind paradigm developed in 1970th (see Sect. 2.2 of Part I). There is no clue if such structures originate close to the Sun and then advected in the interplanetary space, or generate locally in the HCS and other SCSs filling the solar wind, due to magnetic reconnection and numerous instabilities (e.g., Khabarova et al. (2015, 2016), Khabarova and Zank (2017), Malandraki et al. (2019), Khabarova et al. (2020b)). Particularly relevant is the contribution given by the MMS mission (Curtis 1999), whose measurements help unravelling the fine-scale structure of the near-Earth interplanetary space. Lots of effort have been dedicated into correlating spacecraft measurements to topological properties of the magnetic field and kinetic properties of plasma, showing also that reconnection sites can generate secondary structures such as reconnection-generated flux ropes within their exhausts (Lapenta et al. 2015, 2018; Burch et al. 2016b; Burch and Phan 2016; Phan et al. 2016; Eastwood et al. 2016; Stawarz et al. 2018, 2019).

Of course, it is not possible to obtain a clear picture, like that provided by simulations, of the surroundings of a spacecraft, but there are powerful tools that can be used to get 2D and 3D information when specific conditions are met. A three-dimensional perspective of magnetic field lines can be recovered using the First Order Taylor Expansion (FOTE) method (Fu et al. 2015) that can be applied in the vicinity of a null point. This method requires multispacecraft measurements and the null point to be enclosed within the spacecrafts configuration volume but, despite the restricted regions of applicability, it can provide important information such as the identification of a 3D reconnection site where kinetic effects can be studied locally and linked to topological properties (Fu et al. 2016; Wang et al. 2019). On the other hand, the Grad-Shafranov (GS) reconstruction method (Hu and Sonnerup 2002) is able to reveal the 2D magnetic field texture around one single spacecraft when it passes through an MHD stationary structure with cylindrical symmetry (e.g. a flux rope, whose 2D section in the plane perpendicular to the symmetry axis is a magnetic island). This technique has been also adopted to study the effect of magnetic clouds on galactic cosmic ray intensity (Benella et al. 2019). Very recently, Pecora et al. (2019a) enhanced the GS method by synergising it with the PVI technique providing additional observational evidence of the complex structure of the solar wind. In fact, the large-scale texture of the solar wind, reconstructed with the GS method at about $10^5 - 10^6$ km, shows flux tubes that are filamentary or “spaghetti-like”. The additional information provided by the PVI technique reveals where strong small-scale gradients of the magnetic fields are located. These regions are found at the boundaries of flux ropes/plasmoids where, possibly, reconnection, heating and particle acceleration are taking place. A few examples are shown in Fig. 16. These structured flux tubes, hence, provide conduits for energetic particle transport and possible trapping and acceleration (see Tassein et al. (2013), Khabarova et al. (2016), Pecora et al. (2018) and Sect. 3).

The possibility to visualise 2D and 3D maps of the magnetic field and locate reconnection sites is extremely valuable when it comes to relating particle properties with the surrounding environment, as simulations already allow to do (Fig. 14). Eventually, one may envision numerous applications in which the structures revealed by the combined GS/PVI method can be relevant to understand complex physics and turbulent interplanetary dynamics.

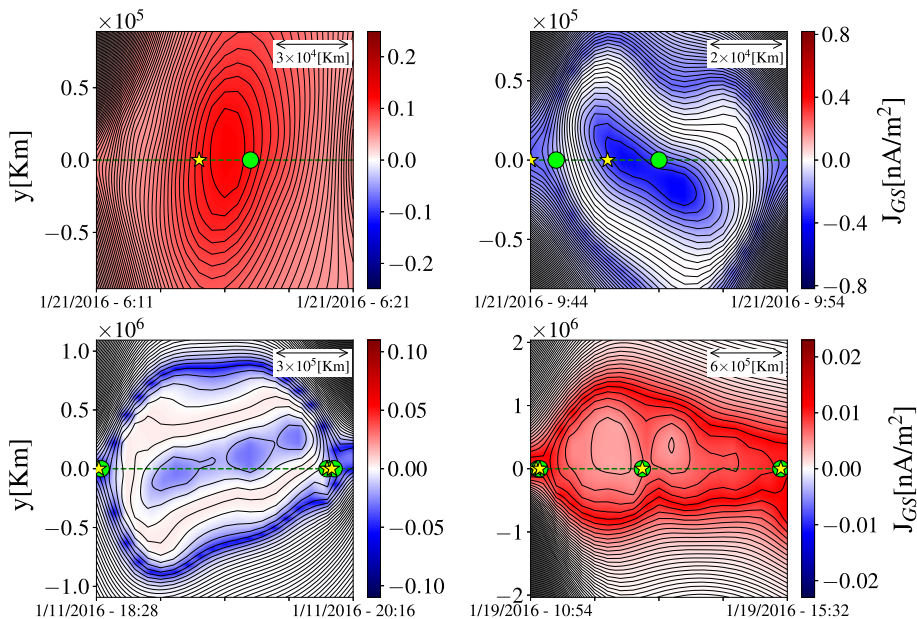


Fig. 16 Reconstructed flux ropes, adapted from Pecora et al. (2019a). The colour represents the out-of-plane current density, the black solid lines are the isocontour of the magnetic potential and the boundaries of a PVI event are indicated with a star (beginning) and a circle (end)

6 Summary and Conclusions

In this review we have depicted the dynamics of magnetic and plasma structures, such as CSs, FRs/MIs and plasmoids/blobs, and their impact on the surrounding medium, especially related to particle energization. The complexity involved within such structures makes the adoption of the fully 3D approach essential since several important pieces of information are inevitably lost by adopting models with explicit symmetries (planar and/or spherical). Observations and numerical simulations in the last decades support these ideas (see, e.g., Lapenta et al. (2015, 2018), Adhikari et al. (2019), Khabarova et al. (2020b), Lazarian et al. (2020)). At the same time, the 2D approach can be employed in some cases. For instance, because of the spectral anisotropy, this is generally applicable for studying turbulence. Indeed, 2D/2.5D models of plasma turbulence are able to describe most of the features of both turbulence dissipation and magnetic reconnection, providing a valid tool for investigation of the related processes and understanding of particle heating and energization in astrophysical plasmas (e.g., Matthaeus et al. (2015)).

Modern theories and observational studies describe the HCS and similarly strong CSs as essentially non-planar complex plasma structures surrounded by a plasma sheet in which numerous small-scale reconnecting CSs separated by plasmoids occur (Khabarova et al. 2015; Malova et al. 2018; Adhikari et al. 2019; Mingalev et al. 2019). CSs are unstable in natural plasmas. Owing to the constantly changing environment, CSs are subject to different instabilities, including the tearing instability (Zelenyi et al. 1998, 2004; Tenerani et al. 2015a). These instabilities may impact CSs simultaneously with various fluctuations, destabilizing, triggering nonlinear processes at CSs and even destroying them. Therefore, strong quasi-stable CSs, such as the HCS and CSs at leading edges of ICMEs and CIRs/SIRs, represent

a well-known source of turbulence and intermittency. On the other hand, numerous thin and unstable CSs are generated in turbulent and intermittent regions (e.g., Servidio et al. (2009), Matthaeus et al. (2015)). This dualism reflects an intrinsic tie between instabilities, wave processes, magnetic reconnection, turbulence, and intermittency in space plasmas.

Summarizing the results of studies of particle acceleration associated with magnetic reconnection, we would like to stress out the fact that, besides the obvious role of the reconnection-induced electric field, charged particles can be energized by the first- and second-order Fermi mechanisms and the so-called anti-reconnection electric field operating during contraction and merging of FRs/plasmoids/MIs (Zank et al. 2014; le Roux et al. 2015, 2016, 2019; Xia and Zharkova 2018, 2020). Numerical simulations of processes occurring in turbulent plasmas successfully describe energization of charged particles by several acceleration mechanisms acting simultaneously. An analysis of observations confirms that theoretical predictions and results of numerical simulations discussed above correspond to reality and show that the ubiquitous occurrence of magnetic reconnection in the heliosphere makes this phenomenon essential for local particle acceleration (Khabarova et al. 2015, 2016, 2020b). Comprehensive studies of the formation, evolution and dynamics of CSs, FRs/plasmoids, MIs in the heliosphere are necessary for better understanding of the transport of energetic particles in the heliosphere, including galactic cosmic rays (Engelbrecht 2019b).

CSs, FRs/MIs, and plasmoids/blobs of various origins and scales exist in the turbulent solar wind. Therefore, we provide an analysis of the main properties of solar wind turbulence, from large (MHD) to smaller (kinetic) scales for convenience of the readers interested in numerical simulations. Here, we particularly focus on the most recent advances in kinetic numerical simulations (e.g., Servidio et al. (2015)). Owing to the weak collisionality, plasma turbulence naturally evolves in the fully 6D phase-space and excites a variety of genuinely kinetic effects in the particle VDF (Valentini et al. 2016; Servidio et al. 2017; Pezzi et al. 2018), ranging from beams along the background magnetic field to a highly-structured velocity-space, as recently found via the Hermite decomposition of the particle VDF.

To conclude, one may offer numerous applications in which the structures revealed by the combined GS/PVI method can be relevant in understanding the complex physics and turbulent dynamics of both the interplanetary magnetic field and the solar wind plasma. It should be emphasized that most of contemporaneous theoretical works describing solar-wind properties have been made in a frame of 2D modeling and reconstructions. Very often, the available methods do not allow complete understanding the real shape of 3D plasma structures, as discussed in Part I of this review. Talking about 2D modeling, one should take into account a certain degree of uncertainty in the interpretation of the results, which is similar to problems of the interpretation of observations. In particular, the shapes and corresponding dynamics of magneto-plasma structures in the solar wind may only be suggested since one considers a cross-section of real 3D structures which may be both FRs and/or finite shaped plasmoids/blobs. That is why we talk about 2D magnetic islands above. We admit that the lack of 3D models due to an obvious complexity of their building as well as the insufficiency of multi-spacecraft data to restore 3D structures are disadvantages of the modern theoretical and observational approaches. Meanwhile, we can conclude that employing contemporary 2D models and corresponding simplified methods widely used in space science allows general understanding of the numerous complex processes if one initially considers various possible 3D topologies occurring in the real space plasmas. The transition from the 2D to 3D models to describe complex 3D processes and non-planar structures in the solar wind is the next step of the development of heliospheric physics.

Acknowledgements This work is supported by the International Space Science Institute (ISSI) in the framework of International Team 405 entitled “Current Sheets, Turbulence, Structures and Particle Acceleration in the Heliosphere.”. O.P. thanks Dr. D. Trotta and Dr. F. Catapano for friendly and precious conversations on some of the topics discussed in this review.

Funding R.K., H.M. and O.K. are partially supported by Russian Foundation for Basic Research (RFBR) grant 19-02-00957. H.M. acknowledges the partial support of Volkswagen Foundation grant Az90 312. J. A. le Roux acknowledges support from NASA Grants 80NSSC19K027, NSF-DOE grant PHY-1707247, and NSF-EPSCoR RII-Track-1 Cooperative Agreement OIA-1655280. S.S. acknowledges the European Union’s Horizon 2020 research and innovation programme under Grant Agreement No. 776262 (AIDA, www.aida-space.eu).

Data availability All data and material used are from public open-access data depositories and archives (see Acknowledgements for details).

Code availability Not applicable.

Conflicts of interest/Competing interests The authors declare no conflict of interests.

Publisher’s Note Springer Nature remains neutral with regard to jurisdictional claims in published maps and institutional affiliations.

References

- L. Adhikari, G.P. Zank, P. Hunana, D. Shiota, R. Bruno, Q. Hu, D. Telloni, II. Transport of nearly incompressible magnetohydrodynamic turbulence from 1 to 75 au. *Astrophys. J.* **841**, 85 (2017). <https://doi.org/10.3847/1538-4357/aa6f5d>
- L. Adhikari, O. Khabarova, G.P. Zank, L.L. Zhao, The role of magnetic reconnection-associated processes in local particle acceleration in the solar wind. *Astrophys. J.* **873**(1), 72 (2019). <https://doi.org/10.3847/1538-4357/ab05c6>
- O. Alexandrova, V. Carbone, P. Veltri, L. Sorriso-Valvo, Small scale energy cascade of the solar wind turbulence. *Astrophys. J.* **674**, 1153–1157 (2008). <https://doi.org/10.1086/524056>
- T. Amano, T. Katou, N. Kitamura, M. Oka, Y. Matsumoto, M. Hoshino, Y. Saito, S. Yokota, B.L. Giles, W.R. Paterson, C.T. Russell, O. Le Contel, R.E. Ergun, P.A. Lindqvist, D.L. Turner, J.F. Fennell, J.B. Blake, Observational evidence for stochastic shock drift acceleration of electrons at the Earth’s bow shock. *Phys. Rev. Lett.* **124**(6), 065101 (2020). <https://doi.org/10.1103/PhysRevLett.124.065101>. [arXiv:2002.06787](https://arxiv.org/abs/2002.06787)
- J. Ambrosiano, W.H. Matthaeus, M.L. Goldstein, D. Plante, Test particle acceleration in turbulent reconnecting magnetic fields. *J. Geophys. Res.* **93**, 14383–14400 (1988). <https://doi.org/10.1029/JA093iA12p14383>
- N. Andrés, F. Sahraoui, S. Galtier, L.Z. Hadid, R. Ferrand, S.Y. Huang, Energy cascade rate measured in a collisionless space plasma with MMS data and compressible Hall magnetohydrodynamic turbulence theory. *Phys. Rev. Lett.* **123**(24), 245101 (2019). <https://doi.org/10.1103/PhysRevLett.123.245101>. [arXiv:1911.09749](https://arxiv.org/abs/1911.09749)
- S.K. Antiochos, C.R. DeVore, The role of magnetic reconnection in solar activity, in *Washington DC American Geophysical Union Geophysical Monograph Series*, vol. 199 (1999), pp. 113–120. [arXiv:astro-ph/9809161](https://arxiv.org/abs/astro-ph/9809161)
- S.V. Apatenkov, V.A. Sergeev, M.V. Kubyshkina, R. Nakamura, W. Baumjohann, A. Runov, I. Alexeev, A. Fazakerley, H. Frey, S. Muhlbachler, P.W. Daly, J.A. Sauvaud, N. Ganushkina, T. Pulkkinen, G.D. Reeves, Y. Khotyaintsev, Multi-spacecraft observation of plasma dipolarization/injection in the inner magnetosphere. *Ann. Geophys.* **25**(3), 801–814 (2007). <https://hal.archives-ouvertes.fr/hal-00330123>
- A.V. Artemyev, A.A. Petrukovich, L. Zelenyi, R. Nakamura, H. Malova, V.Y. Popov, Thin embedded current sheets: Cluster observations of ion kinetic structure and analytical models. *Ann. Geophys.* **27**(10), 4075–4087 (2009a). <https://doi.org/10.5194/angeo-27-4075-2009>
- A.V. Artemyev, L.M. Zelenyi, H.V. Malova, G. Zimbardo, D. Delcourt, Acceleration and transport of ions in turbulent current sheets: Formation of non-Maxwellian energy distribution. *Nonlinear Process. Geophys.* **16**(6), 631–639 (2009b). <https://doi.org/10.5194/npg-16-631-2009>. <https://www.nonlinearprocesses-geophys.net/16/631/2009/>

M. Ashour-Abdalla, J.P. Berchem, J. Buechner, L.M. Zelenyi, Shaping of the magnetotail from the mantle: Global and local structuring. *J. Geophys. Res.* **98**(A4), 5651–5676 (1993). <https://doi.org/10.1029/92JA01662>

N. Aunai, M. Hesse, M. Kuznetsova, Electron nongyrotropy in the context of collisionless magnetic reconnection. *Phys. Plasmas* **20**(9), 092903 (2013). <https://doi.org/10.1063/1.4820953>

D. Ball, L. Sironi, F. Öznel, Electron and proton acceleration in trans-relativistic magnetic reconnection: Dependence on plasma beta and magnetization. *Astrophys. J.* **862**(1), 80 (2018). <https://doi.org/10.3847/1538-4357/aac820>

R. Bandyopadhyay, W.H. Matthaeus, T.N. Parashar, Y. Yang, A. Chasapis, B.L. Giles, D.J. Gershman, C.J. Pollock, C.T. Russell, R.J. Strangeway, R.B. Torbert, T.E. Moore, J.L. Burch, Statistics of kinetic dissipation in the Earth's magnetosheath: MMS observations. *Phys. Rev. Lett.* **124**(25), 255101 (2020a). <https://doi.org/10.1103/PhysRevLett.124.255101>. arXiv:2005.09232

R. Bandyopadhyay, R.A. Qudsi, W.H. Matthaeus, T.N. Parashar, B.A. Maruca, S.P. Gary, V. Roytershteyn, A. Chasapis, B.L. Giles, D.J. Gershman, C.J. Pollock, C.T. Russell, R.J. Strangeway, R.B. Torbert, T.E. Moore, J.L. Burch, Interplay of turbulence and proton-microinstability growth in space plasmas (2020b). arXiv:e-prints. arXiv:2006.10316

G. Batchelor, Brownian diffusion of particles with hydrodynamic interaction. *J. Fluid Mech.* **74**(1), 1–29 (1976)

M. Battarbee, S. Dalla, M.S. Marsh, Solar energetic particle transport near a heliospheric current sheet. *Astrophys. J.* **836**(1), 138 (2017). <https://doi.org/10.3847/1538-4357/836/1/138>

M. Battarbee, S. Dalla, M.S. Marsh, Modeling solar energetic particle transport near a wavy heliospheric current sheet. *Astrophys. J.* **854**(1), 23 (2018). <https://doi.org/10.3847/1538-4357/aaa3fa>. arXiv:1712.03729

W. Baumjohann, A. Matsuoka, K.H. Glassmeier, C.T. Russell, T. Nagai, M. Hoshino, T. Nakagawa, A. Balogh, J.A. Slavin, R. Nakamura, W. Magnes, The magnetosphere of Mercury and its solar wind environment: Open issues and scientific questions. *Adv. Space Res.* **38**(4), 604–609 (2006). <https://doi.org/10.1016/j.asr.2005.05.117>

K.W. Behannon, F.M. Neubauer, H. Barnstorf, Fine-scale characteristics of interplanetary sector boundaries. *J. Geophys. Res.* **86**(A5), 3273–3287 (1981). <https://doi.org/10.1029/JA086iA05p03273>

H.J. Beinroth, F.M. Neubauer, Properties of whistler mode waves between 0.3 and 1.0 au from Helios observations. *J. Geophys. Res. Space Phys.* **86**(A9), 7755–7760 (1981). <https://doi.org/10.1029/JA086iA09p07755>. <https://agupubs.onlinelibrary.wiley.com/doi/pdf/10.1029/JA086iA09p07755>

A.R. Bell, The acceleration of cosmic rays in shock fronts - I. *Mon. Not. R. Astron. Soc.* **182**, 147–156 (1978a). <https://doi.org/10.1093/mnras/182.2.147>

A.R. Bell, The acceleration of cosmic rays in shock fronts - II. *Mon. Not. R. Astron. Soc.* **182**, 443–455 (1978b). <https://doi.org/10.1093/mnras/182.3.443>

S. Benella, C. Grimaldi, M. Laurenza, G. Consolini, Grad-Shafranov reconstruction of a magnetic cloud: Effects of the magnetic-field topology on the galactic cosmic-ray intensity. *Nuovo Cimento C* **42**(1), 44 (2019). <https://doi.org/10.1393/ncc/2019-19044-7>

J.W. Bieber, W.H. Matthaeus, Perpendicular diffusion and drift at intermediate cosmic-ray energies. *Astrophys. J.* **485**(2), 655–659 (1997). <https://doi.org/10.1086/304464>

J.W. Bieber, W.H. Matthaeus, C.W. Smith, W. Wanner, M. Kallenrode, G. Wibberenz, Proton and electron mean free paths: The Palmer consensus revisited. *Astrophys. J.* **420**, 294–306 (1994). <https://doi.org/10.1086/173559>

J.W. Bieber, W. Wanner, W.H. Matthaeus, Dominant two-dimensional solar wind turbulence with implications for cosmic ray transport. *J. Geophys. Res.* **101**, 2511–2522 (1996). <https://doi.org/10.1029/95JA02588>

J. Birn, M. Hesse, K. Schindler, Filamentary structure of a three-dimensional plasmoid. *J. Geophys. Res.* **94**, 241 (1989)

J. Birn, J. Drake, M. Shay, B. Rogers, R. Denton, M. Hesse, M. Kuznetsova, Z. Ma, A. Bhattacharjee, A. Otto et al., Geospace environmental modeling (gem) magnetic reconnection challenge. *J. Geophys. Res. Space Phys.* **106**(A3), 3715–3719 (2001)

R.D. Blandford, J.P. Ostriker, Particle acceleration by astrophysical shocks. *Astrophys. J. Lett.* **221**, L29–L32 (1978). <https://doi.org/10.1086/182658>

D. Borgogno, D. Grasso, F. Porcelli, F. Califano, F. Pegoraro, D. Farina, Aspects of three-dimensional magnetic reconnection. *Phys. Plasmas* **12**(3), 032309 (2005). <https://doi.org/10.1063/1.1857912>

J.E. Borovsky, Flux tube texture of the solar wind: Strands of the magnetic carpet at 1 AU? *J. Geophys. Res. Space Phys.* **113**(A8), A08110 (2008). <https://doi.org/10.1029/2007JA012684>

S. Braginskii, Transport processes in a plasma. *Rev. Plasma Phys.* **1**, 205 (1965)

H. Breuillard, L. Matteini, M.R. Argall, F. Sahraoui, M. Andriopoulou, O.L. Contel, A. Retinò, L. Mirioni, S.Y. Huang, D.J. Gershman, R.E. Ergun, F.D. Wilder, K.A. Goodrich, N. Ahmadi, E. Yordanova, A. Vaivads, D.L. Turner, Y.V. Khotyaintsev, D.B. Graham, P.A. Lindqvist, A. Chasapis, J.L. Burch, R.B.

Torbert, C.T. Russell, W. Magnes, R.J. Strangeway, F. Plaschke, T.E. Moore, B.L. Giles, W.R. Paterson, C.J. Pollock, B. Lavraud, S.A. Fuselier, I.J. Cohen, New insights into the nature of turbulence in the Earth's magnetosheath using magnetospheric MultiScale mission data. *Astrophys. J.* **859**(2), 127 (2018). <https://doi.org/10.3847/1538-4357/aabae8>

M.R. Brown, C.D. Cothran, J. Fung, Two fluid effects on three-dimensional reconnection in the Swarthmore Spheromak Experiment with comparisons to space data. *Phys. Plasmas* **13**(5), 056503 (2006). <https://doi.org/10.1063/1.2180729>

R. Bruno, V. Carbone, *Turbulence in the Solar Wind* (Springer, Berlin, 2016). <https://doi.org/10.1007/978-3-319-43440-7>

R. Bruno, V. Carbone, P. Veltri, E. Pietropaolo, B. Bavassano, Identifying intermittency events in the solar wind. *Planet. Space Sci.* **49**(12), 1201–1210 (2001). [https://doi.org/10.1016/S0032-0633\(01\)00061-7](https://doi.org/10.1016/S0032-0633(01)00061-7)

J. Büchner, J.P. Kuska, Sausage mode instability of thin current sheets as a cause of magnetospheric substorms. *Ann. Geophys.* **17**(5), 604–612 (1999). <https://doi.org/10.1007/s00585-999-0604-5>

J. Buechner, L.M. Zelenyi, Regular and chaotic charged particle motion in magnetotaillike field reversals. 1. Basic theory of trapped motion. *J. Geophys. Res.* **94**(A9), 11821–11842 (1989). <https://doi.org/10.1029/JA094iA09p11821>

J.L. Burch, T.D. Phan, Magnetic reconnection at the dayside magnetopause: Advances with MMS. *Geophys. Res. Lett.* **43**(16), 8327–8338 (2016). <https://doi.org/10.1002/2016GL069787>

J.L. Burch, T.E. Moore, R.B. Torbert, B.L. Giles, Magnetospheric multiscale overview and science objectives. *Space Sci. Rev.* **199**, 5–21 (2016a). <https://doi.org/10.1007/s11214-015-0164-9>

J. Burch, R. Torbert, T. Phan, L.J. Chen, T. Moore, R. Ergun, J. Eastwood, D. Gershman, P. Cassak, M. Argall et al., Electron-scale measurements of magnetic reconnection in space. *Science* **352**(6290), aaf2939 (2016b)

R.A. Burger, Modeling drift along the heliospheric wavy neutral sheet. *Astrophys. J.* **760**(1), 60 (2012). <https://doi.org/10.1088/0004-637X/760/1/60>

R.A. Burger, D.J. Visser, Reduction of drift effects due to solar wind turbulence. *Astrophys. J.* **725**(1), 1366–1372 (2010). <https://doi.org/10.1088/0004-637X/725/1/1366>

R.A. Burger, H. Moraal, G.M. Webb, Drift theory of charged particles in electric and magnetic fields. *Astrophys. Space Sci.* **116**(1), 107–129 (1985). <https://doi.org/10.1007/BF00649278>

R.A. Burger, T.P.J. Krüger, M. Hitge, N.E. Engelbrecht, A Fisk-Parker hybrid heliospheric magnetic field with a solar-cycle dependence. *Astrophys. J.* **674**(1), 511–519 (2008). <https://doi.org/10.1086/525039>

D. Burgess, Shock drift acceleration at low energies. *J. Geophys. Res.* **92**(A2), 1119–1130 (1987). <https://doi.org/10.1029/JA092iA02p01119>

R.A. Caballero-Lopez, N.E. Engelbrecht, J.D. Richardson, Correlation of long-term cosmic-ray modulation with solar activity parameters. *Astrophys. J.* **883**(1), 73 (2019). <https://doi.org/10.3847/1538-4357/ab3c57>

F. Califano, S.S. Cerri, M. Faganello, D. Laveder, M. Sisti, M.W. Kunz, Electron-only reconnection in plasma turbulence. *Front. Phys.* **8**, 317 (2020). <https://doi.org/10.3389/fphy.2020.00317>

V. Carbone, P. Veltri, A shell model for anisotropic magnetohydrodynamic turbulence. *Geophys. Astrophys. Fluid Dyn.* **52**(1–3), 153–181 (1990)

M.L. Cartwright, M.B. Moldwin, Heliospheric evolution of solar wind small-scale magnetic flux ropes. *J. Geophys. Res.* **115**, A08102 (2010)

P.A. Cassak, M.A. Shay, J.F. Drake, Catastrophe model for fast magnetic reconnection onset. *Phys. Rev. Lett.* **95**, 235002 (2005). <https://doi.org/10.1103/PhysRevLett.95.235002>

P.A. Cassak, J.F. Drake, M.A. Shay, B. Eckhardt, Onset of fast magnetic reconnection. *Phys. Rev. Lett.* **98**, 215001 (2007). <https://doi.org/10.1103/PhysRevLett.98.215001>

F. Catapano, A.V. Artemyev, G. Zimbardo, I.Y. Vasko, Current sheets with inhomogeneous plasma temperature: Effects of polarization electric field and 2D solutions. *Phys. Plasmas* **22**(9), 092905 (2015). <https://doi.org/10.1063/1.4931736>

F. Catapano, G. Zimbardo, S. Perri, A. Greco, A.V. Artemyev, Proton and heavy ion acceleration by stochastic fluctuations in the Earth's magnetotail. *Ann. Geophys.* **34**(10), 917–926 (2016). <https://doi.org/10.5194/angeo-34-917-2016>

F. Catapano, G. Zimbardo, S. Perri, A. Greco, D. Delcourt, A. Retinò, I.J. Cohen, Charge proportional and weakly mass-dependent acceleration of different ion species in the Earth's magnetotail. *Geophys. Res. Lett.* **44**(20), 10108–10115 (2017). <https://doi.org/10.1002/2017GL075092>. arXiv:1709.09926

S.S. Cerri, F. Califano, Reconnection and small-scale fields in 2D-3V hybrid-kinetic driven turbulence simulations. *New J. Phys.* **19**(2), 025007 (2017). <https://doi.org/10.1088/1367-2630/aa5c4a>

S.S. Cerri, S. Servidio, F. Califano, Kinetic cascade in solar-wind turbulence: 3D3V hybrid-kinetic simulations with electron inertia. *Astrophys. J.* **846**(2), L18 (2017). <https://doi.org/10.3847/2041-8213/aa87b0>

S.S. Cerri, M.W. Kunz, F. Califano, Dual phase-space cascades in 3D hybrid-Vlasov–Maxwell turbulence. *Astrophys. J.* **856**(1), L13 (2018). <https://doi.org/10.3847/2041-8213/aab557>

B.D.G. Chandran, B. Li, B.N. Rogers, E. Quataert, K. Germaschewski, Perpendicular ion heating by low-frequency Alfvén-wave turbulence in the solar wind. *Astrophys. J.* **720**, 503–515 (2010). <https://doi.org/10.1088/0004-637X/720/1/503>. [arXiv:1001.2069](https://arxiv.org/abs/1001.2069)

S. Chandrasekhar, Stochastic problems in physics and astronomy. *Rev. Mod. Phys.* **15**(1), 1 (1943)

A. Chasapis, W.H. Matthaeus, T.N. Parashar, M. Wan, C.C. Haggerty, C.J. Pollock, B.L. Giles, W.R. Paterson, J. Dorelli, D.J. Gershman, R.B. Torbert, C.T. Russell, P.A. Lindqvist, Y. Khotyaintsev, T.E. Moore, R.E. Ergun, J.L. Burch, In situ observation of intermittent dissipation at kinetic scales in the Earth's magnetosheath. *Astrophys. J.* **856**(1), L19 (2018a). <https://doi.org/10.3847/2041-8213/aaadf8>

A. Chasapis, Y. Yang, W.H. Matthaeus, T.N. Parashar, C.C. Haggerty, J.L. Burch, T.E. Moore, C.J. Pollock, J. Dorelli, D.J. Gershman, R.B. Torbert, C.T. Russell, Energy conversion and collisionless plasma dissipation channels in the turbulent magnetosheath observed by the magnetospheric multiscale mission. *Astrophys. J.* **862**(1), 32 (2018b). <https://doi.org/10.3847/1538-4357/aac775>

C.H.K. Chen, S. Boldyrev, Q. Xia, J.C. Perez, Nature of subproton scale turbulence in the solar wind. *Phys. Rev. Lett.* **110**, 225002 (2013). <https://doi.org/10.1103/PhysRevLett.110.225002>

Y. Chen, Q. Hu, J.A. le Roux, Analysis of small-scale magnetic flux ropes covering the whole Ulysses mission. *Astrophys. J.* **881**(1), 58 (2019a). <https://doi.org/10.3847/1538-4357/ab2ccf>. [arXiv:1905.00986](https://arxiv.org/abs/1905.00986)

C.H.K. Chen, K.G. Klein, G.G. Howes, Evidence for electron Landau damping in space plasma turbulence. *Nat. Commun.* **10**, 740 (2019b). <https://doi.org/10.1038/s41467-019-10843-3>. [arXiv:1902.05785](https://arxiv.org/abs/1902.05785)

L.J. Chen, S. Wang, M. Hesse, R.E. Ergun, T. Moore, B. Giles, N. Bessho, C. Russell, J. Burch, R.B. Torbert, K.J. Genestreti, W. Paterson, C. Pollock, B. Lavraud, O. Le Contel, R. Strangeway, Y.V. Khotyaintsev, P.A. Lindqvist, Electron diffusion regions in magnetotail reconnection under varying guide fields. *Geophys. Res. Lett.* **46**(12), 6230–6238 (2019c). <https://doi.org/10.1029/2019GL082393>

R. Chhiber, A. Usmanov, W. Matthaeus, M. Goldstein, Solar wind collisional age from a global magnetohydrodynamics simulation. *Astrophys. J.* **821**(1), 34 (2016). <https://doi.org/10.3847/0004-637X/821/1/34>

R. Chhiber, A.V. Usmanov, W.H. Matthaeus, T.N. Parashar, M.L. Goldstein, Contextual predictions for Parker solar probe. II. Turbulence properties and Taylor hypothesis. *Astrophys. J. Suppl. Ser.* **242**(1), 12 (2019). <https://doi.org/10.3847/1538-4365/ab16d7>. [arXiv:1902.03340](https://arxiv.org/abs/1902.03340)

S.P. Christon, D.J. Williams, D.G. Mitchell, L.A. Frank, C.Y. Huang, Spectral characteristics of plasma sheet ion and electron populations during undisturbed geomagnetic conditions. *J. Geophys. Res.* **94**(A10), 13409–13424 (1989). <https://doi.org/10.1029/JA094iA10p13409>

M.R. Collier, Evolution of kappa distributions under velocity space diffusion: A model for the observed relationship between their spectral parameters. *J. Geophys. Res.* **104**(A12), 28559–28564 (1999). <https://doi.org/10.1029/1999JA900355>

L. Comisso, L. Sironi, Particle acceleration in relativistic plasma turbulence. *Phys. Rev. Lett.* **121**(25), 255101 (2018)

L. Comisso, L. Sironi, The interplay of magnetically dominated turbulence and magnetic reconnection in producing nonthermal particles. *Astrophys. J.* **886**(2), 122 (2019). <https://doi.org/10.3847/1538-4357/ab4c33>

B. Coppi, G. Laval, R. Pellat, Dynamics of the geomagnetic tail. *Phys. Rev. Lett.* **16**, 1207–1210 (1966). <https://doi.org/10.1103/PhysRevLett.16.1207>

F.V. Coroniti, On the tearing mode in quasi-neutral sheets. *J. Geophys. Res.* **85**(A12), 6719–6728 (1980). <https://doi.org/10.1029/JA085iA12p06719>

S.W.H. Cowley, J.P. Shull, Current sheet acceleration of ions in the geomagnetic tail and the properties of ion bursts observed at the lunar distance. *Planet. Space Sci.* **31**(2), 235–245 (1983). [https://doi.org/10.1016/0032-0633\(83\)90058-2](https://doi.org/10.1016/0032-0633(83)90058-2)

N.U. Crooker, G.L. Siscoe, S. Shodhan, D.F. Webb, J.T. Gosling, E.J. Smith, Multiple heliospheric current sheets and coronal streamer belt dynamics. *J. Geophys. Res.* **98**(A6), 9371–9382 (1993). <https://doi.org/10.1029/93JA00636>

N.U. Crooker, S.W. Kahler, D.E. Larson, R.P. Lin, Large-scale magnetic field inversions at sector boundaries. *J. Geophys. Res. Space Phys.* **109**(A3), A03108 (2004). <https://doi.org/10.1029/2003JA010278>

S. Curtis, *The Magnetospheric Multiscale Mission. Resolving Fundamental Processes in Space Plasmas* (NASA Goddard Space Flight Center, 1999)

R.B. Dahlburg, J.T. Karpen, A triple current sheet model for adjoining coronal helmet streamers. *J. Geophys. Res.* **100**(A12), 23489–23498 (1995). <https://doi.org/10.1029/95JA02496>

J.T. Dahlin, J.F. Drake, M. Swisdak, Parallel electric fields are inefficient drivers of energetic electrons in magnetic reconnection. *Phys. Plasmas* **23**, 120704 (2016)

J.T. Dahlin, J.F. Drake, M. Swisdak, The role of three-dimensional transport in driving enhanced electron acceleration during magnetic reconnection. *Phys. Plasmas* **24**, 092110 (2017)

L.K.S. Daldorff, G. Tóth, T.I. Gombosi, G. Lapenta, J. Amaya, S. Markidis, J.U. Brackbill, Two-way coupling of a global Hall magnetohydrodynamics model with a local implicit particle-in-cell model. *J. Comput. Phys.* **268**, 236–254 (2014). <https://doi.org/10.1016/j.jcp.2014.03.009>

S. Dalena, A. Greco, A.F. Rappazzo, R.L. Mace, W.H. Matthaeus, Magnetic moment nonconservation in magnetohydrodynamic turbulence models. *Phys. Rev. E* **86**(1, Part 2), 016402 (2012). <https://doi.org/10.1103/PhysRevE.86.016402>

S. Dalena, A.F. Rappazzo, P. Dmitruk, A. Greco, W.H. Matthaeus, Test-particle acceleration in a hierarchical three-dimensional turbulence model. *Astrophys. J.* **783**, 143 (2014). <https://doi.org/10.1088/0004-637X/783/2/143>. [arXiv:1402.3745](https://arxiv.org/abs/1402.3745)

S. Dalla, M.S. Marsh, J. Kelly, T. Laitinen, Solar energetic particle drifts in the Parker spiral. *J. Geophys. Res. Space Phys.* **118**(10), 5979–5985 (2013). <https://doi.org/10.1002/jgra.50589>. [arXiv:1307.2165](https://arxiv.org/abs/1307.2165)

W. Daughton, The unstable eigenmodes of a neutral sheet. *Phys. Plasmas* **6**(4), 1329–1343 (1999). <https://doi.org/10.1063/1.873374>

W. Daughton, V. Roytershteyn, H. Karimabadi, L. Yin, B.J. Albright, B. Bergen, K.J. Bowers, Role of electron physics in the development of turbulent magnetic reconnection in collisionless plasmas. *Nat. Phys.* **7**, 539–542 (2011). <https://doi.org/10.1038/nphys1965>

D.C. Delcourt, Particle acceleration by inductive electric fields in the inner magnetosphere. *J. Atmos. Sol.-Terr. Phys.* **64**(5–6), 551–559 (2002). [https://doi.org/10.1016/S1364-6826\(02\)00012-3](https://doi.org/10.1016/S1364-6826(02)00012-3)

D.C. Delcourt, J.A. Sauvaud, Plasma sheet ion energization during dipolarization events. *J. Geophys. Res.* **99**(A1), 97–108 (1994). <https://doi.org/10.1029/93JA01895>

D.C. Delcourt, K. Seki, N. Terada, Y. Miyoshi, Electron dynamics during substorm dipolarization in Mercury's magnetosphere. *Ann. Geophys.* **23**(10), 3389–3398 (2005). <https://doi.org/10.5194/angeo-23-3389-2005>

G. Delzanno, Multi-dimensional, fully-implicit, spectral method for the Vlasov–Maxwell equations with exact conservation laws in discrete form. *J. Comput. Phys.* **301**, 338–356 (2015). <https://doi.org/10.1016/j.jcp.2015.07.028>

P. Dmitruk, W.H. Matthaeus, Structure of the electromagnetic field in three-dimensional Hall magnetohydrodynamic turbulence. *Phys. Plasmas* **13**(4), 042307 (2006). <https://doi.org/10.1063/1.2192757>

P. Dmitruk, W.H. Matthaeus, N. Seenu, Test particle energization by current sheets and nonuniform fields in magnetohydrodynamic turbulence. *Astrophys. J.* **617**, 667–679 (2004). <https://doi.org/10.1086/425301>

M. Dobrowolny, A. Mangeney, P. Veltri, Fully developed anisotropic hydromagnetic turbulence in interplanetary space. *Phys. Rev. Lett.* **45**(2), 144–147 (1980a). <https://doi.org/10.1103/PhysRevLett.45.144>

M. Dobrowolny, A. Mangeney, P. Veltri, Properties of magnetohydrodynamic turbulence in the solar wind. *Astron. Astrophys.* **83**(1–2), 26–32 (1980b)

S. Donato, S. Servidio, P. Dmitruk, V. Carbone, M.A. Shay, P.A. Cassak, W.H. Matthaeus, Reconnection events in two-dimensional Hall magnetohydrodynamic turbulence. *Phys. Plasmas* **19**(9), 092307 (2012). <https://doi.org/10.1063/1.4754151>

J.F. Drake, J. Gerber, R.G. Kleva, Turbulence and transport in the magnetopause current layer. *J. Geophys. Res.* **99**(A6), 11211–11224 (1994). <https://doi.org/10.1029/93JA03253>

J.F. Drake, M. Swisdak, H. Che, M.A. Shay, Electron acceleration from contracting magnetic islands during reconnection. *Nature* **443**(7111), 553–556 (2006a). <https://doi.org/10.1038/nature05116>

J. Drake, M. Swisdak, K. Schoeffler, B. Rogers, S. Kobayashi, Formation of secondary islands during magnetic reconnection. *Geophys. Res. Lett.* **33**(13), L13105 (2006b)

J.F. Drake, M. Opher, M. Swisdak, J.N. Chamoun, A magnetic reconnection mechanism for the generation of anomalous cosmic rays. *Astrophys. J.* **709**, 963–974 (2010). <https://doi.org/10.1088/0004-637X/709/2/963>. [arXiv:0911.3098](https://arxiv.org/abs/0911.3098)

J.F. Drake, M. Swisdak, R. Fermo, The power-law spectra of energetic particles during multi-island magnetic reconnection. *Astrophys. J.* **763**, L5 (2013). <https://doi.org/10.1088/2041-8205/763/1/L5>. [arXiv:1210.4830](https://arxiv.org/abs/1210.4830)

J.F. Drake, M. Swisdak, P.A. Cassak, T.D. Phan, On the 3-D structure and dissipation of reconnection-driven flow bursts. *Geophys. Res. Lett.* **41**(11), 3710–3716 (2014). <https://doi.org/10.1002/2014GL060249>. [arXiv:1401.7056](https://arxiv.org/abs/1401.7056)

J.F. Drake, H. Arnold, M. Swisdak, J.T. Dahlin, A computational model for exploring particle acceleration during reconnection in macroscale systems. *Phys. Plasmas* **26**(1), 012901 (2019). <https://doi.org/10.1063/1.5058140>. [arXiv:1809.04568](https://arxiv.org/abs/1809.04568)

S. Du, F. Guo, G.P. Zank, X. Li, A. Stanier, Plasma energization in colliding magnetic flux ropes. *Astrophys. J.* **867**, 16 (2018)

A. Dundovic, O. Pezzi, P. Blasi, C. Evoli, W.H. Matthaeus, Novel aspects of cosmic ray diffusion in synthetic magnetic turbulence. *Phys. Rev. D* **102**, 103016 (2020). <https://doi.org/10.1103/PhysRevD.102.103016>

J.P. Eastwood, T.D. Phan, P.A. Cassak, D.J. Gershman, C. Haggerty, K. Malakit, M.A. Shay, R. Mistry, M. Øieroset, C.T. Russell, J.A. Slavin, M.R. Argall, L.A. Avanov, J.L. Burch, L.J. Chen, J.C. Dorelli, R.E. Ergun, B.L. Giles, Y. Khotyaintsev, B. Lavraud, P.A. Lindqvist, T.E. Moore, R. Nakamura, W. Paterson, C. Pollock, R.J. Strangeway, R.B. Torbert, S. Wang, Ion-scale secondary flux ropes generated by magnetopause reconnection as resolved by MMS. *Geophys. Res. Lett.* **43**(10), 4716–4724 (2016). <https://doi.org/10.1002/2016GL068747>

F. Effenberger, Y.E. Litvinenko, The diffusion approximation versus the telegraph equation for modeling solar energetic particle transport with adiabatic focusing. I. Isotropic pitch-angle scattering. *Astrophys. J.* **783**, 15 (2014)

N.E. Engelbrecht, On the pitch-angle-dependent perpendicular diffusion coefficients of solar energetic protons in the inner heliosphere. *Astrophys. J.* **880**(1), 60 (2019a). <https://doi.org/10.3847/1538-4357/ab2871>

N.E. Engelbrecht, The implications of simple estimates of the 2D outer scale based on measurements of magnetic islands for the modulation of galactic cosmic-ray electrons. *Astrophys. J.* **872**(2), 124 (2019b). <https://doi.org/10.3847/1538-4357/aafe7f>

N.E. Engelbrecht, R.A. Burger, An ab initio model for cosmic-ray modulation. *Astrophys. J.* **772**, 46 (2013). <https://doi.org/10.1088/0004-637X/772/1/46>

N.E. Engelbrecht, R.A. Burger, Sensitivity of cosmic-ray proton spectra to the low-wavenumber behavior of the 2D turbulence power spectrum. *Astrophys. J.* **814**(2), 152 (2015). <https://doi.org/10.1088/0004-637X/814/2/152>

N.E. Engelbrecht, R.D. Strauss, J.A. le Roux, R.A. Burger, Toward a greater understanding of the reduction of drift coefficients in the presence of turbulence. *Astrophys. J.* **841**(2), 107 (2017). <https://doi.org/10.3847/1538-4357/aa7058>

N.E. Engelbrecht, S.T. Mohlolo, S.E.S. Ferreira, An improved treatment of neutral sheet drift in the inner heliosphere. *Astrophys. J. Lett.* **884**(2), L54 (2019). <https://doi.org/10.3847/2041-8213/ab4ad6>

R.E. Ergun, N. Ahmadi, L. Kromyda, S.J. Schwartz, A. Chasapis, S. Hoilijoki, F.D. Wilder, P.A. Cassak, J.E. Stawarz, K.A. Goodrich, D.L. Turner, F. Pucci, A. Pouquet, W.H. Matthaeus, J.F. Drake, M. Hesse, M.A. Shay, R.B. Torbert, J.L. Burch, Particle acceleration in strong turbulence in the Earth's magnetotail. *Astrophys. J.* **898**(2), 153 (2020a). <https://doi.org/10.3847/1538-4357/ab9ab5>

R.E. Ergun, N. Ahmadi, L. Kromyda, S.J. Schwartz, A. Chasapis, S. Hoilijoki, F.D. Wilder, J.E. Stawarz, K.A. Goodrich, D.L. Turner, I.J. Cohen, S.T. Bingham, J.C. Holmes, R. Nakamura, F. Pucci, R.B. Torbert, J.L. Burch, P.A. Lindqvist, R.J. Strangeway, O. Le Contel, B.L. Giles, Observations of particle acceleration in magnetic reconnection-driven turbulence. *Astrophys. J.* **898**(2), 154 (2020b). <https://doi.org/10.3847/1538-4357/ab9ab6>

E. Fermi, On the origin of the cosmic radiation. *Phys. Rev.* **75**(8), 1169–1174 (1949). <https://doi.org/10.1103/PhysRev.75.1169>

E. Fermi, Galactic magnetic fields and the origin of cosmic radiation. *Astrophys. J.* **119**, 1 (1954). <https://doi.org/10.1086/145789>

S.E.S. Ferreira, M.S. Potgieter, B. Heber, H. Fichtner, Charge-sign dependent modulation in the heliosphere over a 22-year cycle. *Ann. Geophys.* **21**(6), 1359–1366 (2003). <https://doi.org/10.5194/angeo-21-1359-2003>

M.A. Forman, J.R. Jokipii, A.J. Owens, Cosmic-ray streaming perpendicular to the mean magnetic field. *Astrophys. J.* **192**, 535–540 (1974)

L. Franci, A. Verdini, L. Matteini, S. Landi, P. Hellinger, Solar wind turbulence from MHD to sub-ion scales: High-resolution hybrid simulations. *Astrophys. J. Lett.* **804**, L39 (2015). <https://doi.org/10.1088/2041-8205/804/2/L39>. [arXiv:1503.05457](https://arxiv.org/abs/1503.05457)

L. Franci, S.S. Cerri, F. Califano, S. Landi, E. Papini, A. Verdini, L. Matteini, F. Jenko, P. Hellinger, Magnetic reconnection as a driver for a sub-ion-scale cascade in plasma turbulence. *Astrophys. J. Lett.* **850**(1), L16 (2017). <https://doi.org/10.3847/2041-8213/aa93fb>. [arXiv:1707.06548](https://arxiv.org/abs/1707.06548)

L. Franci, S. Landi, A. Verdini, L. Matteini, P. Hellinger, Solar wind turbulent cascade from MHD to sub-ion scales: Large-size 3D hybrid particle-in-cell simulations. *Astrophys. J.* **853**(1), 26 (2018). <https://doi.org/10.3847/1538-4357/aaa3e8>

L. Franci, J.E. Stawarz, E. Papini, P. Hellinger, T. Nakamura, D. Burgess, S. Landi, A. Verdini, L. Matteini, R. Ergun, O. Le Contel, P.A. Lindqvist, Modeling MMS observations at the Earth's magnetopause with hybrid simulations of Alfvénic turbulence. *Astrophys. J.* **898**(2), 175 (2020). <https://doi.org/10.3847/1538-4357/ab9a47>

H.S. Fu, A. Vaivads, Y.V. Khotyaintsev, V. Olshevsky, M. André, J.B. Cao, S.Y. Huang, A. Retinò, G. Lapenta, How to find magnetic nulls and reconstruct field topology with MMS data? *J. Geophys. Res. Space Phys.* **120**, 3758–3782 (2015). <https://doi.org/10.1002/2015JA021082>

H.S. Fu, J.B. Cao, A. Vaivads, Y.V. Khotyaintsev, M. André, M. Dunlop, W.L. Liu, H.Y. Lu, S.Y. Huang, Y.D. Ma, E. Eriksson, Identifying magnetic reconnection events using the FOTE method. *J. Geophys. Res. Space Phys.* **121**(2), 1263–1272 (2016). <https://doi.org/10.1002/2015JA021701>

S.A. Fuselier, W.S. Lewis, C. Schiff, R. Ergun, J.L. Burch, S.M. Petrinec, K.J. Trattner, Magnetospheric multiscale science mission profile and operations. *Space Sci. Rev.* **199**(1), 77–103 (2016). <https://doi.org/10.1007/s11214-014-0087-x>

S. Fuselier, S. Vines, J. Burch, S. Petrinec, K. Trattner, P. Cassak, L.J. Chen, R. Ergun, S. Eriksson, B. Giles et al., Large-scale characteristics of reconnection diffusion regions and associated magnetopause crossings observed by MMS. *J. Geophys. Res. Space Phys.* **122**(5), 5466–5486 (2017)

A.A. Galeev, L.M. Zelenyi, Tearing instability in plasma configurations. *Zh. Eksp. Teor. Fiz.* **70**, 2133–2151 (1976)

C. Garrel, L. Vlahos, H. Isliker, T. Pisokas, Diffusive shock acceleration and turbulent reconnection. *Mon. Not. R. Astron. Soc.* **478**(3), 2976–2986 (2018). <https://doi.org/10.1093/mnras/sty1260>

S.P. Gary, L. Yin, D. Winske, L. Ofman, B.E. Goldstein, M. Neugebauer, Consequences of proton and alpha anisotropies in the solar wind: Hybrid simulations. *J. Geophys. Res. Space Phys.* **108**(A2), 1068 (2003). <https://doi.org/10.1029/2002JA009654>

S.P. Gary, S. Saito, Y. Narita, Whistler turbulence wavevector anisotropies: Particle-in-cell simulations. *Astrophys. J.* **716**(2), 1332–1335 (2010). <https://doi.org/10.1088/0004-637X/716/2/1332>

S.P. Gary, R.S. Hughes, J. Wang, Whistler turbulence heating of electrons and ions: Three-dimensional particle-in-cell simulations. *Astrophys. J.* **816**(2), 102 (2016). <https://doi.org/10.3847/0004-637X/816/2/102>

W. Gekelman, S.W. Tang, T. DeHaas, S. Vincena, P. Pribyl, R. Sydora, Spiky electric and magnetic field structures in flux rope experiments. *Proc. Natl. Acad. Sci. USA* **116**(37), 18239–18244 (2019). <https://doi.org/10.1073/pnas.1721343115>

A. Ghizzo, M. Sarrat, D. Del Sarto, Vlasov models for kinetic Weibel-type instabilities. *J. Plasma Phys.* **83**(1), 705830101 (2017). <https://doi.org/10.1017/S0022377816001215>

S. Ghosh, W. Matthaeus, D. Roberts, M. Goldstein, The evolution of slab fluctuations in the presence of pressure-balanced magnetic structures and velocity shears. *J. Geophys. Res. Space Phys.* **103**(A10), 23691–23704 (1998)

J. Giacalone, Shock drift acceleration of energetic protons at a planetary bow shock. *J. Geophys. Res.* **97**(A6), 8307–8318 (1992). <https://doi.org/10.1029/92JA00313>

J. Gieseler, B. Heber, K. Herbst, An empirical modification of the force field approach to describe the modulation of galactic cosmic rays close to Earth in a broad range of rigidities. *J. Geophys. Res.* **122**(11), 10964–10979 (2017). <https://doi.org/10.1002/2017JA024763>. [arXiv:1710.10834](https://arxiv.org/abs/1710.10834)

K.H. Glassmeier, P.N. Mager, D.Y. Klimushkin, Concerning ULF pulsations in Mercury's magnetosphere. *Geophys. Res. Lett.* **30**(18), 1928 (2003). <https://doi.org/10.1029/2003GL017175>

M.L. Goldstein, D.A. Roberts, Magnetohydrodynamic turbulence in the solar wind. *Phys. Plasmas* **6**, 4154 (1999). <https://doi.org/10.1063/1.873680>

T. Gomez, H. Politano, A. Pouquet, Exact relationship for third-order structure functions in helical flows. *Phys. Rev. E* **61**(5), 5321 (2000)

C.A. González, T.N. Parashar, D. Gomez, W.H. Matthaeus, P. Dmitruk, Turbulent electromagnetic fields at sub-proton scales: Two-fluid and full-kinetic plasma simulations. *Phys. Plasmas* **26**(1), 012306 (2019). <https://doi.org/10.1063/1.5054110>. [arXiv:1809.00985](https://arxiv.org/abs/1809.00985)

J.T. Gosling, Observations of magnetic reconnection in the turbulent high-speed solar wind. *Astrophys. J. Lett.* **671**(1), L73–L76 (2007). <https://doi.org/10.1086/524842>

H. Grad, On the kinetic theory of rarefied gases. *Commun. Pure Appl. Math.* **2**, 331 (1949)

P.C. Gray, W.H. Matthaeus, MHD turbulence, reconnection, and test-particle acceleration, in *Particle Acceleration in Cosmic Plasmas*, ed. by G.P. Zank, T.K. Gaisser. American Institute of Physics Conference Series, vol. 264 (1992), pp. 261–266. <https://doi.org/10.1063/1.42738>

A. Greco, W.H. Matthaeus, S. Servidio, P. Chuychai, P. Dmitruk, Statistical analysis of discontinuities in solar wind ACE data and comparison with intermittent MHD turbulence. *Astrophys. J.* **691**, L111–L114 (2009). <https://doi.org/10.1088/0004-637X/691/2/L111>

A. Greco, F. Valentini, S. Servidio, W. Matthaeus, Inhomogeneous kinetic effects related to intermittent magnetic discontinuities. *Phys. Rev. E* **86**(6), 066405 (2012)

E.E. Grigorenko, H.V. Malova, A.V. Artemyev, O.V. Mingalev, E.A. Kronberg, R. Koleva, P.W. Daly, J.B. Cao, J.A. Sauvad, C.J. Owen, L.M. Zelenyi, Current sheet structure and kinetic properties of plasma flows during a near-Earth magnetic reconnection under the presence of a guide field. *J. Geophys. Res. Space Phys.* **118**(6), 3265–3287 (2013). <https://doi.org/10.1002/jgra.50310>

D. Grošelj, S.S. Cerri, A.B. Navarro, C. Willmott, D. Told, N.F. Loureiro, F. Califano, F. Jenko, Fully kinetic versus reduced-kinetic modeling of collisionless plasma turbulence. *Astrophys. J.* **847**(1), 28 (2017). <https://doi.org/10.3847/1538-4357/aa894d>

F. Guo, Y.H. Liu, W. Daughton, H. Li, Particle acceleration and plasma dynamics during magnetic reconnection in the magnetically dominated regime. *Astrophys. J.* **806**(2), 167 (2015). <https://doi.org/10.1088/0004-637X/806/2/167>

F. Guo, H. Li, W. Daughton, X. Li, Y.H. Liu, Particle acceleration during magnetic reconnection in a low-beta pair plasma. *Phys. Plasmas* **23**(5), 055708 (2016a). <https://doi.org/10.1063/1.4948284>

F. Guo, X. Li, H. Li, W. Daughton, B. Zhang, N. Lloyd-Ronning, Y.H. Liu, H. Zhang, W. Deng, Efficient production of high-energy nonthermal particles during magnetic reconnection in a magnetically dominated ion-electron plasma. *Astrophys. J.* **818**(1), L9 (2016b). <https://doi.org/10.3847/2041-8205/818/1/9>

L.Z. Hadid, F. Sahraoui, S. Galtier, S.Y. Huang, Compressible magnetohydrodynamic turbulence in the Earth's magnetosheath: Estimation of the energy cascade rate using in situ spacecraft data. *Phys. Rev. Lett.* **120**(5), 055102 (2018). <https://doi.org/10.1103/PhysRevLett.120.055102>. arXiv:1710.04691

C.C. Haggerty, T.N. Parashar, W.H. Matthaeus, M.A. Shay, Y. Yang, M. Wan, P. Wu, S. Servidio, Exploring the statistics of magnetic reconnection x-points in kinetic particle-in-cell turbulence. *Phys. Plasmas* **24**(10), 102308 (2017). <https://doi.org/10.1063/1.5001722>

E.G. Harris, On a plasma sheath separating regions of oppositely directed magnetic field. *Nuovo Cimento* **23**(1), 115–121 (1962)

C.T. Haynes, D. Burgess, E. Camporeale, Reconnection and electron temperature anisotropy in sub-proton scale plasma turbulence. *Astrophys. J.* **783**, 38 (2014). <https://doi.org/10.1088/0004-637X/783/1/38>. arXiv:1304.1444

B. Heber, T.R. Sanderson, M. Zhang, Corotating interaction regions. *Adv. Space Res.* **23**(3), 567–579 (1999). [https://doi.org/10.1016/S0273-1177\(99\)80013-1](https://doi.org/10.1016/S0273-1177(99)80013-1)

P. Hellinger, M. Velli, P. Trávníček, S.P. Gary, B.E. Goldstein, P.C. Liewer, Alfvén wave heating of heavy ions in the expanding solar wind: Hybrid simulations. *J. Geophys. Res. Space Phys.* **110**(A12), A12109 (2005). <https://doi.org/10.1029/2005JA011244>

P. Hellinger, P. Trávníček, J.C. Kasper, A.J. Lazarus, Solar wind proton temperature anisotropy: Linear theory and WIND/SWE observations. *Geophys. Res. Lett.* **33**, L09101 (2006). <https://doi.org/10.1029/2006GL025925>

P. Hellinger, L. Matteini, S. Landi, L. Verdini, E. Papini, Turbulence versus fire-hose instabilities: 3D hybrid expanding box simulations. *Astrophys. J.* **883**(2), 178 (2019). <https://doi.org/10.3847/1538-4357/ab3e01>. arXiv:1908.07760

M. Hesse, K. Schindler, J. Birn, M. Kuznetsova, The diffusion region in collisionless magnetic reconnection. *Phys. Plasmas* **6**(5), 1781–1795 (1999). <https://doi.org/10.1063/1.873436>

M. Hesse, N. Aunai, J. Birn, P. Cassak, R.E. Denton, J.F. Drake, T. Gombosi, M. Hoshino, W. Matthaeus, D. Sibeck, S. Zenitani, Theory and modeling for the magnetospheric multiscale mission. *Space Sci. Rev.* **199**(1), 577–630 (2016). <https://doi.org/10.1007/s11214-014-0078-y>

M. Hesse, L.J. Chen, Y.H. Liu, N. Bessho, J.L. Burch, Population mixing in asymmetric magnetic reconnection with a guide field. *Phys. Rev. Lett.* **118**, 145101 (2017). <https://doi.org/10.1103/PhysRevLett.118.145101>

A.K. Higgins, B.J. Lynch, Structured slow solar wind variability: Streamer-blob flux ropes and torsional Alfvén waves. *Astrophys. J.* **859**(1), 6 (2018). <https://doi.org/10.3847/1538-4357/aabc08>

J.T. Hoeksema, J.M. Wilcox, P.H. Scherrer, The structure of the heliospheric current sheet: 1978–1982. *J. Geophys. Res. Space Phys.* **88**(A12), 9910–9918 (1983). <https://doi.org/10.1029/JA088iA12p09910>. <https://agupubs.onlinelibrary.wiley.com/doi/pdf/10.1029/JA088iA12p09910>

M. Hoshino, Electron surfing acceleration in magnetic reconnection. *J. Geophys. Res.* **110**, A10215 (2005). <https://doi.org/10.1029/2005JA011229>

G.G. Howes, The inherently three-dimensional nature of magnetized plasma turbulence. *J. Plasma Phys.* **81**(2), 325810203 (2015). <https://doi.org/10.1017/S0022377814001056>. arXiv:1306.4589

G.G. Howes, S.C. Cowley, W. Dorland, G.W. Hammett, E. Quataert, A.A. Schekochihin, A model of turbulence in magnetized plasmas: Implications for the dissipation range in the solar wind. *J. Geophys. Res. Space Phys.* **113**, A05103 (2008a)

G. Howes, W. Dorland, S. Cowley, G. Hammett, E. Quataert, A. Schekochihin, T. Tatsuno, Kinetic simulations of magnetized turbulence in astrophysical plasmas. *Phys. Rev. Lett.* **100**(6), 065004 (2008b)

Q. Hu, B.U. Sonnerup, Reconstruction of magnetic clouds in the solar wind: Orientations and configurations. *J. Geophys. Res. Space Phys.* **107**(A7), SSH-10 (2002)

C. Huang, Q. Lu, R. Wang, F. Guo, M. Wu, S. Lu, S. Wang, Development of turbulent magnetic reconnection in a magnetic island. *Astrophys. J.* **835**(2), 245 (2017). <https://doi.org/10.3847/1538-4357/835/2/245>

M. Hussein, A. Shalchi, Simulations of energetic particles interacting with dynamical magnetic turbulence. *Astrophys. J.* **817**(2), 136 (2016)

P.A. Isenberg, A hemispherical model of anisotropic interstellar pickup ions. *J. Geophys. Res.* **102**, 4719 (1997). <https://doi.org/10.1029/96JA03671>

M. Janvier, P. Démoulin, S. Dasso, Are there different populations of flux ropes in the solar wind? *Sol. Phys.* **289**(7), 2633–2652 (2014). <https://doi.org/10.1007/s11207-014-0486-x>. arXiv:1401.6812

K. Jiang, S.Y. Huang, Z.G. Yuan, F. Sahraoui, X.H. Deng, X.D. Yu, L.H. He, D. Deng, Y.Y. Wei, S.B. Xu, The role of upper hybrid waves in the magnetotail reconnection electron diffusion region. *Astrophys. J. Lett.* **881**(2), L28 (2019). <https://doi.org/10.3847/2041-8213/ab36b9>

J.R. Johnson, C.Z. Cheng, Stochastic ion heating at the magnetopause due to kinetic Alfvén waves. *Geophys. Res. Lett.* **28**(23), 4421–4424 (2001). <https://doi.org/10.1029/2001GL013509>

J. Jokipii, Cosmic-ray propagation. I. Charged particles in a random magnetic field. *Astrophys. J.* **146**, 480 (1966)

J.R. Jokipii, D.A. Kopriva, Effects of particle drift on the transport of cosmic rays. III. Numerical models of galactic cosmic-ray modulation. *Astrophys. J.* **234**, 384–392 (1979). <https://doi.org/10.1086/157506>

J. Jokipii, E. Parker, Stochastic aspects of magnetic lines of force with application to cosmic-ray propagation. *Astrophys. J.* **155**, 777 (1969)

J.R. Jokipii, B. Thomas, Effects of drift on the transport of cosmic rays. IV - Modulation by a wavy interplanetary current sheet. *Astrophys. J.* **243**, 1115–1122 (1981). <https://doi.org/10.1086/158675>

J.R. Jokipii, E.H. Levy, W.B. Hubbard, Effects of particle drift on cosmic-ray transport. I. General properties, application to solar modulation. *Astrophys. J.* **213**, 861–868 (1977). <https://doi.org/10.1086/155218>

J. Juno, A. Hakim, J. TenBarge, E. Shi, W. Dorland, Discontinuous Galerkin algorithms for fully kinetic plasmas. *J. Comput. Phys.* **353**, 110–147 (2018). <https://doi.org/10.1016/j.jcp.2017.10.009>

H. Karimabadi, P.L. Pritchett, W. Daughton, D. Krauss-Varban, Ion-ion kink instability in the magnetotail: 2. Three-dimensional full particle and hybrid simulations and comparison with observations. *J. Geophys. Res. Space Phys.* **108**(A11), 1401 (2003). <https://doi.org/10.1029/2003JA010109>

H. Karimabadi, V. Roytershteyn, M. Wan, W.H. Matthaeus, W. Daughton, P. Wu, M. Shay, B. Loring, J. Borovsky, E. Leonardis, S.C. Chapman, T.K.M. Nakamura, Coherent structures, intermittent turbulence, and dissipation in high-temperature plasmas. *Phys. Plasmas* **20**(1), 012303 (2013). <https://doi.org/10.1063/1.4773205>

J. Kasper, A. Lazarus, S. Gary, Hot solar-wind helium: Direct evidence for local heating by Alfvén-cyclotron dissipation. *Phys. Rev. Lett.* **101**(26), 261103 (2008)

T. Katou, T. Amano, Theory of stochastic shock drift acceleration for electrons in the shock transition region. *Astrophys. J.* **874**(2), 119 (2019). <https://doi.org/10.3847/1538-4357/ab0d8a>

O.V. Khabarova, G.P. Zank, Energetic particles of keV–MeV energies observed near reconnecting current sheets at 1 au. *Astrophys. J.* **843**(1), 4 (2017). <https://doi.org/10.3847/1538-4357/aa7686>

O.V. Khabarova, G.P. Zank, G. Li, J.A. le Roux, G.M. Webb, A. Dosch, O.E. Malandraki, Small-scale magnetic islands in the solar wind and their role in particle acceleration. I. Dynamics of magnetic islands near the heliospheric current sheet. *Astrophys. J.* **808**(2), 181 (2015). <https://doi.org/10.1088/0004-637X/808/2/181>. [arXiv:1504.06616](https://arxiv.org/abs/1504.06616)

O.V. Khabarova, G.P. Zank, G. Li, O.E. Malandraki, J.A. le Roux, G.M. Webb, Small-scale magnetic islands in the solar wind and their role in particle acceleration. II. Particle energization inside magnetically confined cavities. *Astrophys. J.* **827**(2), 122 (2016)

O.V. Khabarova, O. Malandraki, H. Malova, R. Kislov, A. Greco, R. Bruno, O. Pezzi, S. Servidio, G. Li, W.H. Matthaeus, J. le Roux, N. Engelbrecht, F. Pecora, L. Zelenyi, V. Obridko, V. Kuznetsov, Current sheets, plasmoids and flux ropes in the heliosphere. Part i. General and observational aspects: 2-d or not 2-d? *Space Sci. Rev.* (2020a). <https://doi.org/10.1007/s11214-021-00814-x> (this journal)

O.V. Khabarova, V. Zharkova, Q. Xia, O.E. Malandraki, Counterstreaming strahls and heat flux dropouts as possible signatures of local particle acceleration in the solar wind. *Astrophys. J. Lett.* **894**(1), L12 (2020b). <https://doi.org/10.3847/2041-8213/ab8cb8>

K.G. Klein, G.G. Howes, Measuring collisionless damping in heliospheric plasmas using field-particle correlations. *Astrophys. J. Lett.* **826**(2), L30 (2016). <https://doi.org/10.3847/2041-8205/826/2/L30>. [arXiv:1607.01738](https://arxiv.org/abs/1607.01738)

K.G. Klein, G.G. Howes, J.M. TenBarge, F. Valentini, Diagnosing collisionless energy transfer using field-particle correlations: Alfvén-ion cyclotron turbulence. *J. Plasma Phys.* **86**(4), 905860402 (2020). <https://doi.org/10.1017/S0022377820000689>. [arXiv:2006.02563](https://arxiv.org/abs/2006.02563)

G. Knorr, Two-dimensional turbulence of electrostatic Vlasov plasmas. *Plasma Phys.* **19**, 529–538 (1977). <https://doi.org/10.1088/0032-1028/19/6/004>

T. Kobak, M. Ostrowski, Energetic particle acceleration in a three-dimensional magnetic field reconnection model: The role of magnetohydrodynamic turbulence. *Mon. Not. R. Astron. Soc.* **317**(4), 973–978 (2000). <https://doi.org/10.1046/j.1365-8711.2000.03722.x>. [arXiv:astro-ph/0006045](https://arxiv.org/abs/astro-ph/0006045)

J. Kota, Energy loss in the solar system and modulation of cosmic radiation, in *International Cosmic Ray Conference*. International Cosmic Ray Conference, vol. 11 (1977), p. 186

J. Kota, J.R. Jokipii, Effects of drift on the transport of cosmic rays. VI - A three-dimensional model including diffusion. *Astrophys. J.* **265**, 573–581 (1983). <https://doi.org/10.1086/160701>

G. Kowal, A. Lazarus, E.T. Vishniac, K. Otmianowska-Mazur, Numerical tests of fast reconnection in weakly stochastic magnetic fields. *Astrophys. J.* **700**(1), 63–85 (2009). <https://doi.org/10.1088/0004-637X/700/1/63>. [arXiv:0903.2052](https://arxiv.org/abs/0903.2052)

G. Kowal, E.M. de Gouveia Dal Pino, A. Lazarus, Magnetohydrodynamic simulations of reconnection and particle acceleration: Three-dimensional effects. *Astrophys. J.* **735**(2), 102 (2011). <https://doi.org/10.1088/0004-637X/735/2/102>. [arXiv:1103.2984](https://arxiv.org/abs/1103.2984)

G. Kowal, E.M. de Gouveia Dal Pino, A. Lazarus, Particle acceleration in turbulence and weakly stochastic reconnection. *Phys. Rev. Lett.* **108**(24), 241102 (2012). <https://doi.org/10.1103/PhysRevLett.108.241102>. [arXiv:1202.5256](https://arxiv.org/abs/1202.5256)

M.M. Kuznetsova, L.M. Zelenyi, Magnetic reconnection in collisionless field reversals the universality of the ion tearing mode. *Geophys. Res. Lett.* **18**(10), 1825–1828 (1991). <https://doi.org/10.1029/91GL02245>

G. Lapenta, Self-feeding turbulent magnetic reconnection on macroscopic scales. *Phys. Rev. Lett.* **100**(23), 235001 (2008)

G. Lapenta, J.U. Brackbill, A kinetic theory for the drift-kink instability. *J. Geophys. Res.* **102**(A12), 27099–27108 (1997). <https://doi.org/10.1029/97JA02140>

G. Lapenta, S. Markidis, M.V. Goldman, D.L. Newman, Secondary reconnection sites in reconnection-generated flux ropes and reconnection fronts. *Nat. Phys.* **11**(8), 690–695 (2015)

G. Lapenta, M. Ashour-Abdalla, R.J. Walker, M. El Alaoui, A multiscale study of ion heating in Earth's magnetotail. *Geophys. Res. Lett.* **43**(2), 515–524 (2016). <https://doi.org/10.1002/2015GL066689>

G. Lapenta, J. Berchem, M. Zhou, R.J. Walker, M. El-Alaoui, M.L. Goldstein, W.R. Paterson, B.L. Giles, C.J. Pollock, C.T. Russell, R.J. Strangeway, R.E. Ergun, Y.V. Khotyaintsev, R.B. Torbert, J.L. Burch, On the origin of the crescent-shaped distributions observed by MMS at the magnetopause. *J. Geophys. Res. Space Phys.* **122**(2), 2024–2039 (2017). <https://doi.org/10.1002/2016JA023290>. [arXiv:1702.03550](https://arxiv.org/abs/1702.03550)

G. Lapenta, F. Pucci, V. Olshevsky, S. Servidio, L. Sorriso-Valvo, D.L. Newman, M.V. Goldman, Nonlinear waves and instabilities leading to secondary reconnection in reconnection outflows. *J. Plasma Phys.* **84**(1), 715840103 (2018). <https://doi.org/10.1017/S002237781800003X>. [arXiv:1808.08612](https://arxiv.org/abs/1808.08612)

G. Lapenta, F. Pucci, M. Goldman, D. Newman, Local regimes of turbulence in 3D magnetic reconnection. *Astrophys. J.* **888**(2), 104 (2020)

A. Lazarian, E.T. Vishniac, Reconnection in a weakly stochastic field. *Astrophys. J.* **517**(2), 700 (1999)

A. Lazarian, G. Elyin, E. Vishniac, G. Kowal, Turbulent reconnection and its implications. *Philos. Trans. R. Soc. Lond. Ser. A* **373**, 20140144 (2015). <https://doi.org/10.1098/rsta.2014.0144>. [arXiv:1502.01396](https://arxiv.org/abs/1502.01396)

A. Lazarian, G.L. Elyin, A. Jafari, G. Kowal, H. Li, S. Xu, E.T. Vishniac, 3D turbulent reconnection: Theory, tests, and astrophysical implications. *Phys. Plasmas* **27**(1), 012305 (2020). <https://doi.org/10.1063/1.5110603>. [arXiv:2001.00868](https://arxiv.org/abs/2001.00868)

O. Le Contel, A. Retinò, H. Breuillard, L. Mirioni, P. Robert, A. Chasapis, B. Lavraud, T. Chust, L. Rezeau, F.D. Wilder, D.B. Graham, M.R. Argall, D.J. Gershman, P.A. Lindqvist, Y.V. Khotyaintsev, G. Marklund, R.E. Ergun, K.A. Goodrich, J.L. Burch, R.B. Torbert, J. Needell, M. Chutter, D. Rau, I. Dors, C.T. Russell, W. Magnes, R.J. Strangeway, K.R. Bromund, H.K. Leinweber, F. Plaschke, D. Fischer, B.J. Anderson, G. Le, T.E. Moore, C.J. Pollock, B.L. Giles, J.C. Dorelli, L. Avanov, Y. Saito, Whistler mode waves and Hall fields detected by MMS during a dayside magnetopause crossing. *Geophys. Res. Lett.* **43**(12), 5943–5952 (2016). <https://doi.org/10.1002/2016GL068968>

J.A. le Roux, W.H. Matthaeus, G.P. Zank, Pickup ion acceleration by turbulent electric fields in the slow solar wind. *Geophys. Res. Lett.* **28**(20), 3831–3834 (2001). <https://doi.org/10.1029/2001GL013400>

J.A. le Roux, G.P. Zank, G.M. Webb, O.V. Khabarova, A kinetic transport theory for particle acceleration and transport in regions of multiple contracting and reconnecting inertial-scale flux ropes. *Astrophys. J.* **801**, 112 (2015). <https://doi.org/10.1088/0004-637X/801/2/112>

J.A. le Roux, G.P. Zank, G.M. Webb, O.V. Khabarova, Combining diffusive shock acceleration with acceleration by contracting and reconnecting small-scale flux ropes at heliospheric shocks. *Astrophys. J.* **827**, 47 (2016)

J.A. le Roux, G.P. Zank, O.V. Khabarova, Self-consistent energetic particle acceleration by contracting and reconnecting small-scale flux ropes: The governing equations. *Astrophys. J.* **864**, 158 (2018)

J.A. le Roux, G.M. Webb, O.V. Khabarova, L.L. Zhao, L. Adhikari, Modeling energetic particle acceleration and transport in a solar wind region with contracting and reconnecting small-scale flux ropes at Earth orbit. *Astrophys. J.* **887**(1), 77 (2019). <https://doi.org/10.3847/1538-4357/ab521f>

R.J. Leamon, W.H. Matthaeus, C.W. Smith, H.K. Wong, Contribution of cyclotron-resonant damping to kinetic dissipation of interplanetary turbulence. *Astrophys. J.* **507**, L181 (1998)

E. Leonardis, S.C. Chapman, W. Daughton, V. Roytershteyn, H. Karimabadi, Identification of intermittent multifractal turbulence in fully kinetic simulations of magnetic reconnection. *Phys. Rev. Lett.* **110**(20), 205002 (2013). <https://doi.org/10.1103/PhysRevLett.110.205002>. [arXiv:1302.1749](https://arxiv.org/abs/1302.1749)

M.M. Leroy, A. Mangeney, A theory of energization of solar wind electrons by the Earth's bow shock. *Ann. Geophys.* **2**, 449–456 (1984)

X. Li, F. Guo, H. Li, G. Li, Nonthermally dominated electron acceleration during magnetic reconnection in a low- β plasma. *Astrophys. J. Lett.* **811**, L24 (2015)

T.C. Li, G.G. Howes, K.G. Klein, J.M. TenBarge, Energy dissipation and Landau damping in two- and three-dimensional plasma turbulence. *Astrophys. J. Lett.* **832**(2), L24 (2016). <https://doi.org/10.3847/2041-8205/832/2/L24>. [arXiv:1510.02842](https://arxiv.org/abs/1510.02842)

X. Li, F. Guo, H. Li, G. Li, Particle acceleration during magnetic reconnection in a low-beta plasma. *Astrophys. J.* **843**(1), 21 (2017). <https://doi.org/10.3847/1538-4357/aa745e>

X. Li, F. Guo, J. Birn, The roles of fluid compression and shear in electron energization during magnetic reconnection. *Astrophys. J.* **855**, 80 (2018)

X. Li, F. Guo, H. Li, Particle acceleration in kinetic simulations of nonrelativistic magnetic reconnection with different ion-electron mass ratios. *Astrophys. J.* **879**(1), 5 (2019). <https://doi.org/10.3847/1538-4357/ab223b>. [arXiv:1905.08797](https://arxiv.org/abs/1905.08797)

H. Liang, P.A. Cassak, S. Servidio, M.A. Shay, J.F. Drake, M. Swisdak, M.R. Argall, J.C. Dorelli, E.E. Scime, W.H. Matthaeus, V. Roytershteyn, G.L. Delzanno, Decomposition of plasma kinetic entropy into position and velocity space and the use of kinetic entropy in particle-in-cell simulations. *Phys. Plasmas* **26**(8), 082903 (2019). <https://doi.org/10.1063/1.5098888>. [arXiv:1902.02733](https://arxiv.org/abs/1902.02733)

H. Liang, M. Hasan Barbhuiya, P.A. Cassak, O. Pezzi, S. Servidio, F. Valentini, G.P. Zank, Kinetic entropy-based measures of distribution function non-Maxwellianity: Theory and simulations (2020). [arXiv:2008.06669](https://arxiv.org/abs/2008.06669)

Y.C.M. Liu, J. Huang, C. Wang, B. Klecker, A.B. Galvin, K.D.C. Simunac, M.A. Popecki, L. Kistler, C. Farrugia, M.A. Lee, H. Kucharek, A. Opitz, J.G. Luhmann, L. Jian, A statistical analysis of heliospheric plasma sheets, heliospheric current sheets, and sector boundaries observed in situ by STEREO. *J. Geophys. Res. Space Phys.* **119**(11), 8721–8732 (2014). <https://doi.org/10.1002/2014JA019956>

N. Loureiro, D. Uzdensky, A. Schekochihin, S. Cowley, T. Yousef, Turbulent magnetic reconnection in two dimensions. *Mon. Not. R. Astron. Soc. Lett.* **399**(1), L146–L150 (2009)

Q. Lu, C. Huang, J. Xie, R. Wang, M. Wu, A. Vaivads, S. Wang, Features of separatrix regions in magnetic reconnection: Comparison of 2-d particle-in-cell simulations and cluster observations. *J. Geophys. Res. Space Phys.* **115**(A11), A11208 (2010). <https://doi.org/10.1029/2010JA015713>. <https://agupubs.onlinelibrary.wiley.com/doi/pdf/10.1029/2010JA015713>

S. Lu, V. Angelopoulos, A.V. Artemyev, P.L. Pritchett, J. Liu, A. Runov, A. Tenerani, C. Shi, M. Velli, Turbulence and particle acceleration in collisionless magnetic reconnection: Effects of temperature inhomogeneity across pre-reconnection current sheet. *Astrophys. J.* **878**(2), 109 (2019a). <https://doi.org/10.3847/1538-4357/ab1f6b>

S. Lu, A.V. Artemyev, V. Angelopoulos, P.L. Pritchett, A. Runov, Effects of cross-sheet density and temperature inhomogeneities on magnetotail reconnection. *Geophys. Res. Lett.* **46**(1), 28–36 (2019b). <https://doi.org/10.1029/2018GL081420>. <https://agupubs.onlinelibrary.wiley.com/doi/pdf/10.1029/2018GL081420>

A.T.Y. Lui, Current disruption in the Earth's magnetosphere: Observations and models. *J. Geophys. Res.* **101**(A6), 13067–13088 (1996). <https://doi.org/10.1029/96JA00079>

V.N. Lutsenko, I.P. Kirpichev, T.V. Grechko, D. Delcourt, Source positions of energetic particles responsible for the fine dispersion structures: Numerical simulation results. *Planet. Space Sci.* **53**(1–3), 275–281 (2005). <https://doi.org/10.1016/j.pss.2004.09.053>

L.R. Lyons, T.W. Speiser, Evidence for current sheet acceleration in the geomagnetic tail. *J. Geophys. Res.* **87**(A4), 2276–2286 (1982). <https://doi.org/10.1029/JA087A04p02276>

M. Lyutikov, Explosive reconnection in magnetars. *Mon. Not. R. Astron. Soc.* **346**(2), 540–554 (2003). <https://doi.org/10.1046/j.1365-2966.2003.07110.x>. <http://oup.prod.sis.lan/mnras/article-pdf/346/2/540/429392/346-2-540.pdf>

Z.W. Ma, A. Bhattacharjee, Hall magnetohydrodynamic reconnection: The geospace environment modeling challenge. *J. Geophys. Res.* **106**, 3773–3782 (2001). <https://doi.org/10.1029/1999JA001004>

O. Malandraki, O. Khabarova, R. Bruno, G.P. Zank, G. Li, B. Jackson, M.M. Bisi, A. Greco, O. Pezzi, W. Matthaeus, A. Chasapis Giannakopoulos, S. Servidio, H. Malova, R. Kislov, F. Effenberger, J. le Roux, Y. Chen, Q. Hu, N.E. Engelbrecht, Current sheets, magnetic islands, and associated particle acceleration in the solar wind as observed by Ulysses near the ecliptic plane. *Astrophys. J.* **881**(2), 116 (2019). <https://doi.org/10.3847/1538-4357/ab289a>

F. Malara, M. Velli, Parametric instability of a large-amplitude nonmonochromatic Alfvén wave. *Phys. Plasmas* **3**(12), 4427–4433 (1996). <https://doi.org/10.1063/1.872043>

F. Malara, P. Veltri, V. Carbone, Competition among nonlinear effects in tearing instability saturation. *Phys. Fluids, B Plasma Phys.* **4**(10), 3070–3086 (1992)

F. Malara, G. Nigro, F. Valentini, L. Sorriso-Valvo, Electron heating by kinetic Alfvén waves in coronal loop turbulence. *Astrophys. J.* **871**(1), 66 (2019). <https://doi.org/10.3847/1538-4357/aaf168>

M.A. Malkov, R.Z. Sagdeev, Cosmic ray transport with magnetic focusing and the “Telegraph” model. *Astrophys. J.* **808**, 157 (2015)

H. Malova, V.Y. Popov, E. Grigorenko, A. Petrukovich, D. Delcourt, A. Sharma, O. Khabarova, L. Zelenyi, Evidence for quasi-adiabatic motion of charged particles in strong current sheets in the solar wind. *Astrophys. J.* **834**(1), 34 (2017). <https://doi.org/10.3847/1538-4357/834/1/34>

H. Malova, V.Y. Popov, O.V. Khabarova, E.E. Grigorenko, A.A. Petrukovich, L.M. Zelenyi, Structure of current sheets with quasi-adiabatic dynamics of particles in the solar wind. *Cosm. Res.* **56**(6), 462–470 (2018). <https://doi.org/10.1134/S0010952518060060>

Y.G. Maneva, S. Poedts, Generation and evolution of anisotropic turbulence and related energy transfer in drifting proton-alpha plasmas. *Astron. Astrophys.* **613**, A10 (2018). <https://doi.org/10.1051/0004-6361/201731204>

Y.G. Maneva, A.F. Viñas, L. Ofman, Turbulent heating and acceleration of He^{++} ions by spectra of Alfvén-cyclotron waves in the expanding solar wind: 1.5-D hybrid simulations. *J. Geophys. Res. Space Phys.* **118**, 2842–2853 (2013). <https://doi.org/10.1002/jgra.50363>

Y.G. Maneva, J.A. Araneda, E. Marsch, Regulation of ion drifts and anisotropies by parametrically unstable finite-amplitude Alfvén-cyclotron waves in the fast solar wind. *Astrophys. J.* **783**(2), 139 (2014). <https://doi.org/10.1088/0004-637X/783/2/139>

Y.G. Maneva, L. Ofman, A. Viñas, Relative drifts and temperature anisotropies of protons and α particles in the expanding solar wind: 2.5D hybrid simulations. *Astron. Astrophys.* **578**, A85 (2015). <https://doi.org/10.1051/0004-6361/201424401>. [arXiv:1410.3358](https://arxiv.org/abs/1410.3358)

A. Mangeney, F. Califano, C. Cavazzoni, P. Travnicek, A numerical scheme for the integration of the Vlasov–Maxwell system of equations. *J. Comput. Phys.* **179**(2), 495–538 (2002)

R. Marino, L. Sorriso-Valvo, V. Carbone, A. Noullez, R. Bruno, B. Bavassano, Heating the solar wind by a magnetohydrodynamic turbulent energy cascade. *Astrophys. J. Lett.* **677**(1), L71 (2008). <https://doi.org/10.1086/587957>

E. Marsch, Kinetic physics of the solar corona and solar wind. *Living Rev. Sol. Phys.* **3**(1), 1 (2006). <https://doi.org/10.12942/lrsp-2006-1>

E. Marsch, C.Y. Tu, Intermittency, non-Gaussian statistics and fractal scaling of MHD fluctuations in the solar wind. *Nonlinear Process. Geophys.* **4**(2), 101–124 (1997)

M.S. Marsh, S. Dalla, J. Kelly, T. Laitinen, Drift-induced perpendicular transport of solar energetic particles. *Astrophys. J.* **774**(1), 4 (2013). <https://doi.org/10.1088/0004-637X/774/1/4>. [arXiv:1307.1585](https://arxiv.org/abs/1307.1585)

B.A. Maruca, J.C. Kasper, S.D. Bale, What are the relative roles of heating and cooling in generating solar wind temperature anisotropies? *Phys. Rev. Lett.* **107**, 201101 (2011). <https://doi.org/10.1103/PhysRevLett.107.201101>

L. Matteini, P. Hellinger, B.E. Goldstein, S. Landi, M. Velli, M. Neugebauer, Signatures of kinetic instabilities in the solar wind. *J. Geophys. Res. Space Phys.* **118**, 2771–2782 (2013). <https://doi.org/10.1002/jgra.50320>

W.H. Matthaeus, S.L. Lamkin, Rapid magnetic reconnection caused by finite amplitude fluctuations. *Phys. Fluids* **28**, 303 (1985)

W.H. Matthaeus, S.L. Lamkin, Turbulent magnetic reconnection. *Phys. Fluids* **29**(8), 2513–2534 (1986)

W.H. Matthaeus, D. Montgomery, Selective decay hypothesis at high mechanical and magnetic Reynolds numbers. *Ann. N.Y. Acad. Sci.* **357**(1), 203–222 (1980)

W.H. Matthaeus, M. Velli, Who needs turbulence? *Space Sci. Rev.* **160**(1–4), 145–168 (2011)

W.H. Matthaeus, J.J. Ambrosiano, M.L. Goldstein, Particle-acceleration by turbulent magnetohydrodynamic reconnection. *Phys. Rev. Lett.* **53**, 1449–1452 (1984). <https://doi.org/10.1103/PhysRevLett.53.1449>

W.H. Matthaeus, M.L. Goldstein, D.A. Roberts, Evidence for the presence of quasi-two-dimensional nearly incompressible fluctuations in the solar wind. *J. Geophys. Res.* **95**, 20673–20683 (1990). <https://doi.org/10.1029/JA095iA12p20673>

W.H. Matthaeus, G. Qin, J.W. Bieber, G.P. Zank, Nonlinear collisionless perpendicular diffusion of charged particles. *Astrophys. J. Lett.* **590**, L53–L56 (2003)

W.H. Matthaeus, J.W. Bieber, D. Ruffolo, P. Chuychai, J. Minnie, Spectral properties and length scales of two-dimensional magnetic field models. *Astrophys. J.* **667**, 956–962 (2007). <https://doi.org/10.1086/520924>

W.H. Matthaeus, M. Wan, S. Servidio, A. Greco, K.T. Osman, S. Oughton, P. Dmitruk, Intermittency, nonlinear dynamics and dissipation in the solar wind and astrophysical plasmas. *Philos. Trans. R. Soc. Lond. Ser. A* **373**(2041), 20140154 (2015). <https://doi.org/10.1098/rsta.2014.0154>

W.H. Matthaeus, Y. Yang, M. Wan, T.N. Parashar, R. Bandyopadhyay, A. Chasapis, O. Pezzi, F. Valentini, Pathways to dissipation in weakly collisional plasmas. *Astrophys. J.* **891**(1), 101 (2020). <https://doi.org/10.3847/1538-4357/ab6d6a>

D.J. McComas, J.L. Phillips, A.J. Hundhausen, J.T. Burkepile, Observations of disconnection of open magnetic structures. *Geophys. Res. Lett.* **18**(1), 73–76 (1991). <https://doi.org/10.1029/90GL02480>

R. Metzler, J. Klafter, The random walk's guide to anomalous diffusion: A fractional dynamics approach. *Phys. Rep.* **339**(1), 1–77 (2000). [https://doi.org/10.1016/S0370-1573\(00\)00070-3](https://doi.org/10.1016/S0370-1573(00)00070-3)

R. Metzler, J. Klafter, TOPICAL REVIEW: The restaurant at the end of the random walk: Recent developments in the description of anomalous transport by fractional dynamics. *J. Phys. A, Math. Gen.* **37**(31), R161–R208 (2004). <https://doi.org/10.1088/0305-4470/37/31/R01>

A.V. Milovanov, L.M. Zelenyi, Development of fractal structure in the solar wind and distribution of magnetic field in the photosphere, in *Washington DC American Geophysical Union Geophysical Monograph Series*, vol. 84 (1994), pp. 43–52. <https://doi.org/10.1029/GM084p0043>

A.V. Milovanov, L.M. Zelenyi, “Strange” Fermi processes and power-law nonthermal tails from a self-consistent fractional kinetic equation. *Phys. Rev. E* **64**, 052101 (2001). <https://doi.org/10.1103/PhysRevE.64.052101>

A.V. Milovanov, L.M. Zelenyi, P. Veltri, G. Zimbardo, A.L. Taktakishvili, Geometric description of the magnetic field and plasma coupling in the near-Earth stretched tail prior to a substorm. *J. Atmos. Sol.-Terr. Phys.* **63**(7), 705–721 (2001). [https://doi.org/10.1016/S1364-6826\(00\)00186-3](https://doi.org/10.1016/S1364-6826(00)00186-3)

O.V. Mingalev, O.V. Khabarova, K.V. Malova, I.V. Mingalev, R.A. Kislov, M.N. Mel’nik, P.V. Setsko, L.M. Zelenyi, G.P. Zank, Modeling of proton acceleration in a magnetic island inside the ripple of the heliospheric current sheet. *Sol. Syst. Res.* **53**(1), 30–55 (2019). <https://doi.org/10.1134/S0038094619010064>

J. Minnie, J.W. Bieber, W.H. Matthaeus, R.A. Burger, Suppression of particle drifts by turbulence. *Astrophys. J.* **670**(2), 1149–1158 (2007). <https://doi.org/10.1086/522026>

K.D. Moloto, N.E. Engelbrecht, R.A. Burger, A simplified ab initio cosmic-ray modulation model with simulated time dependence and predictive capability. *Astrophys. J.* **859**(2), 107 (2018). <https://doi.org/10.3847/1538-4357/aac174>

A.B. Navarro, B. Teaca, D. Told, D. Groselj, P. Crandall, F. Jenko, Structure of plasma heating in gyrokinetic Alfvénic turbulence. *Phys. Rev. Lett.* **117**, 245101 (2016). <https://doi.org/10.1103/PhysRevLett.117.245101>

L. Ofman, A.F. Viñas, Two-dimensional hybrid model of wave and beam heating of multi-ion solar wind plasma. *J. Geophys. Res. Space Phys.* **112**(A6), A06104 (2007). <https://doi.org/10.1029/2006JA012187>

L. Ofman, A.F. Viñas, P.S. Moya, Hybrid models of solar wind plasma heating. *Ann. Geophys.* **29**(6), 1071–1079 (2011). <https://doi.org/10.5194/angeo-29-1071-2011>

M. Øieroset, T.D. Phan, M. Fujimoto, R.P. Lin, R.P. Lepping, In situ detection of collisionless reconnection in the Earth’s magnetotail. *Nature* **412**(6845), 414–417 (2001). <https://doi.org/10.1038/35086520>

M. Oka, T.D. Phan, S. Krucker, M. Fujimoto, I. Shinohara, Electron acceleration by multi-island coalescence. *Astrophys. J.* **714**, 915–926 (2010). <https://doi.org/10.1088/0004-637X/714/1/915>. arXiv:1004.1154

K.T. Osman, W.H. Matthaeus, A. Greco, S. Servidio, Evidence for inhomogeneous heating in the solar wind. *Astrophys. J. Lett.* **727**, L11 (2011). <https://doi.org/10.1088/2041-8205/727/1/L11>

K.T. Osman, W.H. Matthaeus, B. Hnat, S.C. Chapman, Kinetic signatures and intermittent turbulence in the solar wind plasma. *Phys. Rev. Lett.* **108**(26), 261103 (2012a). <https://doi.org/10.1103/PhysRevLett.108.261103>. arXiv:1203.6596

K.T. Osman, W.H. Matthaeus, M. Wan, A.F. Rappazzo, Intermittency and local heating in the solar wind. *Phys. Rev. Lett.* **108**(26), 261102 (2012b). <https://doi.org/10.1103/PhysRevLett.108.261102>

S. Oughton, W.H. Matthaeus, Critical balance and the physics of magnetohydrodynamic turbulence. *Astrophys. J.* **897**(1), 37 (2020). <https://doi.org/10.3847/1538-4357/ab8f2a>. arXiv:2006.04677

S. Oughton, E.R. Priest, W.H. Matthaeus, The influence of a mean magnetic field on three-dimensional magnetohydrodynamic turbulence. *J. Fluid Mech.* **280**, 95–117 (1994)

S. Oughton, W.H. Matthaeus, C.W. Smith, B. Breech, P.A. Isenberg, Transport of solar wind fluctuations: A two-component model. *J. Geophys. Res.* **116**, A08105 (2011). <https://doi.org/10.1029/2010JA016365>

S. Oughton, W.H. Matthaeus, P. Dmitruk, Reduced MHD in astrophysical applications: Two-dimensional or three-dimensional? *Astrophys. J.* **839**(1), 2 (2017). <https://doi.org/10.3847/1538-4357/aa67e2>

I.D. Palmer, Transport coefficients of low-energy cosmic rays in interplanetary space. *Rev. Geophys. Space Phys.* **20**, 335–351 (1982). <https://doi.org/10.1029/RG020i002p00335>

E.V. Panov, J. Büchner, M. Fränz, A. Korth, S.P. Savin, H. Rème, K.H. Fornacon, High-latitude Earth’s magnetopause outside the cusp: Cluster observations. *J. Geophys. Res. Space Phys.* **113**(A1), A01220 (2008). <https://doi.org/10.1029/2006JA012123>

E. Papini, L. Franci, S. Landi, A. Verdini, L. Matteini, P. Hellinger, Can Hall magnetohydrodynamics explain plasma turbulence at sub-ion scales? *Astrophys. J.* **870**(1), 52 (2019). <https://doi.org/10.3847/1538-4357/aaef03>. arXiv:1810.02210

T.N. Parashar, W.H. Matthaeus, Propinquity of current and vortex structures: Effects on collisionless plasma heating. *Astrophys. J.* **832**(1), 57 (2016). <https://doi.org/10.3847/0004-637X/832/1/57>

T.N. Parashar, M.A. Shay, P.A. Cassak, W.H. Matthaeus, Kinetic dissipation and anisotropic heating in a turbulent collisionless plasma. *Phys. Plasmas* **16**(3), 032310 (2009). <https://doi.org/10.1063/1.3094062>

T.N. Parashar, W.H. Matthaeus, M.A. Shay, Dependence of kinetic plasma turbulence on plasma β . *Astrophys. J.* **864**(1), L21 (2018). <https://doi.org/10.3847/2041-8213/aadb8b>. arXiv:1807.11371

E.N. Parker, Sweet’s mechanism for merging magnetic fields in conducting fluids. *J. Geophys. Res.* **62**, 509–520 (1957). <https://doi.org/10.1029/JZ062i004p00509>

E.I. Parkhomenko, H.V. Malova, E.E. Grigorenko, V.Y. Popov, A.A. Petrukovich, D.C. Delcourt, E.A. Kronberg, P.W. Daly, L.M. Zelenyi, Acceleration of plasma in current sheet during substorm dipolarizations

in the Earth's magnetotail: Comparison of different mechanisms. *Phys. Plasmas* **26**(4), 042901 (2019). <https://doi.org/10.1063/1.5082715>

F. Pecora, S. Servidio, A. Greco, W.H. Matthaeus, D. Burgess, C.T. Haynes, V. Carbone, P. Veltri, Ion diffusion and acceleration in plasma turbulence. *J. Plasma Phys.* **84**(6), 725840601 (2018)

F. Pecora, A. Greco, Q. Hu, S. Servidio, A.G. Chasapis, W.H. Matthaeus, Single-spacecraft identification of flux tubes and current sheets in the solar wind. *Astrophys. J.* **881**(1), L11 (2019a). <https://doi.org/10.3847/2041-8213/ab32d9>

F. Pecora, F. Pucci, G. Lapenta, D. Burgess, S. Servidio, Statistical analysis of ions in two-dimensional plasma turbulence. *Sol. Phys.* **294**(9), 114 (2019b). <https://doi.org/10.1007/s11207-019-1507-6>

C. Pei, J.W. Bieber, R.A. Burger, J. Clem, Three-dimensional wavy heliospheric current sheet drifts. *Astrophys. J.* **744**(2), 170 (2012). <https://doi.org/10.1088/0004-637X/744/2/170>

R. Pellat, F.V. Coroniti, P.L. Pritchett, Does ion tearing exist? *Geophys. Res. Lett.* **18**(2), 143–146 (1991). <https://doi.org/10.1029/91GL00123>

S. Perri, G. Zimbardo, Evidence of superdiffusive transport of electrons accelerated at interplanetary shocks. *Astrophys. J. Lett.* **671**(2), L177–L180 (2007). <https://doi.org/10.1086/525523>

S. Perri, G. Zimbardo, Superdiffusive shock acceleration. *Astrophys. J.* **750**(2), 87 (2012). <https://doi.org/10.1088/0004-637X/750/2/87>

S. Perri, D. Perrone, E. Yordanova, L. Sorriso-Valvo, W.R. Paterson, D.J. Gershman, B.L. Giles, C.J. Pollock, J.C. Dorelli, L.A. Avanov, B. Lavraud, Y. Saito, R. Nakamura, D. Fischer, W. Baumjohann, F. Plaschke, Y. Narita, W. Magnes, C.T. Russell, R.J. Strangeway, O.L. Contel, Y. Khotyaintsev, F. Valentini, On the deviation from Maxwellian of the ion velocity distribution functions in the turbulent magnetosheath. *J. Plasma Phys.* **86**(1), 905860108 (2020). <https://doi.org/10.1017/S0022377820000021>. arXiv:1905.09466

D. Perrone, F. Valentini, P. Veltri, The role of alpha particles in the evolution of the solar-wind turbulence toward short spatial scales. *Astrophys. J.* **741**(1), 43 (2011). <http://stacks.iop.org/0004-637X/741/i=1/a=43>

D. Perrone, F. Valentini, S. Servidio, S. Dalena, P. Veltri, Vlasov simulations of multi-ion plasma turbulence in the solar wind. *Astrophys. J.* **762**(2), 99 (2013). <http://stacks.iop.org/0004-637X/762/i=2/a=99>

D. Perrone, S. Bourouaine, F. Valentini, E. Marsch, P. Veltri, Generation of temperature anisotropy for alpha particle velocity distributions in solar wind at 0.3 AU: Vlasov simulations and Helios observations. *J. Geophys. Res. Space Phys.* **119**(4), 2400–2410 (2014a). <https://doi.org/10.1002/2013JA019564>

D. Perrone, F. Valentini, S. Servidio, S. Dalena, P. Veltri, Analysis of intermittent heating in a multi-component turbulent plasma. *Eur. Phys. J. D* **68**(7), 209 (2014b). <https://doi.org/10.1140/epjd/e2014-50152-1>

D. Perrone, T. Passot, D. Laveder, F. Valentini, P.L. Sulem, I. Zouganelis, P. Veltri, S. Servidio, Fluid simulations of plasma turbulence at ion scales: Comparison with Vlasov-Maxwell simulations. *Phys. Plasmas* **25**(5), 052302 (2018). <https://doi.org/10.1063/1.5026656>

O. Pezzi, Solar wind collisional heating. *J. Plasma Phys.* **83**(3), 555830301 (2017). <https://doi.org/10.1017/S0022377817000368>

O. Pezzi, F. Valentini, P. Veltri, Collisional relaxation: Landau versus Dougherty operator. *J. Plasma Phys.* **81**(1), 305810107 (2015). <https://doi.org/10.1017/S0022377814000877>

O. Pezzi, E. Camporeale, F. Valentini, Collisional effects on the numerical recurrence in Vlasov-Poisson simulations. *Phys. Plasmas* **23**(2), 022103 (2016a). <https://doi.org/10.1063/1.4940963>

O. Pezzi, F. Valentini, P. Veltri, Collisional relaxation of fine velocity structures in plasmas. *Phys. Rev. Lett.* **116**(14), 145001 (2016b). <https://doi.org/10.1103/PhysRevLett.116.145001>

O. Pezzi, F. Malara, S. Servidio, F. Valentini, T.N. Parashar, W.H. Matthaeus, P. Veltri, Turbulence generation during the head-on collision of Alfvénic wave packets. *Phys. Rev. E* **96**, 023201 (2017a). <https://doi.org/10.1103/PhysRevE.96.023201>

O. Pezzi, T.N. Parashar, S. Servidio, F. Valentini, C.L. Vásconez, Y. Yang, F. Malara, W.H. Matthaeus, P. Veltri, Colliding Alfvénic wave packets in magnetohydrodynamics, Hall and kinetic simulations. *J. Plasma Phys.* **83**(1), 705830108 (2017b). <https://doi.org/10.1017/S0022377817000113>

O. Pezzi, T.N. Parashar, S. Servidio, F. Valentini, C.L. Vásconez, Y. Yang, F. Malara, W.H. Matthaeus, P. Veltri, Revisiting a classic: The Parker–Moffatt problem. *Astrophys. J.* **834**(2), 166 (2017c). <http://stacks.iop.org/0004-637X/834/i=2/a=166>

O. Pezzi, S. Servidio, D. Perrone, F. Valentini, L. Sorriso-Valvo, A. Greco, W.H. Matthaeus, P. Veltri, Velocity-space cascade in magnetized plasmas: Numerical simulations. *Phys. Plasmas* **25**(6), 060704 (2018). <https://doi.org/10.1063/1.5027685>

O. Pezzi, G. Cozzani, F. Califano, F. Valentini, M. Guarrazi, E. Camporeale, G. Brunetti, A. Retinò, P. Veltri, Vida: A Vlasov–Darwin solver for plasma physics at electron scales. *J. Plasma Phys.* **85**(5), 905850506 (2019a). <https://doi.org/10.1017/S0022377819000631>

O. Pezzi, D. Perrone, S. Servidio, F. Valentini, L. Sorriso-Valvo, P. Veltri, Proton-proton collisions in the turbulent solar wind: Hybrid Boltzmann-Maxwell simulations. *Astrophys. J.* **887**, 208 (2019b). <https://iopscience.iop.org/article/10.3847/1538-4357/ab5285>

O. Pezzi, Y. Yang, F. Valentini, S. Servidio, A. Chasapis, W.H. Matthaeus, P. Veltri, Energy conversion in turbulent weakly collisional plasmas: Eulerian hybrid Vlasov-Maxwell simulations. *Phys. Plasmas* **26**(7), 072301 (2019c). <https://doi.org/10.1063/1.5100125>. [arXiv:1904.07715](https://arxiv.org/abs/1904.07715)

O. Pezzi et al., Dissipation measures in weakly-collisional plasmas. *J. Plasma Phys.* (subm) (2020)

T.D. Phan, J.P. Eastwood, P.A. Cassak, M. Øieroset, J.T. Gosling, D.J. Gershman, F.S. Mozer, M.A. Shay, M. Fujimoto, W. Daughton, J.F. Drake, J.L. Burch, R.B. Torbert, R.E. Ergun, L.J. Chen, S. Wang, C. Pollock, J.C. Dorelli, B. Lavraud, B.L. Giles, T.E. Moore, Y. Saito, L.A. Avanov, W. Paterson, R.J. Strangeway, C.T. Russell, Y. Khotyaintsev, P.A. Lindqvist, M. Oka, F.D. Wilder, MMS observations of electron-scale filamentary currents in the reconnection exhaust and near the x line. *Geophys. Res. Lett.* **43**(12), 6060–6069 (2016). <https://doi.org/10.1002/2016GL069212>

T.D. Phan, J.P. Eastwood, M. Shay, J. Drake, B.Ö. Sonnerup, M. Fujimoto, P. Cassak, M. Øieroset, J. Burch, R. Torbert et al., Electron magnetic reconnection without ion coupling in Earth's turbulent magnetosheath. *Nature* **557**(7704), 202 (2018)

M.S. Potgieter, Solar modulation of cosmic rays. *Living Rev. Sol. Phys.* **10**(1), 3 (2013). <https://doi.org/10.12942/lrsp-2013-3>. [arXiv:1306.4421](https://arxiv.org/abs/1306.4421)

E.R. Priest, D.I. Pontin, Three-dimensional null point reconnection regimes. *Phys. Plasmas* **16**(12), 122101 (2009). <https://doi.org/10.1063/1.3257901>

L. Primavera, F. Malara, S. Servidio, G. Nigro, P. Veltri, Parametric instability in two-dimensional Alfvénic turbulence. *Astrophys. J.* **880**(2), 156 (2019). <https://doi.org/10.3847/1538-4357/ab29f5>

P. Pritchett, Collisionless magnetic reconnection in an asymmetric current sheet. *J. Geophys. Res. Space Phys.* **113**, A06210 (2008)

P.L. Pritchett, The influence of intense electric fields on three-dimensional asymmetric magnetic reconnection. *Phys. Plasmas* **20**(6), 061204 (2013). <https://doi.org/10.1063/1.4811123>

P.L. Pritchett, Three-dimensional structure and kinetic features of reconnection exhaust jets. *J. Geophys. Res. Space Phys.* **121**(1), 214–226 (2016). <https://doi.org/10.1002/2015JA022053>

P.L. Pritchett, F.V. Coroniti, V.K. Decyk, Three-dimensional stability of thin quasi-neutral current sheets. *J. Geophys. Res.* **101**(A12), 27413–27430 (1996). <https://doi.org/10.1029/96JA02665>

F. Pucci, C.L. Vásconez, O. Pezzi, S. Servidio, F. Valentini, W.H. Matthaeus, F. Malara, From Alfvén waves to kinetic Alfvén waves in an inhomogeneous equilibrium structure. *J. Geophys. Res. Space Phys.* **121**(2), 1024–1045 (2016). <https://doi.org/10.1002/2015JA022216>

F. Pucci, S. Servidio, L. Sorriso-Valvo, V. Olshevsky, W.H. Matthaeus, F. Malara, M.V. Goldman, D.L. Newman, G. Lapenta, Properties of turbulence in the reconnection exhaust: Numerical simulations compared with observations. *Astrophys. J.* **841**(1), 60 (2017a). <https://doi.org/10.3847/1538-4357/aa704f>

F. Pucci, M. Velli, A. Tenerani, Fast magnetic reconnection: “Ideal” tearing and the Hall effect. *Astrophys. J.* **845**(1), 25 (2017b). <https://doi.org/10.3847/1538-4357/aa7b82>. [arXiv:1704.08793](https://arxiv.org/abs/1704.08793)

F. Pucci, W.H. Matthaeus, A. Chasapis, S. Servidio, L. Sorriso-Valvo, V. Olshevsky, D.L. Newman, M.V. Goldman, G. Lapenta, Generation of turbulence in colliding reconnection jets. *Astrophys. J.* **867**(1), 10 (2018a). <https://doi.org/10.3847/1538-4357/aadd0a>

F. Pucci, M. Velli, A. Tenerani, D. Del Sarto, Onset of fast “ideal” tearing in thin current sheets: Dependence on the equilibrium current profile. *Phys. Plasmas* **25**(3), 032113 (2018b). <https://doi.org/10.1063/1.5022988>. [arXiv:1801.08412](https://arxiv.org/abs/1801.08412)

R.A. Qudsi, R. Bandyopadhyay, B.A. Maruca, T.N. Parashar, W.H. Matthaeus, C. Ar, S.P. Gary, B.L. Giles, D.J. Gershman, C.J. Pollock, R.J. Strangeway, R.B. Torbert, T.E. Moore, J.L. Burch, Intermittency and ion temperature-anisotropy instabilities: Simulation and magnetosheath observation. *Astrophys. J.* **895**(2), 83 (2020). <https://doi.org/10.3847/1538-4357/ab89ad>. [arXiv:2004.06164](https://arxiv.org/abs/2004.06164)

A.F. Rappazzo, M. Velli, G. Einaudi, R.B. Dahlburg, Coronal heating, weak MHD turbulence, and scaling laws. *Astrophys. J. Lett.* **657**(1), L47–L51 (2007). <https://doi.org/10.1086/512975>. [arXiv:astro-ph/0701872](https://arxiv.org/abs/astro-ph/0701872)

A.F. Rappazzo, M. Velli, G. Einaudi, Shear photospheric forcing and the origin of turbulence in coronal loops. *Astrophys. J.* **722**(1), 65–78 (2010). <https://doi.org/10.1088/0004-637X/722/1/65>. [arXiv:1003.3872](https://arxiv.org/abs/1003.3872)

A.F. Rappazzo, W.H. Matthaeus, D. Ruffolo, M. Velli, S. Servidio, Coronal heating topology: The interplay of current sheets and magnetic field lines. *Astrophys. J.* **844**(1), 87 (2017). <https://doi.org/10.3847/1538-4357/aa79f2>. [arXiv:1706.08983](https://arxiv.org/abs/1706.08983)

A. Retinò, D. Sundkvist, A. Vaivads, F. Mozer, M. André, C.J. Owen, In situ evidence of magnetic reconnection in turbulent plasma. *Nat. Phys.* **3**, 236–238 (2007). <https://doi.org/10.1038/nphys574>

V. Réville, M. Velli, A.P. Rouillard, B. Lavraud, A. Tenerani, C. Shi, A. Strugarek, Tearing instability and periodic density perturbations in the slow solar wind. *Astrophys. J. Lett.* **895**(1), L20 (2020). <https://doi.org/10.3847/2041-8213/ab911d>. [arXiv:2005.02679](https://arxiv.org/abs/2005.02679)

B.B. Rossi, S. Olbert, *Introduction to the Physics of Space* (McGraw-Hill, New York, 1970)

V. Roytershteyn, S. Boldyrev, G.L. Delzanno, C.H.K. Chen, D. Grošelj, N.F. Loureiro, Numerical study of inertial kinetic-Alfvén turbulence. *Astrophys. J.* **870**(2), 103 (2019). <https://doi.org/10.3847/1538-4357/aaf288>

A. Ruffenach, B. Lavraud, M.J. Owens, J.A. Sauvaud, N.P. Savani, A.P. Rouillard, P. Démoulin, C. Fouillon, A. Opitz, A. Fedorov, C.J. Jacquey, V. Génot, P. Louarn, J.G. Luhmann, C.T. Russell, C.J. Farrugia, A.B. Galvin, Multispacecraft observation of magnetic cloud erosion by magnetic reconnection during propagation. *J. Geophys. Res. Space Phys.* **117**(A9), A09101 (2012). <https://doi.org/10.1029/2012JA017624>

D. Ruffolo, W.H. Matthaeus, P. Chuychai, Trapping of solar energetic particles by the small-scale topology of solar wind turbulence. *Astrophys. J. Lett.* **597**, L169–L172 (2003). <https://doi.org/10.1086/379847>

D. Ruffolo, T. Pianpanit, W.H. Matthaeus, P. Chuychai, Random ballistic interpretation of nonlinear guiding center theory. *Astrophys. J. Lett.* **747**, L34 (2012). <https://doi.org/10.1088/2041-8205/747/2/L34>

A. Runov, V.A. Sergeev, W. Baumjohann, R. Nakamura, S. Apatenkov, Y. Asano, M. Volwerk, Z. Vörös, T.L. Zhang, A. Petrukovich, A. Balogh, J.A. Sauvaud, B. Klecker, H. Rème, Electric current and magnetic field geometry in flapping magnetotail current sheets. *Ann. Geophys.* **23**(4), 1391–1403 (2005). <https://doi.org/10.5194/angeo-23-1391-2005>

A. Runov, V.A. Sergeev, R. Nakamura, W. Baumjohann, S. Apatenkov, Y. Asano, T. Takada, M. Volwerk, Z. Vörös, T.L. Zhang, J.A. Sauvaud, H. Rème, A. Balogh, Local structure of the magnetotail current sheet: 2001 cluster observations. *Ann. Geophys.* **24**(1), 247–262 (2006). <https://doi.org/10.5194/angeo-24-247-2006>

F. Sahraoui, M.L. Goldstein, P. Robert, Y.V. Khotyaintsev, Evidence of a cascade and dissipation of solar-wind turbulence at the electron gyroscale. *Phys. Rev. Lett.* **102**(23), 231102 (2009). <https://doi.org/10.1103/PhysRevLett.102.231102>

C.S. Salem, G.G. Howes, D. Sundkvist, S.D. Bale, C.C. Chaston, C.H.K. Chen, F.S. Mozer, Identification of kinetic Alfvén wave turbulence in the solar wind. *Astrophys. J. Lett.* **745**(1), L9 (2012). <https://doi.org/10.1088/2041-8205/745/1/L9>

E. Sanchez-Diaz, A.P. Rouillard, B. Lavraud, E. Kilpua, J.A. Davies, In situ measurements of the variable slow solar wind near sector boundaries. *Astrophys. J.* **882**(1), 51 (2019). <https://doi.org/10.3847/1538-4357/ab341c>

E.T. Sarris, S.M. Krimigis, C.O. Bostrom, T. Iijima, T.P. Armstrong, Location of the source of magnetospheric energetic particle bursts by multispacecraft observations. *Geophys. Res. Lett.* **3**(8), 437–440 (1976). <https://doi.org/10.1029/GL003i008p00437>

K.H. Schatten, Large-scale properties of the interplanetary magnetic field. *Rev. Geophys. Space Phys.* **9**, 773–812 (1971). <https://doi.org/10.1029/RG009i003p00773>

A.A. Schekochihin, S.C. Cowley, W. Dorland, G.W. Hammett, G.G. Howes, E. Quataert, T. Tatsuno, Astrophysical gyrokinetics: Kinetic and fluid turbulent cascades in magnetized weakly collisional plasmas. *Astrophys. J. Suppl. Ser.* **182**(1), 310–377 (2009). <https://doi.org/10.1088/0067-0049/182/1/310>. [arXiv:0704.0044](https://arxiv.org/abs/0704.0044)

A.A. Schekochihin, J.T. Parker, E.G. Highcock, P.J. Dellar, W. Dorland, G.W. Hammett, Phase mixing versus nonlinear advection in drift-kinetic plasma turbulence. *J. Plasma Phys.* **82**(2), 905820212 (2016). <https://doi.org/10.1017/S0022377816000374>. [arXiv:1508.05988](https://arxiv.org/abs/1508.05988)

K. Schindler, Theories of tail structures. *Space Sci. Rev.* **23**(3), 365–374 (1979). <https://doi.org/10.1007/BF00172245>. (Article published in the special issues: Proceedings of the Symposium on Solar Terrestrial Physics held in Innsbruck, May–June 1978 (pp. 137–538).)

K. Schindler, M. Hesse, J. Birn, General magnetic reconnection, parallel electric fields, and helicity. *J. Geophys. Res.* **93**, 5547–5557 (1988). <https://doi.org/10.1029/JA093iA06p05547>

H. Schmitz, R. Grauer, Darwin–Vlasov simulations of magnetised plasmas. *J. Comput. Phys.* **214**(2), 738–756 (2006)

J.D. Scudder, W. Daughton, “Illuminating” electron diffusion regions of collisionless magnetic reconnection using electron agyrotropy. *J. Geophys. Res.* **113**, A06222 (2008). <https://doi.org/10.1029/2008JA013035>

A. Serianni, D. Ruffolo, W.H. Matthaeus, P. Chuychai, Dropouts in solar energetic particles: Associated with local trapping boundaries or current sheets? *Astrophys. J.* **711**, 980–989 (2010). <https://doi.org/10.1088/0004-637X/711/2/980>

S. Servidio, V. Carbone, L. Primavera, P. Veltri, K. Stasiewicz, Compressible turbulence in Hall magnetohydrodynamics. *Planet. Space Sci.* **55**(15), 2239–2243 (2007). <https://doi.org/10.1016/j.pss.2007.05.023>

S. Servidio, W.H. Matthaeus, M.A. Shay, P.A. Cassak, P. Dmitruk, Magnetic reconnection in two-dimensional magnetohydrodynamic turbulence. *Phys. Rev. Lett.* **102**(11), 115003 (2009). <https://doi.org/10.1103/PhysRevLett.102.115003>

S. Servidio, W.H. Matthaeus, M.A. Shay, P. Dmitruk, P.A. Cassak, M. Wan, Statistics of magnetic reconnection in two-dimensional magnetohydrodynamic turbulence. *Phys. Plasmas* **17**(3), 032315 (2010). <https://doi.org/10.1063/1.3368798>

S. Servidio, P. Dmitruk, A. Greco, M. Wan, S. Donato, P. Cassak, M. Shay, V. Carbone, W. Matthaeus, Magnetic reconnection as an element of turbulence. *Nonlinear Process. Geophys.* **18**(5), 675–695 (2011a)

S. Servidio, A. Greco, W.H. Matthaeus, K.T. Osman, P. Dmitruk, Statistical association of discontinuities and reconnection in magnetohydrodynamic turbulence. *J. Geophys. Res. Space Phys.* **116**(A9), A09102 (2011b). <https://doi.org/10.1029/2011JA016569>

S. Servidio, F. Valentini, F. Califano, P. Veltri, Local kinetic effects in two-dimensional plasma turbulence. *Phys. Rev. Lett.* **108**(4), 045001 (2012). <https://doi.org/10.1103/PhysRevLett.108.045001>

S. Servidio, K.T. Osman, F. Valentini, D. Perrone, F. Califano, S. Chapman, W.H. Matthaeus, P. Veltri, Proton kinetic effects in Vlasov and solar wind turbulence. *Astrophys. J. Lett.* **781**(2), L27 (2014). <https://doi.org/10.1088/2041-8205/781/2/L27>. [arXiv:1306.6455](https://arxiv.org/abs/1306.6455)

S. Servidio, F. Valentini, D. Perrone, A. Greco, F. Califano, W.H. Matthaeus, P. Veltri, A kinetic model of plasma turbulence. *J. Plasma Phys.* **81**(1), 325810107 (2015). <https://doi.org/10.1017/S0022377814000841>

S. Servidio, C.T. Haynes, W.H. Matthaeus, D. Burgess, V. Carbone, P. Veltri, Explosive particle dispersion in plasma turbulence. *Phys. Rev. Lett.* **117**, 095101 (2016). <https://doi.org/10.1103/PhysRevLett.117.095101>

S. Servidio, A. Chasapis, W.H. Matthaeus, D. Perrone, F. Valentini, T.N. Parashar, P. Veltri, D. Gershman, C.T. Russell, B. Giles, S.A. Fuselier, T.D. Phan, J. Burch, Magnetospheric multiscale observation of plasma velocity-space cascade: Hermite representation and theory. *Phys. Rev. Lett.* **119**, 205101 (2017). <https://doi.org/10.1103/PhysRevLett.119.205101>

A. Shalchi, *Nonlinear Cosmic Ray Diffusion Theories*. Astrophysics and Space Science Library, vol. 362 (Springer, Berlin, 2009). <https://doi.org/10.1007/978-3-642-00309-7>

A. Shalchi, A unified particle diffusion theory for cross-field scattering: Subdiffusion, recovery of diffusion, and diffusion in three-dimensional turbulence. *Astrophys. J. Lett.* **720**(2), L127–L130 (2010). <https://doi.org/10.1088/2041-8205/720/2/L127>

A. Shalchi, G. Li, G.P. Zank, Analytic forms of the perpendicular cosmic ray diffusion coefficient for an arbitrary turbulence spectrum and applications on transport of Galactic protons and acceleration at interplanetary shocks. *Astrophys. Space Sci.* **325**(1), 99–111 (2010). <https://doi.org/10.1007/s10509-009-0168-6>

M.A. Shay, J.F. Drake, M. Swisdak, Two-scale structure of the electron dissipation region during collisionless magnetic reconnection. *Phys. Rev. Lett.* **99**(15), 155002 (2007). <https://doi.org/10.1103/PhysRevLett.99.155002>. [arXiv:0704.0818](https://arxiv.org/abs/0704.0818)

M.A. Shay, C.C. Haggerty, T.D. Phan, J.F. Drake, P.A. Cassak, P. Wu, M. Oieroset, M. Swisdak, K. Malakit, Electron heating during magnetic reconnection: A simulation scaling study. *Phys. Plasmas* **21**(12), 122902 (2014). <https://doi.org/10.1063/1.4904203>. [arXiv:1410.1206](https://arxiv.org/abs/1410.1206)

M.A. Shay, T.D. Phan, C.C. Haggerty, M. Fujimoto, J.F. Drake, K. Malakit, P.A. Cassak, M. Swisdak, Kinetic signatures of the region surrounding the X line in asymmetric (magnetopause) reconnection. *Geophys. Res. Lett.* **43**(9), 4145–4154 (2016). <https://doi.org/10.1002/2016GL069034>. [arXiv:1602.00779](https://arxiv.org/abs/1602.00779)

M.A. Shay, C.C. Haggerty, W.H. Matthaeus, T.N. Parashar, M. Wan, P. Wu, Turbulent heating due to magnetic reconnection. *Phys. Plasmas* **25**(1), 012304 (2018). <https://doi.org/10.1063/1.4993423>

J.V. Shebalin, W.H. Matthaeus, D. Montgomery, Anisotropy in MHD turbulence due to a mean magnetic field. *J. Plasma Phys.* **29**, 525–547 (1983). <https://doi.org/10.1017/S0022377800000933>

J.R. Shuster, D.J. Gershman, L.J. Chen, S. Wang, N. Bessho, J.C. Dorelli, D.E. da Silva, B.L. Giles, W.R. Paterson, R.E. Denton, S.J. Schwartz, C. Norgren, F.D. Wilder, P.A. Cassak, M. Swisdak, V. Uritsky, C. Schiff, A.C. Rager, S. Smith, L.A. Avanov, A.F. Viñas, MMS measurements of the Vlasov equation: Probing the electron pressure divergence within thin current sheets. *Geophys. Res. Lett.* **46**(14), 7862–7872 (2019). <https://doi.org/10.1029/2019GL083549>

I. Silin, J. Büchner, L. Zelenyi, Instabilities of collisionless current sheets: Theory and simulations. *Phys. Plasmas* **9**, 1104–1112 (2002). <https://doi.org/10.1063/1.1459056>

N. Sioulas, H. Isliker, L. Vlahos, Stochastic turbulent acceleration in a fractal environment. *Astrophys. J. Lett.* **895**(1), L14 (2020). <https://doi.org/10.3847/2041-8213/ab9092>. [arXiv:2005.02668](https://arxiv.org/abs/2005.02668)

M.I. Sitnov, H.V. Malova, A.T.Y. Lui, Quasi-neutral sheet tearing instability induced by electron preferential acceleration from stochasticity. *J. Geophys. Res.* **102**(A1), 163–174 (1997). <https://doi.org/10.1029/96JA01872>

M.I. Sitnov, A.S. Sharma, P.N. Guzdar, P.H. Yoon, Reconnection onset in the tail of Earth’s magnetosphere. *J. Geophys. Res. Space Phys.* **107**(A9), 1256 (2002). <https://doi.org/10.1029/2001JA009148>

M.I. Sitnov, A.T.Y. Lui, P.N. Guzdar, P.H. Yoon, Current-driven instabilities in forced current sheets. *J. Geophys. Res. Space Phys.* **109**(A3), A03205 (2004). <https://doi.org/10.1029/2003JA010123>

V. Skoutnev, A. Hakim, J. Juno, J.M. TenBarge, Temperature-dependent saturation of Weibel-type instabilities in counter-streaming plasmas. *Astrophys. J. Lett.* **872**(2), L28 (2019). <https://doi.org/10.3847/2041-8213/ab0556>. [arXiv:1902.08672](https://arxiv.org/abs/1902.08672)

J.A. Slavin, Mercury's magnetosphere. *Adv. Space Res.* **33**(11), 1859–1874 (2004). <https://doi.org/10.1016/j.asr.2003.02.019>

J.A. Slavin, M.H. Acuña, B.J. Anderson, D.N. Baker, M. Benna, G. Gloeckler, R.E. Gold, G.C. Ho, R.M. Killen, H. Korth, S.M. Krimigis, R.L. McNutt, L.R. Nittler, J.M. Raines, D. Schriver, S.C. Solomon, R.D. Starr, P. Trávníček, T.H. Zurbuchen, Mercury's magnetosphere after MESSENGER's first flyby. *Science* **321**(5885), 85 (2008). <https://doi.org/10.1126/science.1159040>

C.W. Smith, W.H. Matthaeus, G.P. Zank, N.F. Ness, S. Oughton, J.D. Richardson, Heating of the low-latitude solar wind by dissipation of turbulent magnetic fluctuations. *J. Geophys. Res. Space Phys.* **106**(A5), 8253–8272 (2001)

D. Smith, S. Ghosh, P. Dmitruk, W.H. Matthaeus, Hall and turbulence effects on magnetic reconnection. *Geophys. Res. Lett.* **31**(2), L02805 (2004). <https://doi.org/10.1029/2003GL018689> <https://agupubs.onlinelibrary.wiley.com/doi/pdf/10.1029/2003GL018689>

C.W. Smith, P.A. Isenberg, W.H. Matthaeus, J.D. Richardson, Turbulent heating of the solar wind by newborn interstellar pickup protons. *Astrophys. J.* **638**(1), 508–517 (2006). <https://doi.org/10.1086/498671>

B.V. Somov, The solar corona: Why it is interesting for us. *Astron. Tsirkulyar* **1596**, 1–6 (2013)

H.Q. Song, Y. Chen, K. Liu, S.W. Feng, L.D. Xia, Quasi-periodic releases of streamer blobs and velocity variability of the slow solar wind near the Sun. *Sol. Phys.* **258**(1), 129–140 (2009). <https://doi.org/10.1007/s11207-009-9411-0> [arXiv:0907.0819](https://arxiv.org/abs/0907.0819)

B.U.Ö. Sonnerup, Magnetic field reconnection, in *Solar System Plasma Physics (A79-53667 24-46)*, vol. 3 (North-Holland, Amsterdam, 1979), pp. 45–108

L. Sorriso-Valvo, V. Carbone, P. Veltri, G. Consolini, R. Bruno, Intermittency in the solar wind turbulence through probability distribution functions of fluctuations. *Geophys. Res. Lett.* **26**(13), 1801–1804 (1999). <https://doi.org/10.1029/1999GL900270> [arXiv:physics/9903043](https://arxiv.org/abs/physics/9903043)

L. Sorriso-Valvo, R. Marino, V. Carbone, A. Noullez, F. Lepreti, P. Veltri, R. Bruno, B. Bavassano, E. Pietropaolo, Observation of inertial energy cascade in interplanetary space plasma. *Phys. Rev. Lett.* **99**(11), 115001 (2007). <https://doi.org/10.1103/PhysRevLett.99.115001> [arXiv:astro-ph/0702264](https://arxiv.org/abs/astro-ph/0702264)

L. Sorriso-Valvo, D. Perrone, O. Pezzi, F. Valentini, S. Servidio, I. Zouganelis, P. Veltri, Local energy transfer rate and kinetic processes: The fate of turbulent energy in two-dimensional hybrid Vlasov–Maxwell numerical simulations. *J. Plasma Phys.* **84**(2), 725840201 (2018). <https://doi.org/10.1017/S0022377818000302>

L. Sorriso-Valvo, F. Catapano, A. Retinò, O. Le Contel, D. Perrone, O.W. Roberts, J.T. Coburn, V. Panebianco, F. Valentini, S. Perri, A. Greco, F. Malara, V. Carbone, P. Veltri, O. Pezzi, F. Fraternale, F. Di Mare, R. Marino, B. Giles, T.E. Moore, C.T. Russell, R.B. Torbert, J.L. Burch, Y.V. Khotyaintsev, Turbulence-driven ion beams in the magnetospheric Kelvin-Helmholtz instability. *Phys. Rev. Lett.* **122**, 035102 (2019). <https://doi.org/10.1103/PhysRevLett.122.035102>

T.W. Speiser, Particle trajectories in model current sheets, 1, analytical solutions. *J. Geophys. Res.* **70**(17), 4219–4226 (1965). <https://doi.org/10.1029/JZ070i017p04219>

J.E. Stawarz, J.P. Eastwood, K.J. Genestreti, R. Nakamura, R.E. Ergun, D. Burgess, J.L. Burch, S.A. Fuselier, D.J. Gershman, B.L. Giles, O. Le Contel, P.A. Lindqvist, C.T. Russell, R.B. Torbert, Intense electric fields and electron-scale substructure within magnetotail flux ropes as revealed by the magnetospheric multiscale mission. *Geophys. Res. Lett.* **45**(17), 8783–8792 (2018). <https://doi.org/10.1029/2018GL079095>

J.E. Stawarz, J.P. Eastwood, T.D. Phan, I.L. Gingell, M.A. Shay, J.L. Burch, R.E. Ergun, B.L. Giles, D.J. Gershman, O.L. Contel, P.A. Lindqvist, C.T. Russell, R.J. Strangeway, R.B. Torbert, M.R. Argall, D. Fischer, W. Magnes, L. Franci, Properties of the turbulence associated with electron-only magnetic reconnection in Earth's magnetosheath. *Astrophys. J.* **877**(2), L37 (2019). <https://doi.org/10.3847/2041-8213/ab21c8>

R.D. Strauss, M.S. Potgieter, I. Büsching, A. Kopp, Modelling heliospheric current sheet drift in stochastic cosmic ray transport models. *Astrophys. Space Sci.* **339**(2), 223–236 (2012). <https://doi.org/10.1007/s10509-012-1003-z>

P.A. Sturrock, Stochastic acceleration. *Phys. Rev.* **141**, 186–191 (1966). <https://doi.org/10.1103/PhysRev.141.186>

D. Sundkvist, A. Retinò, A. Vaivads, S.D. Bale, Dissipation in turbulent plasma due to reconnection in thin current sheets. *Phys. Rev. Lett.* **99**, 025004 (2007). <https://doi.org/10.1103/PhysRevLett.99.025004>

S.I. Syrovatskiĭ, Formation of current sheets in a plasma with a frozen-in strong magnetic field. *Sov. Phys. JETP* **33**, 933 (1971)

T. Tatsuno, W. Dorland, A.A. Schekochihin, G.G. Plunk, M. Barnes, S.C. Cowley, G.G. Howes, Nonlinear phase mixing and phase-space cascade of entropy in gyrokinetic plasma turbulence. *Phys. Rev. Lett.* **103**(1), 015003 (2009). <https://doi.org/10.1103/PhysRevLett.103.015003> [arXiv:0811.2538](https://arxiv.org/abs/0811.2538)

R.C. Tautz, A. Shalchi, Drift coefficients of charged particles in turbulent magnetic fields. *Astrophys. J.* **744**(2), 125 (2012). <https://doi.org/10.1088/0004-637X/744/2/125>

J.M. TenBarge, G.G. Howes, Current sheets and collisionless damping in kinetic plasma turbulence. *Astrophys. J. Lett.* **771**, L27 (2013). <https://doi.org/10.1088/2041-8205/771/2/L27>. [arXiv:1304.2958](https://arxiv.org/abs/1304.2958)

J.M. TenBarge, G.G. Howes, W. Dorland, Collisionless damping at electron scales in solar wind turbulence. *Astrophys. J.* **774**(2), 139 (2013). <https://doi.org/10.1088/0004-637X/774/2/139>

A. Tenerani, A.F. Rappazzo, M. Velli, F. Pucci, The tearing mode instability of thin current sheets: The transition to fast reconnection in the presence of viscosity. *Astrophys. J.* **801**(2), 145 (2015a)

A. Tenerani, M. Velli, A.F. Rappazzo, F. Pucci, Magnetic reconnection: Recursive current sheet collapse triggered by “ideal” tearing. *Astrophys. J. Lett.* **813**(2), L32 (2015b)

J.A. Tassein, W.H. Matthaeus, M. Wan, K.T. Osman, D. Ruffolo, J. Giacalone, Association of suprathermal particles with coherent structures and shocks. *Astrophys. J.* **776**, L8 (2013). <https://doi.org/10.1088/2041-8205/776/1/L8>

S.V. Thampi, C. Krishnaprasad, P.R. Shreedevi, T.K. Pant, A. Bhardwaj, Acceleration of energetic ions in corotating interaction region near 1.5 au: Evidence from MAVEN. *Astrophys. J. Lett.* **880**(1), L3 (2019). <https://doi.org/10.3847/2041-8213/ab2b43>. [arXiv:1908.00816](https://arxiv.org/abs/1908.00816)

P. Tooprakai, P. Chuchai, J. Minnie, D. Ruffolo, J.W. Bieber, W.H. Matthaeus, Temporary topological trapping and escape of charged particles in a flux tube as a cause of delay in time asymptotic transport. *Geophys. Res. Lett.* **34**, 17105 (2007). <https://doi.org/10.1029/2007GL030672>

P. Tooprakai, A. Seripienlert, D. Ruffolo, P. Chuchai, W.H. Matthaeus, Simulations of lateral transport and dropout structure of energetic particles from impulsive solar flares. *Astrophys. J.* **831**, 195 (2016). <https://doi.org/10.3847/0004-637X/831/2/195>

R.B. Torbert, J.L. Burch, B.L. Giles, D. Gershman, C.J. Pollock, J. Dorelli, L. Avanov, M.R. Argall, J. Shuster, R.J. Strangeway, C.T. Russell, R.E. Ergun, F.D. Wilder, K. Goodrich, H.A. Faith, C.J. Farrugia, P.A. Lindqvist, T. Phan, Y. Khotyaintsev, T.E. Moore, G. Marklund, W. Daughton, W. Magnes, C.A. Kletzing, S. Bounds, Estimates of terms in ohm’s law during an encounter with an electron diffusion region. *Geophys. Res. Lett.* **43**(12), 5918–5925 (2016). <https://doi.org/10.1002/2016GL069553>. <https://agupubs.onlinelibrary.wiley.com/doi/pdf/10.1002/2016GL069553>

R.B. Torbert, J.L. Burch, T.D. Phan, M. Hesse, M.R. Argall, J. Shuster, R.E. Ergun, L. Alm, R. Nakamura, K.J. Genestreti, D.J. Gershman, W.R. Paterson, D.L. Turner, I. Cohen, B.L. Giles, C.J. Pollock, S. Wang, L.J. Chen, J.E. Stawarz, J.P. Eastwood, K.J. Hwang, C. Farrugia, I. Dors, H. Vaith, C. Mouikis, A. Ardakanian, B.H. Mauk, S.A. Fuselier, C.T. Russell, R.J. Strangeway, T.E. Moore, J.F. Drake, M.A. Shay, Y.V. Khotyaintsev, P.A. Lindqvist, W. Baumjohann, F.D. Wilder, N. Ahmadi, J.C. Dorelli, L.A. Avanov, M. Oka, D.N. Baker, J.F. Fennell, J.B. Blake, A.N. Jaynes, O. Le Contel, S.M. Petrinec, B. Lavraud, Y. Saito, Electron-scale dynamics of the diffusion region during symmetric magnetic reconnection in space. *Science* **362**(6421), 1391–1395 (2018). <https://doi.org/10.1126/science.aat2998>. <https://science.sciencemag.org/content/362/6421/1391.full.pdf>

C. Tronci, E. Camporeale, Neutral Vlasov kinetic theory of magnetized plasmas. *Phys. Plasmas* **22**(2), 020704 (2015). <https://doi.org/10.1063/1.4907665>

D. Trotta, L. Franci, D. Burgess, P. Hellinger, Fast acceleration of transrelativistic electrons in astrophysical turbulence. *Astrophys. J.* **894**(2), 136 (2020). <https://doi.org/10.3847/1538-4357/ab873c>. [arXiv:1910.11935](https://arxiv.org/abs/1910.11935)

A.Y. Ukhorskiy, M.I. Sitnov, V.G. Merkin, M. Gkioulidou, D.G. Mitchell, Ion acceleration at dipolarization fronts in the inner magnetosphere. *J. Geophys. Res. Space Phys.* **122**(3), 3040–3054 (2017). <https://doi.org/10.1002/2016JA023304>

T. Umeda, Y. Wada, Secondary instabilities in the collisionless Rayleigh-Taylor instability: Full kinetic simulation. *Phys. Plasmas* **23**(11), 112117 (2016). <https://doi.org/10.1063/1.4967859>

T. Umeda, Y. Wada, Non-MHD effects in the nonlinear development of the MHD-scale Rayleigh-Taylor instability. *Phys. Plasmas* **24**(7), 072307 (2017). <https://doi.org/10.1063/1.4991409>

T. Umeda, K. Togano, T. Ogino, Two-dimensional full-electromagnetic Vlasov code with conservative scheme and its application to magnetic reconnection. *Comput. Phys. Commun.* **180**(3), 365–374 (2009). <https://doi.org/10.1016/j.cpc.2008.11.001>

T. Umeda, J.i. Miwa, Y. Matsumoto, T.K.M. Nakamura, K. Togano, K. Fukazawa, I. Shinohara, Full electromagnetic Vlasov code simulation of the Kelvin-Helmholtz instability. *Phys. Plasmas* **17**(5), 052311 (2010). <https://doi.org/10.1063/1.3422547>

D.A. Uzdensky, Magnetic reconnection in extreme astrophysical environments. *Space Sci. Rev.* **160**(1), 45–71 (2011). <https://doi.org/10.1007/s11214-011-9744-5>

S. Vafin, M. Riazantseva, M. Pohl, Coulomb collisions as a candidate for temperature anisotropy constraints in the solar wind. *Astrophys. J. Lett.* **871**(1), L11 (2019). <https://doi.org/10.3847/2041-8213/aafb11>

A. Vaivads, Y. Khotyaintsev, M. André, A. Retinò, S.C. Buchert, B.N. Rogers, P. Décréau, G. Paschmann, T.D. Phan, Structure of the magnetic reconnection diffusion region from four-spacecraft observations. *Phys. Rev. Lett.* **93**, 105001 (2004). <https://doi.org/10.1103/PhysRevLett.93.105001>

A. Vaivads, A. Retinò, J. Soucek, Y.V. Khotyaintsev, F. Valentini, C.P. Escoubet, O. Alexandrova, M. André, S.D. Bale, M. Balikhin et al., Turbulence heating observer – satellite mission proposal. *J. Plasma Phys.* **82**(5), 905820501 (2016). <https://doi.org/10.1017/S0022377816000775>

F. Valentini, P. Trávníček, F. Califano, P. Hellinger, A. Mangeney, A hybrid-Vlasov model based on the current advance method for the simulation of collisionless magnetized plasma. *J. Comput. Phys.* **225**(1), 753–770 (2007)

F. Valentini, P. Veltri, F. Califano, A. Mangeney, Cross-scale effects in solar-wind turbulence. *Phys. Rev. Lett.* **101**(2), 025006 (2008). <https://doi.org/10.1103/PhysRevLett.101.025006>

F. Valentini, F. Califano, D. Perrone, F. Pegoraro, P. Veltri, New ion-wave path in the energy cascade. *Phys. Rev. Lett.* **106**(16), 165002 (2011a). <https://doi.org/10.1103/PhysRevLett.106.165002>

F. Valentini, D. Perrone, P. Veltri, Short-wavelength electrostatic fluctuations in the solar wind. *Astrophys. J.* **739**(1), 54 (2011b). <https://doi.org/10.1088/0004-637X/739/1/54>

F. Valentini, S. Servidio, D. Perrone, F. Califano, W. Matthaeus, P. Veltri, Hybrid Vlasov-Maxwell simulations of two-dimensional turbulence in plasmas. *Phys. Plasmas* **21**(8), 082307 (2014)

F. Valentini, D. Perrone, S. Stabile, O. Pezzi, S. Servidio, R.D. Marco, F. Marcucci, R. Bruno, B. Lavraud, J.D. Keyser, G. Consolini, D. Brienza, L. Sorriso-Valvo, A. Retinò, A. Vaivads, M. Salatti, P. Veltri, Differential kinetic dynamics and heating of ions in the turbulent solar wind. *New J. Phys.* **18**(12), 125001 (2016). <http://stacks.iop.org/1367-2630/18/i=12/a=125001>

F. Valentini, C.L. Vásconez, O. Pezzi, S. Servidio, F. Malara, F. Pucci, Transition to kinetic turbulence at proton scales driven by large-amplitude kinetic Alfvén fluctuations. *Astron. Astrophys.* **599**, A8 (2017). <https://doi.org/10.1051/0004-6361/201629240>

C.L. Vásconez, F. Pucci, F. Valentini, S. Servidio, W.H. Matthaeus, F. Malara, Kinetic Alfvén wave generation by large-scale phase mixing. *Astrophys. J.* **815**(1), 7 (2015). <http://stacks.iop.org/0004-637X/815/i=1/a=7>

I.Y. Vasko, I.V. Kuzichev, A.V. Artemyev, S.D. Bale, J.W. Bonnell, F.S. Mozer, On quasi-parallel whistler waves in the solar wind. *Phys. Plasmas* **27**(8), 082902 (2020). <https://doi.org/10.1063/5.0003401>

B.J. Vasquez, C.W. Smith, K. Hamilton, B.T. MacBride, R.J. Leamon, Evaluation of the turbulent energy cascade rates from the upper inertial range in the solar wind at 1 AU. *J. Geophys. Res. Space Phys.* **112**(A7), A07101 (2007). <https://doi.org/10.1029/2007JA012305>

V.M. Vasyliunas, Low-energy electrons in the magnetosphere as observed by ogo-1 and ogo-3, in *Physics of the Magnetosphere* (Springer, Berlin, 1968), pp. 622–640

D. Vech, K.G. Klein, J.C. Kasper, Nature of stochastic ion heating in the solar wind: Testing the dependence on plasma beta and turbulence amplitude. *Astrophys. J. Lett.* **850**(1), L11 (2017). <https://doi.org/10.3847/2041-8213/aa9887>. arXiv:1711.01508

M. Verma, D. Roberts, M. Goldstein, Turbulent heating and temperature evolution in the solar wind plasma. *J. Geophys. Res. Space Phys.* **100**(A10), 19839–19850 (1995)

D. Verscharen, K.G. Klein, B.A. Maruca, The multi-scale nature of the solar wind. *Living Rev. Sol. Phys.* **16**(1), 5 (2019)

M. Wan, W.H. Matthaeus, S. Servidio, S. Oughton, Generation of X-points and secondary islands in 2D magnetohydrodynamic turbulence. *Phys. Plasmas* **20**, 042307 (2013). <https://doi.org/10.1063/1.4802985>

M. Wan, A.F. Rappazzo, W.H. Matthaeus, S. Servidio, S. Oughton, Dissipation and reconnection in boundary-driven reduced magnetohydrodynamics. *Astrophys. J.* **797**, 63 (2014). <https://doi.org/10.1088/0004-637X/797/1/63>

M. Wan, W.H. Matthaeus, V. Roytershteyn, H. Karimabadi, T. Parashar, P. Wu, M. Shay, Intermittent dissipation and heating in 3D kinetic plasma turbulence. *Phys. Rev. Lett.* **114**(17), 175002 (2015). <https://doi.org/10.1103/PhysRevLett.114.175002>

M. Wan, W.H. Matthaeus, V. Roytershteyn, T.N. Parashar, P. Wu, H. Karimabadi, Intermittency, coherent structures and dissipation in plasma turbulence. *Phys. Plasmas* **23**(4), 042307 (2016). <https://doi.org/10.1063/1.4945631>

Y.M. Wang, P. Hess, Gradual streamer expansions and the relationship between blobs and inflows. *Astrophys. J.* **859**(2), 135 (2018). <https://doi.org/10.3847/1538-4357/aabfd5>

Y.M. Wang, J.N.R. Sheeley, J.H. Walters, G.E. Brueckner, R.A. Howard, D.J. Michels, P.L. Lamy, R. Schwenn, G.M. Simnett, Origin of streamer material in the outer corona. *Astrophys. J. Lett.* **498**(2), L165–L168 (1998). <https://doi.org/10.1086/311321>

Y.M. Wang, N.R. Sheeley, D.G. Socker, R.A. Howard, N.B. Rich, The dynamical nature of coronal streamers. *J. Geophys. Res.* **105**(A11), 25133–25142 (2000). <https://doi.org/10.1029/2000JA000149>

B. Wang, J. Kuo, S.C. Bae, S. Granick, When Brownian diffusion is not Gaussian. *Nat. Mater.* **11**(6), 481 (2012)

Z. Wang, H.S. Fu, C.M. Liu, Y.Y. Liu, G. Cozzani, B.L. Giles, K.J. Hwang, J.L. Burch, Electron distribution functions around a reconnection X-line resolved by the FOTE method. *Geophys. Res. Lett.* **46**(3), 1195–1204 (2019). <https://doi.org/10.1029/2018GL081708>

S. Wang, R. Wang, Q. Lu, H. Fu, S. Wang, Direct evidence of secondary reconnection inside filamentary currents of magnetic flux ropes during magnetic reconnection. *Nat. Commun.* **11**(1), 1–8 (2020)

G.M. Webb, N.J. Martinic, H. Moraal, Scatter free propagation and drifts of cosmic-rays in the heliosphere, in *International Cosmic Ray Conference*. International Cosmic Ray Conference, vol. 10 (1981), p. 109

J.M. Wilcox, J.T. Hoeksema, P.H. Scherrer, Origin of the warped heliospheric current sheet. *Science* **209**, 603–605 (1980). <https://doi.org/10.1126/science.209.4456.603>

F. Wilder, R. Ergun, J. Burch, N. Ahmadi, S. Eriksson, T. Phan, K. Goodrich, J. Shuster, A. Rager, R. Torbert et al., The role of the parallel electric field in electron-scale dissipation at reconnecting currents in the magnetosheath. *J. Geophys. Res. Space Phys.* **123**(8), 6533–6547 (2018)

P. Wu, S. Perri, K. Osman, M. Wan, W.H. Matthaeus, M.A. Shay, M.L. Goldstein, H. Karimabadi, S. Chapman, Intermittent heating in solar wind and kinetic simulations. *Astrophys. J. Lett.* **763**(2), L30 (2013). <https://doi.org/10.1088/2041-8205/763/2/L30>

Q. Xia, V. Zharkova, Particle acceleration in coalescent and squashed magnetic islands - I. Test particle approach. *Astron. Astrophys.* **620**, A121 (2018). <https://doi.org/10.1051/0004-6361/201833599>

Q. Xia, V. Zharkova, Particle acceleration in coalescent and squashed magnetic islands. II. Particle-in-cell approach. *Astron. Astrophys.* **635**, A116 (2020). <https://doi.org/10.1051/0004-6361/201936420>

X. Xu, F. Wei, X. Feng, Observations of reconnection exhausts associated with large-scale current sheets within a complex ICME at 1 AU. *J. Geophys. Res. Space Phys.* **116**(A5), A05105 (2011). <https://doi.org/10.1029/2010JA016159>. <https://agupubs.onlinelibrary.wiley.com/doi/pdf/10.1029/2010JA016159>

F. Xu, G. Li, L. Zhao, Y. Zhang, O. Khabarova, B. Miao, J. le Roux, Angular distribution of solar wind magnetic field vector at 1 AU. *Astrophys. J.* **801**(1), 58 (2015). <https://doi.org/10.1088/0004-637X/801/1/58>

Y. Yang, W.H. Matthaeus, T.N. Parashar, C.C. Haggerty, V. Roytershteyn, W. Daughton, M. Wan, Y. Shi, S. Chen, Energy transfer, pressure tensor, and heating of kinetic plasma. *Phys. Plasmas* **24**(7), 072306 (2017a). <https://doi.org/10.1063/1.4990421>

Y. Yang, W.H. Matthaeus, T.N. Parashar, P. Wu, M. Wan, Y. Shi, S. Chen, V. Roytershteyn, W. Daughton, Energy transfer channels and turbulence cascade in Vlasov-Maxwell turbulence. *Phys. Rev. E* **95**, 061201 (2017b). <https://doi.org/10.1103/PhysRevE.95.061201>

S.T. Yao, Q.Q. Shi, R.L. Guo, Z.H. Yao, H.S. Fu, A.W. Degeling, Q.G. Zong, X.G. Wang, C.T. Russell, A.M. Tian, Y.C. Xiao, H. Zhang, S.M. Wang, H.Q. Hu, J. Liu, H. Liu, B. Li, B.L. Giles, Kinetic-scale flux rope in the magnetosheath boundary layer. *Astrophys. J.* **897**(2), 137 (2020). <https://doi.org/10.3847/1538-4357/ab9620>

P.H. Yoon, A.T.Y. Lui, On the drift-sausage mode in one-dimensional current sheet. *J. Geophys. Res.* **106**(A2), 1939–1948 (2001). <https://doi.org/10.1029/2000JA000130>

G.P. Zank, W.K.M. Rice, C.C. Wu, Particle acceleration and coronal mass ejection driven shocks: A theoretical model. *J. Geophys. Res. Space Phys.* **105**(A11), 25079–25095 (2000). <https://doi.org/10.1029/1999JA000455>. <https://agupubs.onlinelibrary.wiley.com/doi/pdf/10.1029/1999JA000455>

G.P. Zank, J.A. le Roux, G.M. Webb, A. Dosch, O. Khabarova, Particle acceleration via reconnection processes in the supersonic solar wind. *Astrophys. J.* **797**, 28 (2014). <https://doi.org/10.1088/0004-637X/797/1/28>

G.P. Zank, P. Hunana, P. Mostafavi, J.A. le Roux, G. Li, G.M. Webb, O.V. Khabarova, Particle acceleration by combined diffusive shock acceleration and downstream multiple magnetic island acceleration. *J. Phys. Conf. Ser.* **642**, 012031 (2015a)

G.P. Zank, P. Hunana, P. Mostafavi, J.A. le Roux, G. Li, G.M. Webb, O. Khabarova, A. Cummings, E. Stone, R. Decker, Diffusive shock acceleration and reconnection acceleration processes. *Astrophys. J.* **814**, 137 (2015b). <https://doi.org/10.1088/0004-637X/814/2/137>

A. Zeiler, D. Biskamp, J.F. Drake, B.N. Rogers, M.A. Shay, M. Scholer, Three-dimensional particle simulations of collisionless magnetic reconnection. *J. Geophys. Res. Space Phys.* **107**(A9), SMP 6–1–SMP 6–9 (2002). <https://doi.org/10.1029/2001JA000287>. <https://agupubs.onlinelibrary.wiley.com/doi/pdf/10.1029/2001JA000287>

L.M. Zelenyi, A.V. Milovanov, REVIEWS OF TOPICAL PROBLEMS: Fractal topology and strange kinetics: From percolation theory to problems in cosmic electrodynamics. *Phys. Usp.* **47**(8), R01 (2004). <https://doi.org/10.1070/PU2004v047n08ABEH001705>

L.M. Zelenyi, A.S. Lipatov, D.G. Lominadze, A.L. Taktakishvili, The dynamics of the energetic proton bursts in the course of the magnetic field topology reconstruction in the Earth's magnetotail. *Planet. Space Sci.* **32**(3), 313–324 (1984). [https://doi.org/10.1016/0032-0633\(84\)90167-3](https://doi.org/10.1016/0032-0633(84)90167-3)

L.M. Zelenyi, J.G. Lominadze, A.L. Taktakishvili, Generation of the energetic proton and electron bursts in planetary magnetotails. *J. Geophys. Res.* **95**(A4), 3883–3891 (1990). <https://doi.org/10.1029/JA095iA04p03883>

L. Zelenyi, A.V. Milovanov, G. Zimbardo, Multiscale magnetic structure of the distant tail: Self-consistent fractal approach, in *Geophysical Monograph-American Geophysical Union*, vol. 105 (1998), pp. 321–339

L. Zelenyi, M. Sitnov, H. Malova, A. Sharma, Thin and superthin ion current sheets. Quasi-adiabatic and nonadiabatic models. *Nonlinear Process. Geophys.* **7**, 127–139 (2000). <https://doi.org/10.5194/npg-7-127-2000>

L.M. Zelenyi, H. Malova, V. Popov, Splitting of thin current sheets in the Earth's magnetosphere. *JETP Lett.* **78**, 296–299 (2003). <https://doi.org/10.1134/1.1625728>

L. Zelenyi, H. Malova, V.Y. Popov, D. Delcourt, A. Sharma, Nonlinear equilibrium structure of thin currents sheets: Influence of electron pressure anisotropy. *Nonlinear Process. Geophys.* **11**, 579–587 (2004). <https://doi.org/10.5194/npg-11-579-2004>

L.M. Zelenyi, H.V. Malova, V.Y. Popov, D.C. Delcourt, N.Y. Ganushkina, A.S. Sharma, "Matreshka" model of multilayered current sheet. *Geophys. Res. Lett.* **33**(5), L05105 (2006). <https://doi.org/10.1029/2005GL025117>

L.M. Zelenyi, M.S. Dolgonosov, E.E. Grigorenko, J.A. Sauvaud, Universal properties of the nonadiabatic acceleration of ions in current sheets. *JETP Lett.* **85**(4), 187–193 (2007). <https://doi.org/10.1134/S0021364007040017>

L. Zelenyi, A. Artemiev, H. Malova, V. Popov, Marginal stability of thin current sheets in the Earth's magnetotail. *J. Atmos. Sol.-Terr. Phys.* **70**(2–4), 325–333 (2008). <https://doi.org/10.1016/j.jastp.2007.08.019>

L.M. Zelenyi, A.V. Artemyev, A.A. Petrukovich, R. Nakamura, H.V. Malova, V.Y. Popov, Low frequency eigenmodes of thin anisotropic current sheets and Cluster observations. *Ann. Geophys.* **27**(2), 861–868 (2009a). <https://doi.org/10.5194/angeo-27-861-2009>

L.M. Zelenyi, A.P. Kropotkin, V.I. Domrin, A.V. Artemyev, H.V. Malova, V.Y. Popov, Tearing mode in thin current sheets of the Earth's magnetosphere: A scenario of transition to unstable state. *Cosm. Res.* **47**(5), 352–360 (2009b). <https://doi.org/10.1134/S0010952509050025>

L.M. Zelenyi, A. Petrukovich, A.V. Artemyev, K.V. Malova, R. Nakamura, Metastability of current sheets. *Phys. Usp.* **53**(9), 933–941 (2010). <https://doi.org/10.3367/UFNr.0180.201009g.0973>

L. Zelenyi, H. Malova, A. Artemyev, V.Y. Popov, A. Petrukovich, Thin current sheets in collisionless plasma: Equilibrium structure, plasma instabilities, and particle acceleration. *Plasma Phys. Rep.* **37**(2), 118–160 (2011). <https://doi.org/10.1134/S1063780X1102005X>

L. Zelenyi, H. Malova, E. Grigorenko, V. Popov, D. Delcourt, Current sheets in planetary magnetospheres. *Plasma Phys. Control. Fusion* **61**(5), 054002 (2019). <https://doi.org/10.1088/1361-6587/aafbbf>

S. Zenitani, M. Hesse, A. Klimas, M. Kuznetsova, New measure of the dissipation region in collisionless magnetic reconnection. *Phys. Rev. Lett.* **106**(19), 195003 (2011)

L.L. Zhao, G.P. Zank, O. Khabarova, S. Du, Y. Chen, L. Adhikari, Q. Hu, An unusual energetic particle flux enhancement associated with solar wind magnetic island dynamics. *Astrophys. J. Lett.* **864**(2), L34 (2018)

L.L. Zhao, G.P. Zank, L. Adhikari, Q. Hu, J.C. Kasper, S.D. Bale, K.E. Korreck, A.W. Case, M. Stevens, J.W. Bonnell, T. Dudok de Wit, K. Goetz, P.R. Harvey, R.J. MacDowall, D.M. Malaspina, M. Pulupa, D.E. Larson, R. Livi, P. Whittlesey, K.G. Klein, Identification of magnetic flux ropes from Parker solar probe observations during the first encounter. *Astrophys. J. Suppl. Ser.* **246**(2), 26 (2020). <https://doi.org/10.3847/1538-4365/ab4ff1>. [arXiv:1912.02349](https://arxiv.org/abs/1912.02349)

V.V. Zharkova, O.V. Khabarova, Particle dynamics in the reconnecting heliospheric current sheet: Solar wind data versus three-dimensional particle-in-cell simulations. *Astrophys. J.* **752**(1), 35 (2012). <https://doi.org/10.1088/0004-637X/752/1/35>

V.V. Zharkova, O.V. Khabarova, Additional acceleration of solar-wind particles in current sheets of the heliosphere. *Ann. Geophys.* **33**(4), 457–470 (2015). <https://doi.org/10.5194/angeo-33-457-2015>

V. Zhdankin, D.A. Uzdensky, J.C. Perez, S. Boldyrev, Statistical analysis of current sheets in three-dimensional magnetohydrodynamic turbulence. *Astrophys. J.* **771**, 124 (2013). <https://doi.org/10.1088/0004-637X/771/2/124>

J. Zheng, Q. Hu, Observational evidence for self-generation of small-scale magnetic flux ropes from intermittent solar wind turbulence. *Astrophys. J. Lett.* **852**, L23 (2018)

X.Z. Zhou, V. Angelopoulos, V.A. Sergeev, A. Runov, Accelerated ions ahead of earthward propagating dipolarization fronts. *J. Geophys. Res. Space Phys.* **115**(A8), A00I03 (2010). <https://doi.org/10.1029/2010JA015481>

Z. Zhu, R.M. Winglee, Tearing instability, flux ropes, and the kinetic current sheet kink instability in the Earth's magnetotail: A three-dimensional perspective from particle simulations. *J. Geophys. Res.* **101**(A3), 4885–4898 (1996). <https://doi.org/10.1029/95JA03144>

G. Zimbardo, S. Perri, From Lévy walks to superdiffusive shock acceleration. *Astrophys. J.* **778**(1), 35 (2013). <https://doi.org/10.1088/0004-637X/778/1/35>

G. Zimbardo, S. Perri, Superdiffusive shock acceleration at galaxy cluster shocks. *Nat. Astron.* **1**, 0163 (2017). <https://doi.org/10.1038/s41550-017-0163>

G. Zimbardo, P. Pommerehne, P. Veltri, Superdiffusive and subdiffusive transport of energetic particles in solar wind anisotropic magnetic turbulence. *Astrophys. J. Lett.* **639**(2), L91–L94 (2006). <https://doi.org/10.1086/502676>

G. Zimbardo, E. Amato, A. Bovet, F. Effenberger, A. Fasoli, H. Fichtner, I. Furno, K. Gustafson, P. Ricci, S. Perri, Superdiffusive transport in laboratory and astrophysical plasmas. *J. Plasma Phys.* **81**(6), 495810601 (2015). <https://doi.org/10.1017/S0022377815001117>

G. Zimbardo, S. Perri, F. Effenberger, H. Fichtner, Fractional Parker equation for the transport of cosmic rays: Steady-state solutions. *Astron. Astrophys.* **607**, A7 (2017). <https://doi.org/10.1051/0004-6361/201731179>